ORNL/TM--12202

DE93 003589

MODELS OF IODINE BEHAVIOR IN REACTOR CONTAINMENTS

C. F. Weber
E. C. Beahm*
T. S. Kress†

Computing and Telecommunications Division
at Oak Ridge National Laboratory
P.O. Box 2008
Oak Ridge, TN 37831

*Chemical Technology Division.
†Engineering Technology Division

Date Published: October 1992

Prepared by the
OAK RIDGE NATIONAL LABORATORY
Oak Ridge, Tennessee 37831
managed by
MARTIN MARIETTA ENERGY SYSTEMS, INC.
for the
U.S. DEPARTMENT OF ENERGY
under contract DE-AC05-84OR21400

CONTENTS

LIST OF FIGURES

LIST OF TABLES

ACKNOWLEDGMENTS

Much of the work described in this report was done under the sponsorship of the U.S. Nuclear Regulatory Commission to enhance the ability to predict releases and consequences of LWR severe accidents. Thus, considerable credit is due to the NRC Office of Nuclear Regulatory Research, and to technical monitors Lisa Chan, Tom Walker, and Richard Lee.

The final publication, however, has been supported by the ORNL Research Reactors Division in order to adequately document models that have been used in the safety analysis of the High Flux Isotope Reactor. The authors are especially grateful to Lamar Lepard, David Cook, and George Flanagan of Research Reactors Division for this sponsorship of this work. Finally, thanks go to Lindy Norris for her diligent efforts in typing and revising the manuscript.

ABSTRACT

Models are developed for many phenomena of interest concerning iodine behavior in reactor containments during severe accidents. Processes include speciation in both gas and liquid phases, reactions with surfaces, airborne aerosols, and other materials, and gas-liquid interface behavior. Although some models are largely empirical formulations, every effort has been made to construct mechanistic and rigorous descriptions of relevant chemical processes. All are based on actual experimental data generated at the Oak Ridge National Laboratory (ORNL) or elsewhere, and, hence, considerable data evaluation and parameter estimation are contained in this study. No application or encoding is attempted, but each model is stated in terms of rate processes, with the intention of allowing mechanistic simulation. Taken together, this collection of models represents a best estimate iodine behavior and transport in reactor accidents.

1. INTRODUCTION

Since the advent of nuclear reactors for commercial power production, safety studies have focused on the behavior of fission-product iodine in determining risks and consequences of various accident scenarios. This element is present in large quantities, has several isotopes that generate large doses, and, under certain conditions, can easily become volatile. Therefore, there is a significant possibility of release to the environment, where considerable hazards to human health could result. In addition, it interacts in many ways with various reactor systems and materials; hence, overall behavior is not easily predictable. Thus, detailed understanding of iodine transport in reactor accidents is both important and complex.

The first attempt to predict iodine behavior[1] involved many assumptions and few models based on experimental data. The large releases that were predicted were not verified by experience, namely the accident at Three Mile Island (TMI). In fact, the predictions were so overly conservative that they were of questionable value. This situation prompted a flurry of research into mechanisms of iodine behavior and motivated the quest for more mechanistic models for predicting accident consequences.

Numerous computer codes have been developed since the TMI accident to predict the thermal and hydraulic behavior of various plant systems.[2-4] The calculation of temperatures, pressures, flows, and inventories of various materials is obviously prerequisite to any meaningful calculation of iodine behavior. Most of these codes have only very primitive iodine transport models, usually limited to the transport of aerosol particles. Because iodine can occur in many other forms, additional models are necessary.

Over the past decade, considerable research has been undertaken to characterize the dominant reactions and transport behavior of iodine. Experiments have focused on chemical interactions of various species in the gas phase, liquid phase, and at interfaces. Reactions with solid surfaces and aerosol particles have also been revisited.

Several specialized codes have been, or are being, developed to predict iodine behavior using models based on the recent experimental results. The models described in this report represent the culmination of these efforts with regard to behavior in reactor containments. All are based predominantly on experimental data, although various assumptions were still necessary.

The model descriptions are grouped into three general categories: gas phase (Sect. 2), liquid phase (Sect. 3), and interface behavior (Sect. 4), although there is occasional overlap. Each model is expressed in terms of a rate process, and together they form an overall model of transient iodine behavior within a single, well-mixed, control volume. When combined with flow patterns connecting multiple control volumes, and transient conditions (e.g., temperature) within these regions, a best estimate of iodine behavior and release in reactor accidents is possible.

2. GAS-PHASE BEHAVIOR

Iodine behavior in the gas space of containment volumes is of particular importance since this is usually the phase of release, both into and out of containment. Iodine sources from the primary system or from molten core debris can remain airborne or can deposit on surfaces, dissolve in sprays, or be otherwise transferred to liquid. While airborne, it can undergo reaction that alters subsequent behavior. Most releases to the environment result form leakage or venting of airborne containment iodine.

The models in this section describe important interactions of gas-phase iodine that do not involve water. These include pure gas-phase speciation reactions (Sects. 2.1 and 2.2) and deposition onto surfaces (Sects. 2.3, 2.4, and 2.5). Interactions involving both gas-phase and aqueous behavior are described in Sect. 4.

2.1 FORMATION OF ORGANIC IODIDES

Inorganic iodine species can react with a wide variety of organic compounds to produce organic iodides. The types of organic compounds susceptible to reaction with iodine species include the following (reacting iodine species shown in brackets): alkenes [I_2, HI], alkynes [I_2, HI]; alcohols [HI]; ethers [HI]; methyl ketones [OI^-]; amines [HI]; diazonium compounds [KI]; and aniline [I_2]. Such an array of possible reactions leading to the formation of organic iodides should make one cautious in assigning a simple reaction mechanism. Clearly, there is more involved than the reaction of methane with elemental iodine (I_2).

In addition to direct reactions of organic compounds and iodine species, radiation in the containment building could bring about reactions not otherwise possible. Free radicals, atoms, or groups of atoms that are quite reactive due to an unpaired electron, can form when radiation interacts with many types of molecules. Iodine is a very effective scavenger of free radicals to the degree that it is used to measure the extent of free-radical formation in studies of the irradiation of organic compounds. The products of iodine reacting with organic free radicals are known as organic iodides.

Reactions to form organic iodides can be both beneficial and detrimental. The resulting iodine compound could be immobilized or it could form a penetrating volatile organic compound. In fact, both processes may occur simultaneously with a given source of organic material. Thus, for example, Rosenburg et al.[5] reported that an epoxy-based coating Amercoat 66 (Amercoat Corp.) sorbed 3.3 mg/cm^2 of I_2 at 90°C. Under similar conditions, at 100°C with the same coating, Bennett et al.[6] clearly show that methyl iodide and ethyl iodide are produced when I_2 is introduced into the system.

Both gas-phase reactions and surface reactions may contribute to the formation of organic iodides. In addition, liquid-phase production of organic iodides may also occur, as described in Sect. 3.5. A review report by Postma and Zavadoski[7] cites gas-phase reactions

under the influence of radiation as the principal source of organic iodides. Alternatively, Durant et al.[8] considered a two-step reaction process where the first stage of the reaction is the addition of I_2 to reactive groups on the coating surface, which is then followed by the formation of low-molecular-weight organic iodine compounds. Thus, it may not be prudent at this time to assign a single source when there exists such a large number of possible reaction types, sites, and conditions. It may be more important to stress the dynamic nature of reactions involving organic iodine. Thus, we may expect a dynamic interaction between sorption and desorption of iodine species, desorption of organic species prior to reaction with iodine, radiation-induced formation and decomposition of organic compounds, and organic compounds containing iodine, as well as interaction with water pools. Regarding the latter, for each I_2 converted to an organic iodide, an equal amount of I_2 would be delivered to the containment atmosphere from the sump in order to maintain the gas-liquid equilibrium. On the other hand, organic iodides may hydrolyze in water to form alcohols and I^-. For example, Lemire et al.[9] report that at 80°C for pH = 10, 43% of the initial methyl iodide in water remained after 1 h for an initial concentration of 10^{-6} mol/L.

For the purpose of constructing a realistic model, the term organic iodide and methyl iodide will henceforth mean the same thing and will refer to organic iodide that is airborne. Iodine that may be associated with an organic material on a surface is treated from the standpoint of adsorption/desorption in our models and not specifically identified as organic or inorganic. Volatile organic iodides other than CH_3I would include ethyl iodide, C_2H_5I, and the propyl iodides, C_3H_7I. The boiling point of CH_3I is ~30°C less than that of C_2H_5I, which is ~30°C less than that of nC_3H_7I. Thus, CH_3I is the most volatile of the organic iodides, and using it to represent all volatile organic iodides will not result in underpredicting the impact of organic iodides unless one of the other organic iodides was produced in significantly larger amounts than CH_3I.

2.1.1 Normal Concentrations of CH_3I in Air

After iodine enters containment during a severe accident sequence, we specify a minimum gaseous organic iodide concentration that is based on reactor building air sampling results from the TMI-2 accident. Approximately 15 months after the accident at TMI-2, the activity of ^{129}I in containment gas was $7.5 \pm 2.0 \times 10^{-11}$ $\mu Ci/cm^3$. This value corresponds to an ^{129}I concentration of $3.3 \pm 0.89 \times 10^{-12}$ mol I/L. At that time, the containment was vented and the ^{129}I was reduced by a factor of 20. Within 15 days it had nearly returned to the prepurge value.

Methyl iodide is a "ubiquitous" halocarbon that is present at concentrations that vary somewhat with distance from the ocean.[10] In a study of halocarbon concentrations at eight locations in the United States, Lillian et al.[10] reported a maximum CH_3I concentration of 3.8 ppb ($\sim 10^{-10}$ mol CH_3I/L) and an over all mean value of 0.05 ppb ($\sim 2 \times 10^{-12}$ mol CH_3I/L). Thus, atmospheric iodine concentrations on the order of 10^{-12} mol I/L are the probable lower limits

based on the evidence from TMI-2 and data on ubiquitous methyl iodide. Isotopic exchange between I_2 and CH_3I has been demonstrated by Behrens and Maddock.[11]

Based on the TMI-2 results and measurements of atmospheric CH_3I, we will establish a minimum organic iodide concentration in containment as 2×10^{-12} mol CH_3I/L which is attained in 14 d. If the gas in containment is purged and this value is decreased by dilution, we assume that it will be restored to its original value in 14 d. The mechanism for this source of organic iodide is isotopic exchange with atmospheric methyl iodide.

2.1.2 Organic Iodine Resulting From Gas or Surface Interactions

Organic iodide in the gas phase which results from gaseous or more likely gas-surface interactions is modeled from empirical data that were obtained from large vessel tests of iodine behavior. Despite several reviews of this subject within the last 15 years, the sources and rates of organic iodide production in containment are not well characterized. The state of knowledge is especially poor with respect to estimation of formation rate within the time span of a core heatup event. Even though surface reactions may play an important role, the empirical models adopted here relate only to gas-phase concentrations.

Postma and Zavodoski[7] reviewed production rates from about 70 containment tests and determined that the asymptotic steady-state conversion to CH_3I was

$$\% \ I_2 \text{ converted} = 0.188 \ C_{mo}^{-0.26} , \tag{1}$$

where C_{mo} = initial I_2 concentration (mg/m^3).

In a more recent review, Beahm et al.[12] described formation using the rate equation

$$\frac{dC_o}{dt} = \alpha(C^* - C_o) , \tag{2}$$

where

α = formation rate constant (s^{-1}),
C_o = organic iodide concentration at time t (mg iodine/m^3),
C^* = steady-state organic iodide concentration (mg iodine/m^3).

In place of Eq. (1), they used

$$C^* = 0.0189 \ C_{mo}^{0.82} , \tag{3}$$

which was based on seven containment tests using radiation environments (unlike those of ref. 7). Observing that equilibrium was attained quickly in all tests, sometimes in a matter of minutes, they assigned the value $\alpha = 0.0051$, derived by solving Eq. (2) and assuming that 0.99 C^* is reached in 1 h.

At the higher temperatures attainable in containment volumes, organic iodide is expected to decompose back onto I_2. Following Wichner et al.,[13] a first-order destruction rate is given by

$$\frac{dC_o}{dt} = - \gamma C_o \, . \tag{4}$$

The coefficient γ is fit to an Arrhenius form using data from Hilliard and Coleman,[14] resulting in

$$\gamma = \exp(0.14 - 4600/T) \quad (T \text{ in K}) \, .$$

At 25°C, this yields $\gamma = 2 \times 10^{-7}$, which agrees with the observation of Borkowski[15] that the destruction rate is on the order of 10^{-7}. Combining Eqs. (2) through (4) yields the empirical conversion-destruction model:

$$- \frac{dC_m}{dt} = \frac{dC_o}{dt} = 0.0189 \, \alpha \, C_{mo}^{0.82} - (\alpha + \gamma) C_o \, .$$

2.2 OXIDATION OF CsI IN HYDROGEN BURNS

Because of both the high temperatures and the presence of free radicals, H_2 combustion presents interesting possibilities for reaction of gas-phase or airborne particulate iodine species. Two recent studies, both sponsored by the Electric Power Research Institute Advanced Containment Experiments (EPRI-ACE) Program, were commissioned to investigate these etfects experimentally.

A number of benchscale experiments were performed at ORNL to investigate CsI conversion to I_2 and IO_3^- in steady-state H_2 flames.[16] These were designed to examine the effects of temperature, hydrogen/air mixture richness, and CsI concentration on conversion. The results were largely qualitative, but showed very little correlation between I_2 formation and mixture richness or flame temperature. There was, however, a slight dependence on the actual quantity of CsI volatilized in the flame and considerable dependence on the presence of excess cesium; hence, a quantitative model must build on these observations.

Conversion is believed to involve homogeneous gas-phase reaction, so it is essential that the CsI boiling point of 1280°C be exceeded. In constructing a quantitative model using the results of ref. 16, we make the following assumptions:

1. All gas flow in the crucial reaction region (immediately above the flame) is g = 6.67 L/min. For simplicity, assume this is independent of temperature variation within the flame.

2. From qualitative observation, it took about 5 s to completely evaporate each sample. Assume that this rate was uniform.

From these assumptions, the concentration of CsI can be determined from ν, the total amount volatilized:

$$C_g = \frac{\nu}{g \cdot \Delta t} = \frac{\nu}{(6.67)(5/60)} = 0.556\ \nu\ , \tag{5}$$

where C_g = concentration of CsI (μmol/L) and ν = amount volatilized (μmol). For the exact stoichiometric ratio of Cs:I=1, Brown[16] fit a quadratic polynomial to get the fraction of I_2 produced as a function of the amount of CsI volatilized. Because this does not allow for any extrapolation without serious error, we suggest a decaying exponential model,

$$F = F_0\ e^{-\alpha \nu}\ , \tag{6}$$

where

F = fraction converted to I_2,
F_0, α = empirical constants.

Taking logarithms of Eq. (5), the data in ref. 16 were fit by linear regression, yielding

$$\alpha = 0.3445, \qquad \ln F_0 = -0.3226\ . \tag{7}$$

Substituting Eq. (5) into Eq. (6) then gives:

$$F_1 = 0.7243\ \exp(-0.6201\ C_g)\ . \tag{8}$$

For the case of excess cesium (more likely the case in actual accidents), Eq. (6) is also used. However, because there are only two data points, the fit is exact, yielding constants

$$\alpha = 1.552 \qquad \ln F_0 = -2.35\ , \tag{9}$$

and the functional form

$$F_{10} = 0.0954\ \exp(-1.55\ C_g)\ . \tag{10}$$

The entire model is then dependent on a variable Cs/I ratio through linear interpolation of the logarithmic form:

$$r = \frac{\text{[Cs] (g·atom from all species)}}{\text{[I] (g·atom from all species)}} \tag{11}$$

$$\ln F(r) = \ln F_1 + \frac{(r-1)}{9} [\ln F_{10} - \ln F_1] . \tag{12}$$

Larger-scale experiments were performed by Kupferschmidt et al.[17] with the primary purpose of evaluating the effects of atmospheric steam on conversion of iodide. Tests using only dry air gave results similar to those of Brown et al.[16] However, when the combustion atmosphere contained 10% steam (by volume), virtually no oxidation of CsI occurred. Both of the two mechanisms suggested by the authors involved mass transfer impediments by the steam. Because the CsI aerosol at room temperature was injected into a gas mixture at 95°C, considerable condensation onto the particulates was likely. Insufficient time was allowed for revaporization, since the H_2 detonation occurred 4 s after aerosol injection. This situation would work to both retard CsI vaporization and to impede diffusion of reacting radicals to the CsI, and is the likely explanation; hence, it requires a model stipulation that all water vapor be evaporated off the CsI before conversion can occur. The model can thus be summarized as follows:

1. Vaporize all water on aerosols. If any liquid water remains, then no conversion of CsI occurs.

2. Determine if the CsI boiling point is exceeded. If not, then no conversion occurs. (This ignores the trivial contribution from the vapor pressure of CsI below the boiling point.)

3. Conversion occurs, according to Eqs. (8), (10), (11), and (12), if all water is vaporized and the CsI boiling point is exceeded.

2.3 CESIUM IODIDE CONDENSATION

Under conditions usually encountered in containment control volumes, CsI exists in condensed form; hence, it would be transported as aerosol particles. However, occasionally conditions occur (e.g., in a BWR drywell) in which temperature and pressure are high enough that a significant vapor-phase inventory could exist even though the temperature remains well below the boiling point of CsI. This gaseous CsI can migrate to and condense onto cooler surfaces within a control volume or can vent into cooler regions where nucleation or condensation onto aerosols or onto fixed surfaces might occur. This form of deposition is limited by a mass-transfer coefficient, and, unlike adsorption processes for I_2, CH_3I, and HI, it does not depend on surface type. Revaporization does not depend on surface concentration, but only on

a departure from equilibrium vapor pressure. A single equation is used to describe both condensation and revaporization:

$$\frac{dC_s}{dt} = h_w(C_g - C_g^*) ,$$

where

C_s, C_g = surface and gas-phase concentrations (mg/cm^2 and mg/cm^3),

C_g^* = equilibrium gas concentration (mg/cm^3),

h_w = mass transfer coefficient (cm/s).

The value of C_g^* is obtained from the equilibrium vapor pressure P^*, by assuming ideal gas behavior:

$$\log_{10} P^* = 17.47 - 9678/T - 3.52 \log_{10} T ,$$

$$C_g^* = \frac{P^* M_{CsI}}{R\,T} \quad (T \text{ in } K) ,$$

where M_{CsI} = molecular weight of CsI. The value of h_w is obtained from the natural convection correlation in Sect. 4.

2.4 GAS-PHASE DEPOSITION ONTO AEROSOLS

Even though many accident sequences indicate that iodine will exist predominantly as CsI in condensed form (i.e., as aerosol), it is possible in certain situations that volatile iodine species (I_2, CH_3I) will be airborne simultaneously with various types of particulate matter. Most studies have been largely qualitative, although they have indicated that substantial deposition may occur. Because such deposition may be a significant mechanism for removing gaseous iodine, it is worthy of thorough and detailed modeling consideration.

Early work in the United Kingdom assumed an irreversible deposition model based on hard spheres or analogy with water drops, but did not include any mechanistic consideration of surface reactions. Chamberlain et al.[18] gave a review and stated the basic equation for removal of a gaseous iodine species. Megaw and May[19] and Megaw[20] used a simplified equation, and applied it to experimental studies of Aitken nuclei particles in the DIDO and PLUTO reactors. Even though this pioneering work was qualitatively useful, it is inadequate for current modeling efforts.

Deposition of volatile species onto aerosol surfaces includes mass transport to the surface (adsorption), revaporization from the surface (desorption), and possibly chemical reaction with the surface material. These mechanisms can be modeled as

$$C_g \underset{k_2}{\overset{k_1}{\rightleftharpoons}} C_p \underset{k_4}{\overset{k_3}{\rightleftharpoons}} C_c, \tag{13}$$

where

C_g = gas phase concentration (mol/cm^3),
C_p = intermediate or physisorbed iodine (mol/cm^2),
C_c = chemisorbed iodine (i.e., reacted with surface material) (mol/cm^2).

The quantities k_1 and k_2 represent mass-transfer coefficients to and from the surface; k_3 and k_4 represent chemical reaction rate constants.

The characteristics of chemical reaction are highly dependent on the type of aerosol material involved. Several studies[21-23] have concerned interactions between various species (usually focusing on CsI) and control rod materials. Recent work at ORNL was concerned with the interaction of I_2 and CH_3I with fission-product aerosols, principally cesium compounds.[24]

Aerosol materials will consist of oxides, metals, and water.[25] In general, water-soluble aerosol materials will be fission products, principally cesium compounds, and in some reactor systems, boron oxides. In addition, chemical changes can occur on aerosol surfaces in containment. Varying amounts of hydration may be expected, as well as reaction of CsOH to form carbonates, borates, and nitrates. Other aerosol oxides and metals may also react with HNO_3 (gas) produced from the interaction of radiation with humid air.

Aerosols that contain liquid water are a special case. The iodine adsorption behavior of an insoluble aerosol in an aqueous droplet would be that of the aqueous phase, and iodine phenomena expected in an aqueous solution such as mass transport, hydrolysis, and radiolysis effects would predominate. With water-soluble aerosols, the same phenomena would occur along with additional pH and ionic strength effects of the aerosol material. Thus, the overall behavior in either case is similar to that of water droplets (cf. Sect. 4.3), but may have additional solution components.

In accident sequence calculations, it is necessary to use a computer code such as VANESA[26] to predict the overall composition of aerosols, although this information may not be directly applicable without further assumptions. For most interactions, the bulk composition is less important than the surface composition (i.e., less-volatile materials are more likely to condense first and can be found on the inside of aerosols). In addition, chemical changes may occur on the surface. Sorption characteristics may vary with aerosol size. Thus, in general, it will be necessary to assume homogeneous material with known geometric characteristics and whose surface characteristics vary only as predicted by interaction models.

Several studies[22-24] have determined that physical adsorption of I_2 without chemical reaction is not a particularly important process. In addition, I_2 does not react readily with most structural components or boric acid.[24] It does react in varying degrees with dry cesium compounds, the likelihood of reaction being well characterized by the iodine potential, as described in ref. 24.

2.4.1 Analysis of Deposition Onto Fission-Product Aerosol

In order to characterize rate processes, some of the data from ref. 24 have been re-evaluated. In each case, the chemical reaction step in Eq. (13) is essentially irreversible, indicating that $k_4 = 0$. The preponderance of data and the principal analyses were done for cesium carbonate aerosol, with the surface reaction[24]

$$I_2 + Cs_2CO_3 \xrightarrow{k_3} \frac{5}{3} CsI + \frac{1}{3} CsIO_3 + CO_2 . \qquad (14)$$

For dry powder, formation of surface iodide and iodate blocks diffusion to lower layers, which results in depletion of the available reaction sites. (The same is not true with wet powder, where diffusion to lower layers in the aerosol occurs readily.)

The rate equations represented by Eqs. (13) and (14) form a set of ordinary differential equations which are, in general, nonlinear. The rate coefficients for several substances have been obtained by the mathematical optimization procedure described elsewhere.[27] The materials, experimental conditions, and resulting parameters $u_i = \ln k_i$ are shown in Table 1. Also obtained from the optimization is the concentration of reactive surface sites, shown in the last column.

Table 1. Iodine deposition onto cesium-containing aerosols

Particulate material	Temp. (°C)	BET area (cm^2/g)	Rate constants[a] u_1	u_2	u_3	C_{so} (mol/cm^2) × 10^{10}
Cs_2CO_3	25	2411	6.4[b]	u_1+4.56	15.5	342
Cs_2CO_3	100	2411	17.8	21.3	15.5	
$Cs_2B_4O_7$	100	6652	-4.8	-9	19	7.8
Cs_2O	100	753	-2.2	0.63	18	648

[a] $u_i = \ln k_i$, units of k_i in min^{-1} for i = 1,2, and min^{-1} $(mol/cm^2)^{-1}$ for i = 3.

[b] Determined from Eq. (15); choices for $u_1 \geq 2$ gave identical results.

In general, it was fairly difficult to obtain optimal values, and there is considerable uncertainty in the values shown. This is primarily because the data were sparse and sometimes unavailable in ranges of greatest use in parameter estimation. However, it is probably adequate for general modeling purposes.

As mentioned previously, the principal material analyzed (for which the most data were available) was Cs_2CO_3. At 25°C, no unique value of u_1 or u_2 could be determined, although the difference between them was clearly defined. That is, for any value of $u_1 \geq 2$ and $u_2 = u_1 + 4.56$, the minimum squared error was attained. This difference actually represents an "equilibrium constant" for mass transfer

$$u_1 - u_2 = \ln \frac{k_1}{k_2} ,$$

and the nonuniqueness indicates that rapid equilibration in the adsorption/desorption processes occurred. No data were taken in the first few minutes where non-equilibrium conditions existed; hence, this is the only information that can be reliably extracted from this data.

It is possible to approximate the individual mass transport parameters using existing correlations. For mass transport to small spheres due to diffusion alone, a theoretical analysis yields[28]

$$\frac{\tilde{k}_1 d}{D} = 2 , \tag{15}$$

where

$\tilde{k}_1$ = $k_1(V_g/A)$ = flux to particle surface/bulk concentration (cm/s),
d = particle diameter (cm),
D = binary diffusion coefficient (cm^2/s),
V_g = gas volume (cm^3),
A = total surface area of particles (cm^2).

The diameter of particles is estimated to be $d = 2 \times 10^{-4}$, and the diffusion coefficient of I_2 in air is calculated using the collision integral to be $D = 0.081$. Then the approximate transfer coefficient can be determined using Eq. (15):

$$k_1 = \frac{2DA}{dV_g} = 627\ \text{min}^{-1}, \qquad u_1 = \ln k_1 = 6.4 ,$$

which is the value shown in Table 1.

The parameters in Table 1 can be used to simulate the rate processes, as shown for a typical transient in Fig. 1. The computed solution matches the general behavior of the system, although the scatter in the data makes it difficult.

Optimization calculations were also performed on Cs_2CO_3 data at 100°C, in which the following activation energies (kJ/mol) were obtained:

$$E_1 = 140 \qquad E_2 = 127 \qquad E_3 = 0\,. \tag{16}$$

These energies were then used with the lower temperature results to obtain the rate coefficients shown in the table.

Optimization calculations were performed for I_2 deposition onto two other powder materials, as shown in Table 1. These data were fairly sparse, with high data uncertainties, resulting in high uncertainties for the parameters. In these cases, both adsorption and desorption were somewhat slower, although the chemical reaction rate constant is comparable to that of Cs_2CO_3.

2.4.2 General Model

As mentioned previously, parameter values in Table 1 have large uncertainties, especially for $Cs_2B_4O_7$ and Cs_2O. The mass-transfer coefficients u_1 and u_2 are not defined uniquely for Cs_2CO_3, although their difference u_2-u_1 can be ascertained with more accuracy. Since equilibration of adsorption/desorption occurs very quickly, these two parameters are not rate determining. (For practical purposes, this equilibration can be assumed to occur instantaneously.)

The principal quantities of importance are the chemical reaction rate u_3 and the concentration of surface sites C_{so}. The former changes very little with temperature for Cs_2CO_3 powder, and this behavior will be assumed for other materials as well. Furthermore, the rate for all three materials is nearly the same, at least when the uncertainties are considered. Because much more data were available for Cs_2CO_3, we assume that the rate coefficient for this material is applicable to all other cesium-containing materials.

The concentration of surface sites controls the extent of reaction, and, therefore, the maximum loading of irreversibly sorbed iodine. For the three materials evaluated, a clear linear relationship exists between C_{so} and the cesium content of the material:

$$C_{so} = a\,x + b, \qquad a = 2.0 \times 10^{-7} \qquad b = -\,1.3 \times 10^{-7}\,, \tag{17}$$

where x = mass fraction due to cesium, and the constants a and b were obtained by linear regression.

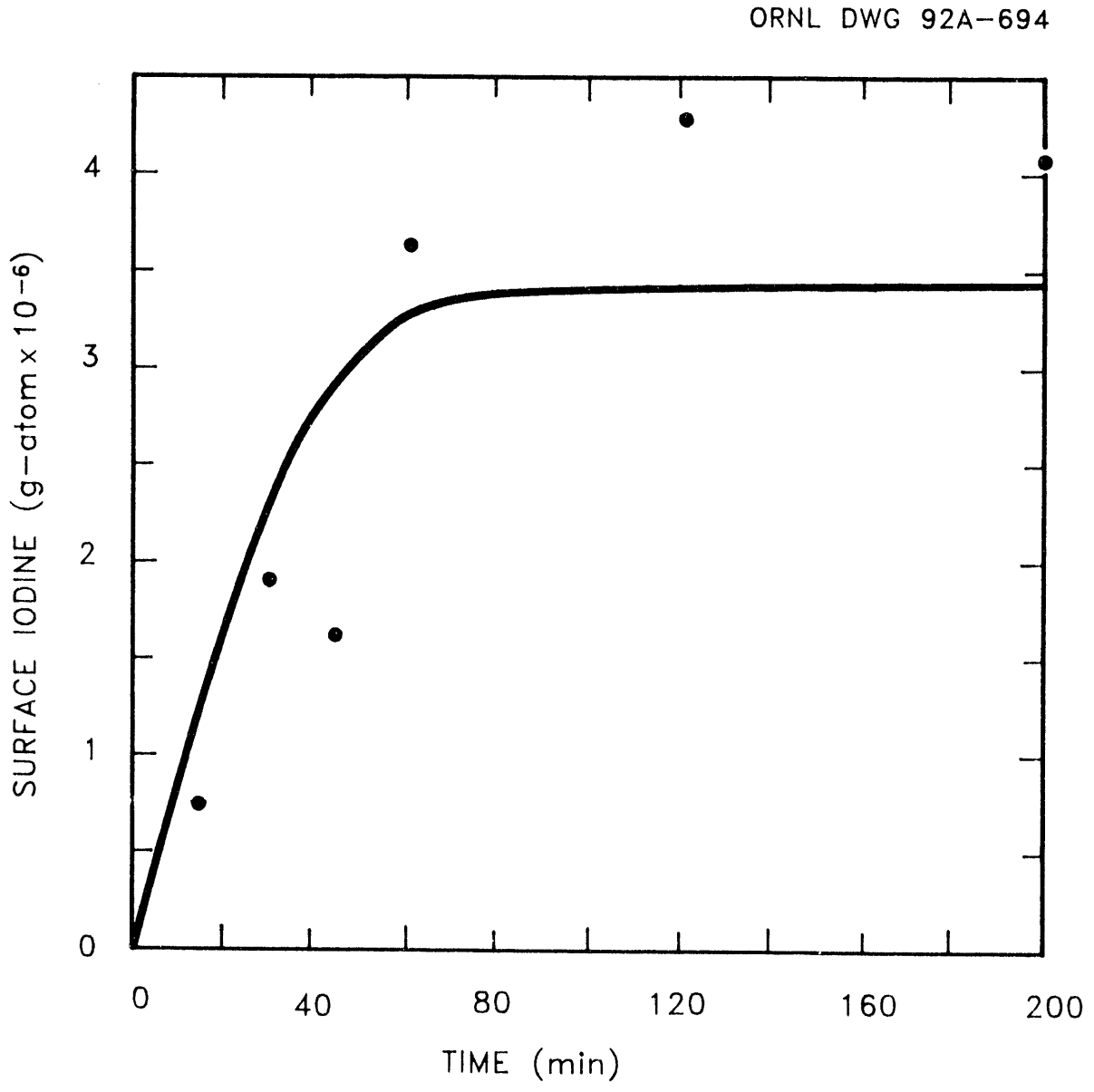

Fig. 1. Iodine deposition onto Cs_2CO_3 aerosol. Comparison of data (•) and calculated (—) values.

In general, the reaction of I_2 with cesium compounds is ultimately due to the basicity of the cesium salt. Some cesium compounds such as CsI or $CsNO_3$ are not basic. However, the chemical forms of aerosol materials are not well defined, and, hence, it is assumed that cesium is in a form that can react with I_2. In this case, Eq. (17) should be applied for any aerosol material, and when it yields $C_{so}<0$, negligible deposition occurs.

2.5 DEPOSITION OF VOLATILE IODINE ON SURFACES

Reactor containments are composed of a great many materials and surfaces with which iodine can react, most notably steel, concrete, and various types of paint. Even though it is impossible to characterize exactly the geometry and interaction mechanisms, it is possible to estimate the overall amounts of principal surface materials and to develop reasonable reaction mechanisms. This effect is of particular importance in the reduction of airborne concentrations of I_2 and CH_3I.

In general, deposition onto fixed surfaces is modeled by Eq. (13), with rate coefficients varying with temperature, surface material, iodine form, and to some extent, humidity. Data to determine kinetic parameters have been adapted from several studies before 1970, and some recent work in conjunction with the ACE program. In most cases, the original authors describe their data in terms of deposition velocities and desorption rates. In order to obtain the kinetic parameters in Eq. (13), it was necessary to perform considerable re-evaluation.

2.5.1 Deposition of I_2 onto Steel

Several previous studies[5,29,30] indicate that considerable deposition of I_2 can occur onto almost any form of steel. Rosenberg et al.[5] studied deposition onto the constituents commonly found in stainless steel. They observed that I_2 reacts most readily with iron, less so with nickel, and only sparingly with chromium, and concluded that the large amounts of irreversibly bound iodine were in the form FeI_2. Morris and Nicholls[29] noted higher deposition on several pure metals (iron, lead, silver, copper, and aluminum) than on either mild or stainless steel, although deposition onto steels was considerable. Both studies note that surface oxidation and iodine deposition are mutually beneficial processes. Thus, deposition is greatly enhanced by the presence of water vapor, but not by liquid water, either as condensate or bulk liquid.

In this situation, Eq. (13) takes the form

$$I_2(g) \underset{k_2}{\overset{k_1}{\rightleftharpoons}} I_2(s) \underset{k_4}{\overset{k_3}{\rightleftharpoons}} FeI_2(s) \ . \tag{18}$$

The determination of rate coefficients under varying conditions is accomplished by re-evaluating the data of previous studies. Descriptions of various data sets, their experimental apparatus and

procedure, and the mathematical procedures used to obtain kinetic parameters are given in Appendix A. A brief summary of the results is given in Table 2 and indicates that irreversible sorption takes place only in the presence of water vapor, but that it can be reversed by eliminating water from the system. Physisorption occurs in any environment although it is enhanced by water vapor.

Table 2. Kinetic parameters for I_2 deposition onto steel

	(s^{-1})				
Conditions	k_1	k_2	k_3	k_4	Ref.
Moist air, 20°C	7.935E-7	6.942E-7	2.947E-6	0	30
Moist air, 115°C	0.0250	1.188E-5	6.878E-5	0	5
Dry air, 115°C	7.469E-5	4.033E-5	0	7.186E-6	5

It is important to note that the moist air experiments involved very different amounts of moisture. In ref. 30, a relative humidity of 85% was used (a water mole fraction of about 0.02); additional data using 65% and 100% yielded very little change in deposition behavior. In ref. 5, steam comprised 44% by volume.[31] It may be that such differences in water content are not important provided they exceed some threshold level. If such is the case, the results from the two moist air experiments can be combined to obtain activation energies

$$E_1 = 103 \quad E_2 = 28.3 \quad E_3 = 31.3 \ \text{(kJ/mol)},$$

where

$$k_i = A_i \exp(-E_i/RT).$$

The evaluation of activation energies in dry air would require data for both adsorption and desorption at some other temperature. Neill[32] reports values of

$$E_1 = -115, \ E_2 = 70 \ \text{(kJ/mol)},$$

although these are based on data at much higher temperatures (316 to 538°C). The negative value for adsorption energy is not unusual, although it obviously does not have chemical kinetic significance (recall this is largely a mass transport process).

Finally, it is necessary to assess the behavior of sorbed iodine if liquid water contacts the surface. Rosenberg[5] performed several experiments in which a substantial loading of iodine was achieved (in moist air, implying considerable surface reaction), followed by immersion in various water solutions. Virtually all iodine was removed within a few minutes by either distilled water or a saturated I_2 solution. Removal in a saturated FeI_2 solution was slower, with about one-third removed after 30 min. It thus seems prudent for reactor safety calculations to assume all iodine is removed quickly, dissolving in water as I^-.

2.5.2 Deposition of I_2 onto Paints

Many of the early researchers who investigated I_2 deposition onto steel also studied I_2 deposition onto paints. In particular, the study of Rosenberg et al.[5] was exceptionally thorough, because they evaluated several different paint types and manufacturers under a variety of conditions. One series of tests was undertaken using single samples at a time, and reevaluation here of the results at 115°C is similar to the previous analysis of deposition onto steel.

We consider the two-step process of iodine deposition onto paint, which is analogous to Eq. (18):

$$I_2(g) \underset{k_2}{\overset{k_1}{\rightleftharpoons}} I_2(s) \tag{19a}$$

$$I_2(s) + R_2 \xrightarrow{k_3} R_2I_2 \, . \tag{19b}$$

The first step constitutes physisorption (i.e., mass transfer to surface material). The second step describes surface reaction in which an acceptable surface site has two adjacent organic groups — each combining with an iodine atom. The reaction product is written in the dimerized form to facilitate calculations (all stoichiometric coefficients are unity), although it may not occur in practice.

Because paints are porous, iodine is likely to diffuse and react in the interior and not just on the surface. Rosenberg et al.[5] have completed a thorough analysis of various modeling approaches, including the diffusion equation with simultaneous chemical reaction. Even though their approach is likely to be more meaningful physically, it poses unnecessary complications and yields simulation results no better than the three-parameter method developed here. Nevertheless, it is expedient to view surface concentrations as relative to paint mass rather than surface area.

The details of data fitting and parameter estimation are described in Appendix B. The results for four paint types are shown in Table 3. Simulation of the transients and comparison with data are shown in Figs. 2 through 5 and indicate excellent agreement.

Table 3. Kinetic parameters for iodine deposition onto paints

Run designator[a]	Paint type	Parameter values[b] u_1	u_2	u_3
VAM HB33-2	Vinyl	11.19	3.678	9.543
VAM 1756-1	Acrylic latex	8.067	1.969	9.297
VAM 66-2	Epoxy	8.380	0.2921	4.772
VP-302-3	Phenolic	5.964	1.228	5.941

[a]*Source*: H. S. Rosenberg, J. M. Genco, and D. L. Morrison, *Fission-Product Deposition and Its Enhancement Under Reactor Accident Conditions: Deposition on Containment-System Surfaces*, BMI-1865, Battelle Memorial Institute, 1969 (reevaluation of data in Table 17).

[b]$u_i = \ln k_i$; units of k_i (i=1,2,3) are h^{-1}, h^{-1}, g/mol·h, respectively.

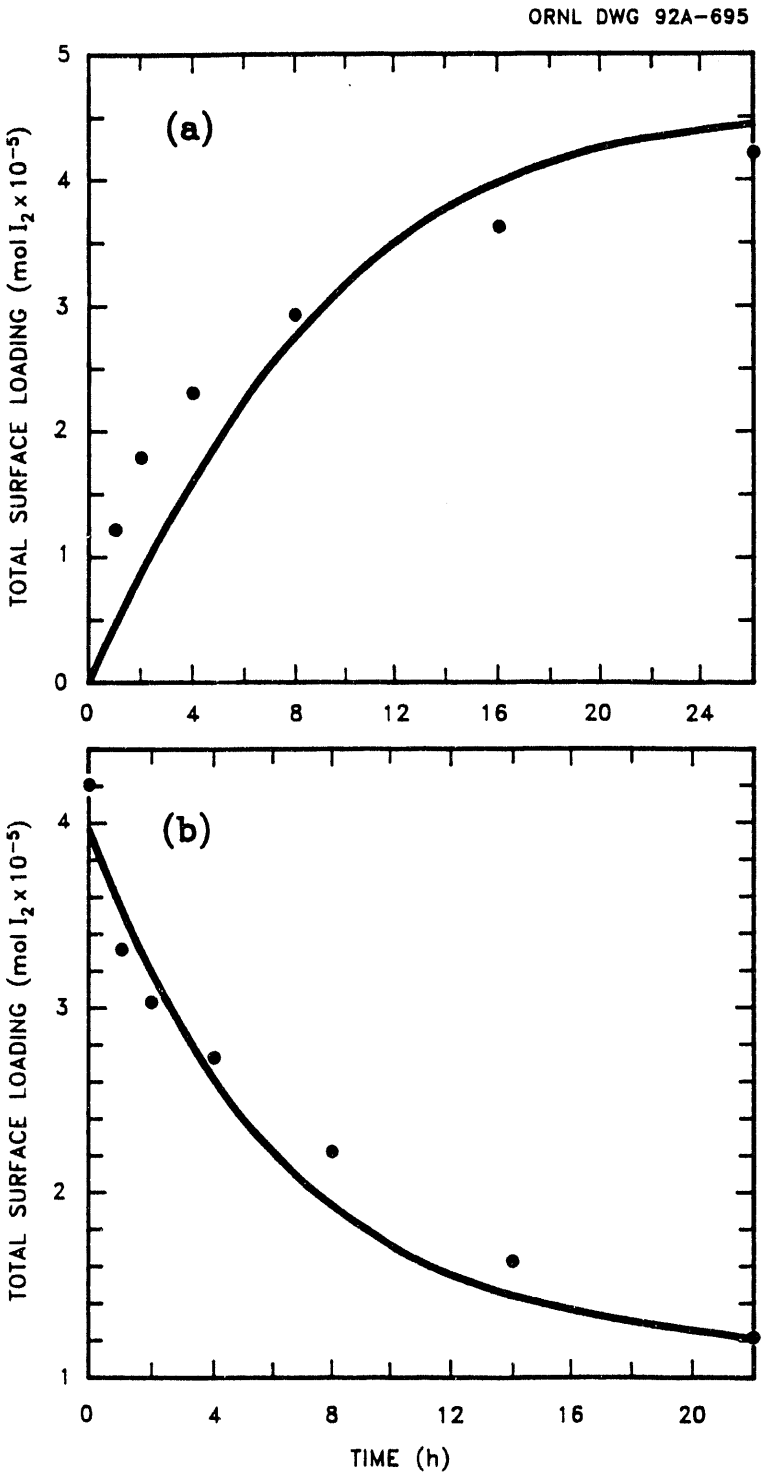

Fig. 2. Comparison of model prediction and data for I_2 deposition onto VAM HB33-2 coating: (a) adsorption, (b) desorption.

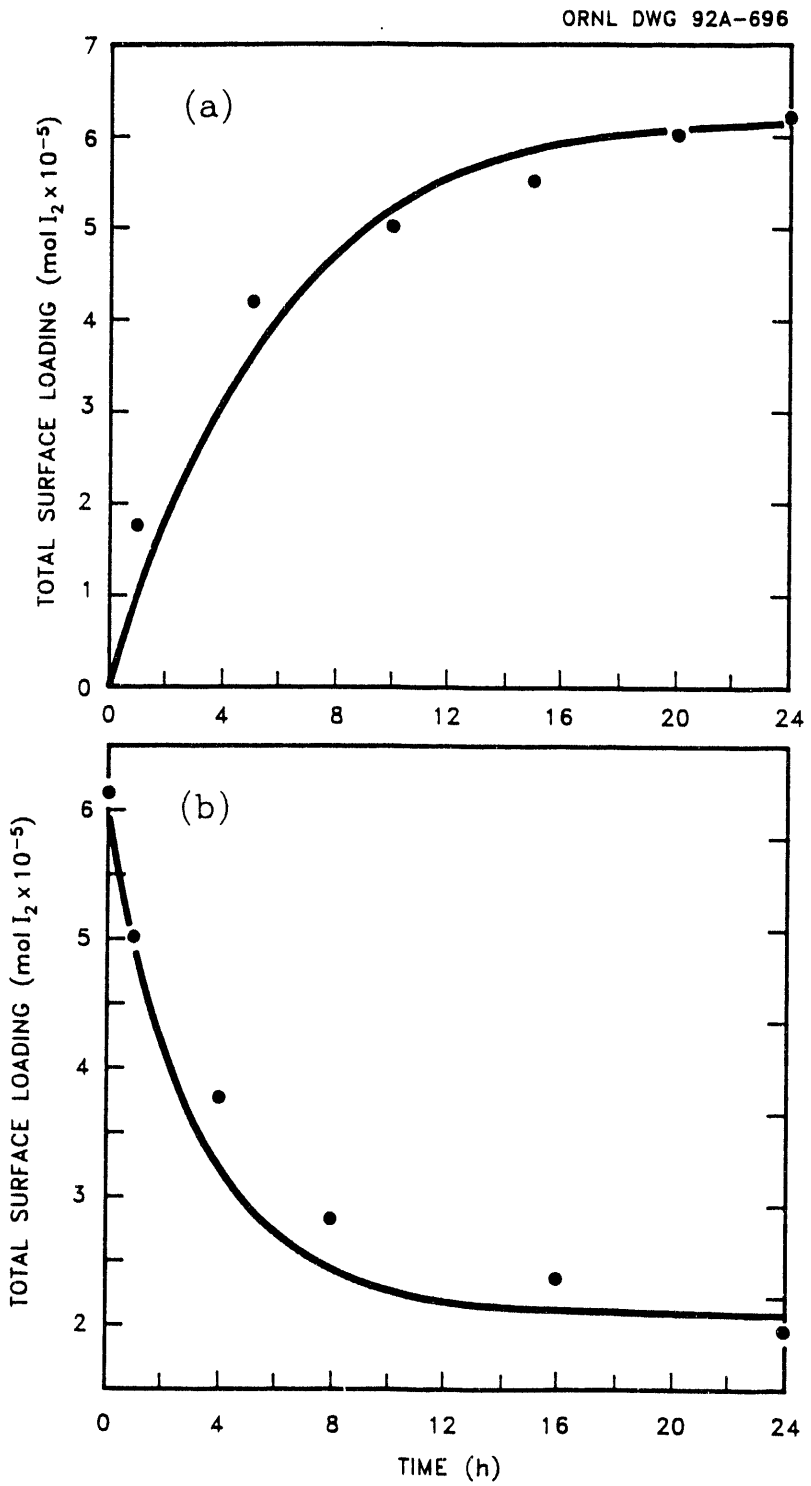

Fig. 3. Comparison of model prediction and data for I_2 deposition onto VAM 1756-1 coating: (a) adsorption, (b) desorption.

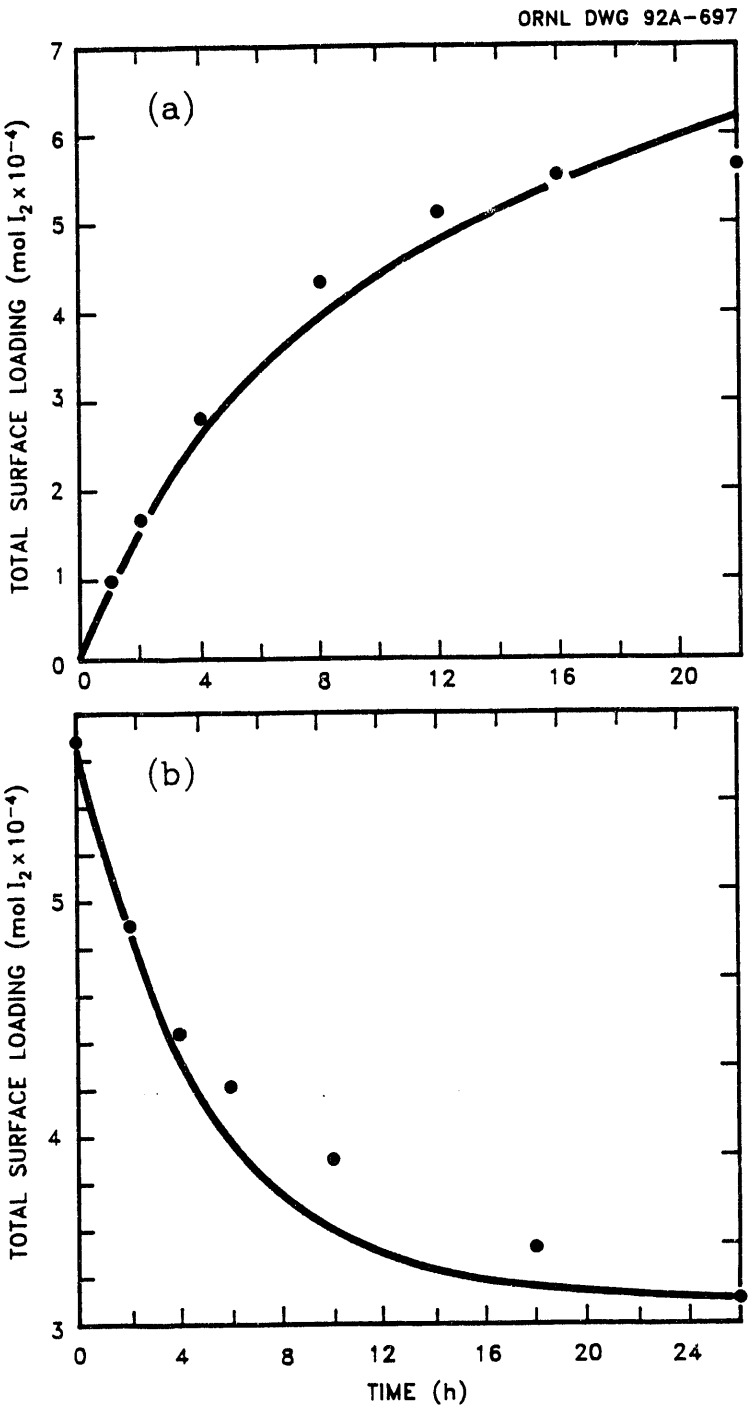

Fig. 4. Comparison of model prediction and data for I_2 deposition onto VAM 66-2 coating: (a) adsorption, (b) desorption.

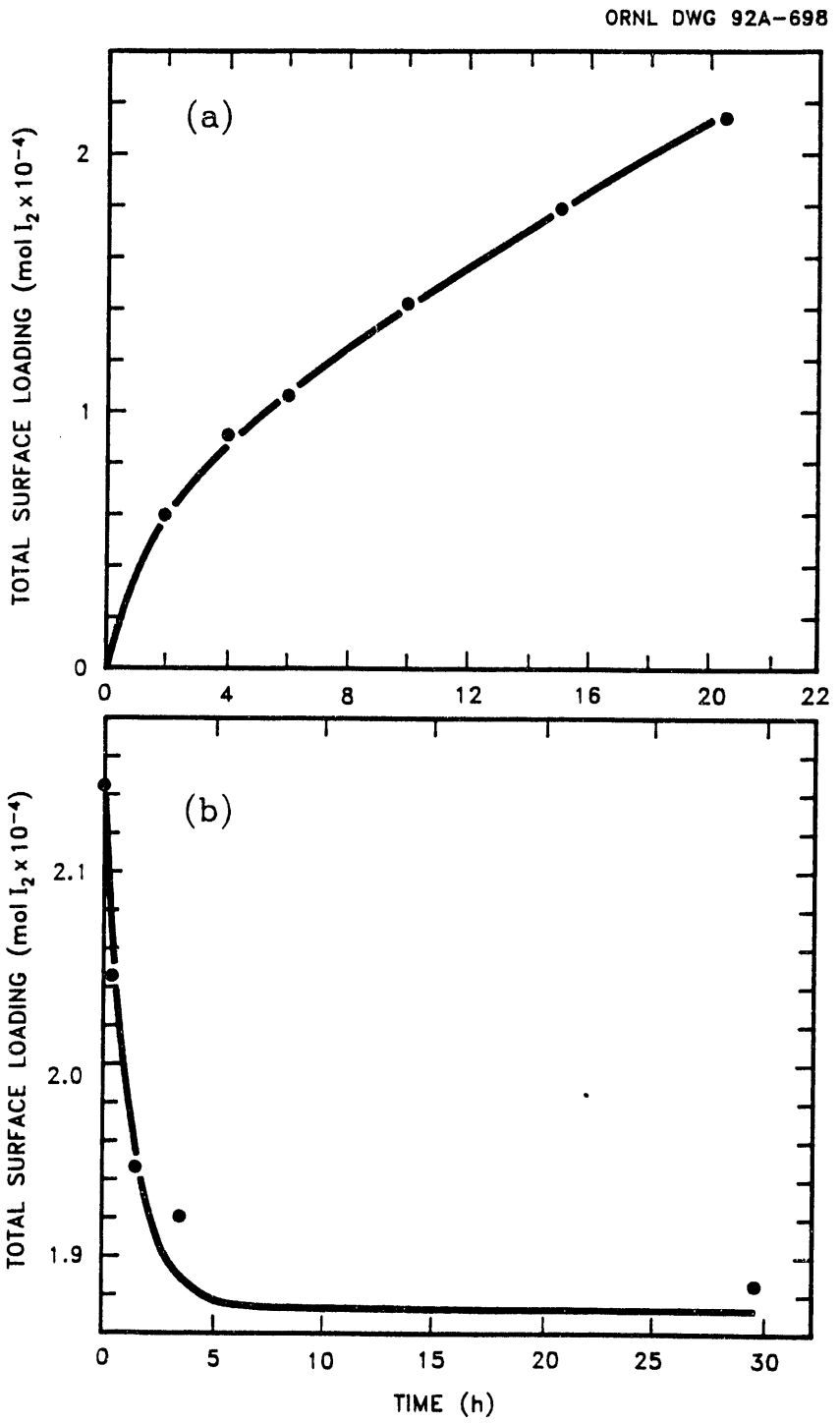

Fig. 5. Comparison of model prediction and data for I_2 deposition onto VP 302-3 coating: (a) adsorption, (b) desorption.

3. LIQUID-PHASE BEHAVIOR

Accident studies suggest that in most sequences substantial quantities of iodine may reside in water pools or sumps. Even if the initial releases into containment are airborne sources, spray water or condensing steam are likely to wash large amounts into system sumps. In this form, the iodine is largely immobile and therefore less hazard exists. However, there are several factors that could produce a reevolution of airborne iodine and a resurgent threat to atmospheric release. It is thus important to carefully consider aqueous behavior of iodine and the other substances which could reside in pools or sumps.

The principal concern is the aqueous speciation of iodine - does it form volatile species which might evaporate, or does it remain highly soluble? This question is evaluated with regard to thermal reactions with water itself in Sect. 3.1. The additional complications posed by irradiation are the subject of Sect. 3.2. Both of these processes are highly dependent on the water pH; an accurate means of calculating this important quantity is described in Sect. 3.3. Interaction with suspended silver aerosol, which may be significant in pressurized-water-reactor (PWR) accidents, is addressed in Sect. 3.4. And, finally, the liquid-phase formation of organic iodides is described in Sect. 3.5.

3.1 HYDROLYSIS

In pure water, I_2 hydrolyzes to form I^- and IO_3^- through processes that can be described by the overall reaction

$$3I_2 + 3H_2O \rightleftharpoons 5I^- + IO_3^- + 6H^+ . \tag{20}$$

At equilibrium, only I^-, I_2, and IO_3^- exist as stable end products (occupying oxidation states -1, 0, and 5, respectively). However, during the transient reaction phase, various intermediate species have been suggested to occupy oxidation states 1, 2, 3, and 4, the most popular being HOI, OI, HIO_2, and IO_2, respectively. In addition, several reaction progressions involving these have been suggested. Although some investigators claim to have measured certain of these intermediates,[33] their involvement in hydrolysis reactions and even their existence remains open to speculation.

The most popular model of iodine hydrolysis is the two-stage reaction[34-36]

$$I_2 + H_2O \rightleftharpoons HOI + I^- + H^+ \tag{21a}$$

$$3HOI \rightleftharpoons IO_3^- + 2I^- + 3H^+ . \tag{21b}$$

The first reaction is usually quite rapid, while the second step is much slower under many pH and temperature conditions.[34] It is unlikely that this actually occurs in a single reaction step; rather, Eq. (21b) is viewed as the result of several reaction subprocesses. This formulation is capable of predicting conversion of I_2 to I^- or IO_3^- in certain limited circumstances.[35] The principal deficiencies are (1) the semi-empirical form of the second equation, and (2) the lack of applicability (and rate coefficients) at higher temperatures.

Several researchers have developed complicated models to describe iodine radiolysis. These models include reactions between many different iodine species and the free radicals that result from irradiating water. Basic hydrolysis processes (the aqueous iodine reactions that would occur in the absence of radiation) are also included, since they would occur simultaneously. These can be extracted and used by themselves under conditions in which radiolysis is not significant. Two such formulations[37,38] include the following reversible steps to model the overall reaction:

$$I_2 + H_2O \underset{k_2}{\overset{k_1}{\rightleftharpoons}} I^- + HOI + H^+ \tag{22a}$$

$$2HOI \underset{k_4}{\overset{k_3}{\rightleftharpoons}} I^- + HIO_2 + H^+ \tag{22b}$$

$$HOI + HIO_2 \underset{k_6}{\overset{k_5}{\rightleftharpoons}} I^- + HIO_3 + H^+ . \tag{22c}$$

Values for the rate constants at 25°C are given in Table 4 and include several values that have been estimated but not measured directly. As seen in the table, there is considerable variation between different researchers. Recent data taken at ORNL were used to revise the estimates of these rate constants and to investigate other reaction schemes as well. It was concluded that Eqs. (22a,b,c) do represent an adequate description of aqueous iodine reactions, although the parameters given in refs. 37 and 38 were inadequate for modeling these data. Using a nonlinear optimization procedure,[27] revised values for these rate coefficients were obtained and are also given in Table 4. Also shown are activation energies, corresponding to the rate coefficients determined at ORNL. The data used and the optimization process are described in greater detail in Appendix C.

Also included in the model are the dissociation equilibrium,

$$K_a = \frac{[H^+][IO_3^-]}{[HIO_3]} , \tag{23a}$$

Table 4. Parameters for iodine hydrolysis model

Parameter	Rate coefficients at 25°C[a]			Activation energy (kJ/mol)
	Ref. 37	Ref. 38	ORNL	
k_1	0.054	31	44.6	68
k_2	5.87×10^{12}	3.5×10^{15}	4.7×10^{14}	0
k_3	10^5	10^{10}	1.3×10^6	175
k_4	5×10^6	10^{10}	5.1×10^{11}	53
k_5	3	2.3×10^5	6.6×10^6	5
k_6	1800	3.7×10^{-5}	1.2×10^8	5

[a]Units are s^{-1} for k_1, $M^{-1}s^{-1}$ for k_3 and k_5, $M^{-2}s^{-1}$ for k_2, k_4, and k_6.

and the side reaction,

$$I^- + I_2 \underset{k_8}{\overset{k_7}{\rightleftharpoons}} I_3^- \,. \tag{23b}$$

The equilibrium constant is well characterized by the form[39]

$$\log_{10} K_a = -657.45/T + 21.589 - 8.158 \log_{10} T \,,$$

while the rate constants are reliably known at 25°C:[40]

$$k_7 = (6.2 \pm 0.8) \times 10^9 \ M^{-1} \ s^{-1}$$
$$k_8 = (8.5 \pm 1.0) \times 10^6 \ s^{-1} \,.$$

Although activation energies are not available from direct experimental measurement, k_7 is near the diffusion controlled limit; hence, an activation energy of 15 to 20 kJ/mol is not unreasonable. From the equilibrium constant for this reaction,[39] it can be determined that

$$E_8 - E_7 = 17.4 \text{ kJ/mol} \,,$$

valid within the range 0 to 100°C. Even though this is an approximation, Eq. (23b) is not usually a major factor in reactor accident calculations; thus, it should suffice.

3.2 RADIOLYTIC CONVERSION OF I^- TO I_2

The task of describing aqueous iodine behavior under radiation conditions involves no less than the complete mechanistic evaluation of iodine in water, including hydrolysis, reverse hydrolysis, oscillatory mechanisms, and redox reactions. Studies of iodine behavior in water began more than 100 years ago. The primary difference between current and previous investigations is the availability of computers and routines for solving large systems of differential equations associated with reaction kinetics. However, the earlier investigators did not try to contend with the interaction of iodine species and the products of water radiolysis. In recent years, this problem was approached by performing experiments on the irradiation of aqueous iodine and setting up methods for solving a large set of differential equations (more than 100 in some cases) in an attempt to reproduce the experimental results by mechanistic simulation.

The practical problem to be considered is the extent of release of iodine from containments during reactor accident events and the ability to compute a realistic estimate of this quantity within the framework of existing accident analysis codes. To some extent, this puts limits on the range of conditions that must be evaluated. For example, the events of interest in a water pool will probably be restricted to a pH range between 3 and 9, since it is not likely that pH values outside this range will be attained in reactor accidents (with the possible exception of evaporation to dryness, which is not considered here; if this did occur, it is not difficult to predict what would happen by using experimental data on radiolysis effects and reverse hydrolysis). Other important parameters, such as temperature, iodine concentrations, and radiation dose rates, may also be delimited if we consider only the conditions of importance in reactor accidents.

Practical considerations also limit the conditions that *can* be evaluated. A useful model must not require information that is not available in normal accident sequence calculations. It must also be efficient, easy to understand and use, and accurately reflect available data. It is desirable to use mechanistic formulations as much as possible; however, empirical elements will no doubt be required as well.

Based on the results of experimental studies, we may summarize the formation of I_2 during the radiolysis of I^- as follows:

1. At $pH < 3$, virtually all iodine is converted to I_2; for $pH > 7$, only a tiny fraction is converted. For $3 < pH < 7$, conversion is highly variable (see Fig. 6).

2. For a given pH and temperature, there is a threshold radiation dose to the water, which, if exceeded, ensures that conversion will reach the steady-state value. If iodine is not added until this dose is reached, then steady-state conversion occurs very rapidly (within a few minutes). If dose is lower than the threshold value, then conversion will occur gradually until the steady state is reached.

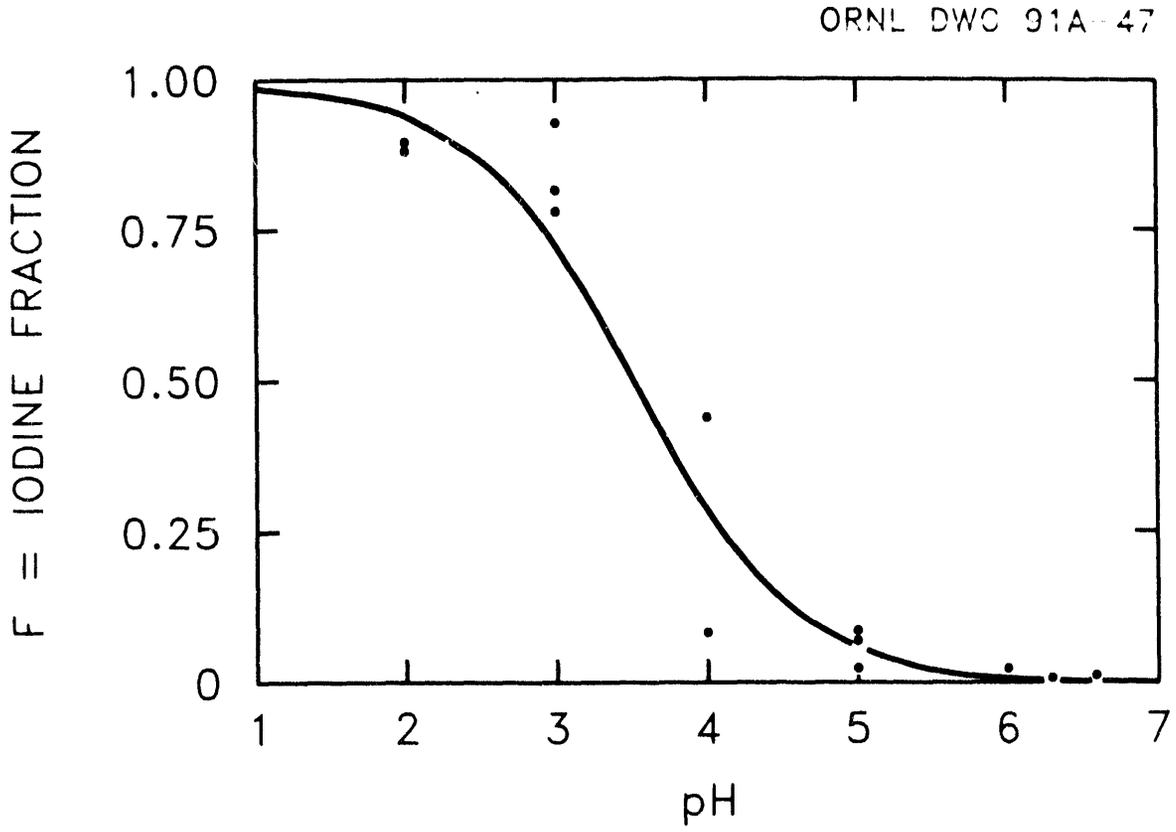

Fig. 6. Radiolytic conversion of I^- to I_2. *Source:* C. C. Lin, "Chemical Effects of Gamma Radiation on Iodine in Aqueous Solutions," *J. Inorg. Nucl. Chem.* **42**, 1101 (1980).

3. At very low aqueous iodine concentrations ($<10^{-6}$ g-atom/L) there is a tendency for iodate formation in the presence of irradiation and a tendency for iodine to show anomalous behavior in the absence of irradiation. Data in this region are less reliable, and, therefore, modeling results will exhibit greater uncertainty.

Our approach to the use of kinetic rate expressions is based on a narrowing of the problem to a range of parameters that are of practical interest and involves identifying the process(es) that determine the steady-state fraction of I^- converted to I_2 at a given pH. This approach was selected rather than using more than 100 individual reactions because many, if not most, of the rate constants in the large set of reactions must be estimated; as a result, large individual uncertainties would be propagated into the overall calculation.

3.2.1 Equilibrium Radiolysis

The plateau in fraction of I^- converted to I_2 implies that a steady-state process is reached during irradiation. During the irradiation of water, free radical products such as OH• or H• are present at very low concentrations (on the order of 10^{-10} *M* or less). However, hydrogen peroxide (H_2O_2) will increase to concentrations that are comparable to iodide concentrations in containment water pools (10^{-4} to 10^{-6} *M*). The concentration of H_2O_2 will depend on the radiation dose and on the extent of reaction with other species in solution, such as I^- or Cl^-.

Hydrogen peroxide reacts with both I^- and I_2 as follows:

$$2I^- + 2H^+ + H_2O_2 \rightarrow I_2 + 2H_2O ,$$

$$I_2 + H_2O_2 \rightarrow 2I^- + 2H^+ + O_2 .$$

These reactions generated much interest in the 1920s and 1930s. Abel[42] proposed a mechanism that gives the following steady-state relationship between I^-, I_2, and H^+:

$$\frac{[H^+]^2\,[I^-]^2}{[I_2]} = a + b\,[H^+] , \qquad (24)$$

where $[H^+]$, $[I^-]$, and $[I_2]$ are concentrations in mol/L (*M*) and *a* and *b* are constants to be determined. His experimental studies indicated that the reaction of I^- with H_2O_2 is first order in $[I^-]$ and in $[H_2O_2]$. These processes can be described by the rates $r_1 = k_1\,[I^-]\,[H_2O_2]$ and $r_2 = k_2\,[H_2O_2]\,[HIO] + k_3\,[H_2O_2]\,[IO^-]$. By definition, the steady state implies $r_1 = r_2$, that is,

$$k_1\,[I^-]\,[H_2O_2] = k_2\,[H_2O_2]\,[HIO] + k_3\,[H_2O_2]\,[IO^-]$$

or

$$k_1\,[I^-] = k_2\,[HIO] + k_3\,[IO^-] . \qquad (25)$$

The equilibria

$$I_2 + H_2O \rightleftharpoons H^+ + I^- + HIO \qquad (26)$$

and

$$HIO \rightleftharpoons H^+ + IO^- \tag{27}$$

are quite rapid, so we may substitute for HIO and IO^- as follows:

$$[HIO] = K_1 \frac{I_2}{[H^+][I^-]}, \tag{28}$$

$$[IO^-] = \frac{K_2\,[HIO]}{[H^+]} = \frac{K_2 K_1\,[I_2]}{[H^+]^2\,[I^-]}, \tag{29}$$

where K_1 and K_2 are the equilibrium constants for Eqs. (26) and (27), respectively. Equations (28) and (29) may be substituted into Eq. (25) to give

$$k_1\,[I^-] = k_2 \cdot \frac{K_1\,[I_2]}{[H^+]\,[I^-]} + k_3 K_2\,\frac{K_1\,[I_2]}{[H^+]^2\,[I^-]} = K_1 \frac{[I_2]}{[H^+]^2 [I^-]}\,(k_3 K_2 + k_2\,[H^+]).$$

This can be rearranged to get

$$\frac{[H^+]^2\,[I^-]^2}{[I_2]} = \frac{K_1}{k_1}\,(k_3 K_2 + k_2\,[H^+]), \tag{30}$$

which is in the form of Eq. (24), with

$$a = \frac{K_1 K_2 k_3}{k_1}, \qquad b = \frac{K_1 k_2}{k_1}. \tag{31}$$

The various rate and equilibrium constants have been measured at 25°C and are given in Table 5.

Data at higher temperatures are sparse and sometimes inconsistent. Some additional experimental evidence reveals that the conversion of I^- to I_2 decreases with increasing temperature. Tests of Burns et al.[47] on irradiation of 1×10^{-4} g-atom I^-/L solutions, gave 45% conversion to I_2 at 30°C, but only 10% conversion at 70°C.

A series of tests were run at ORNL at 92°C. In these tests, samples were taken by pressurizing the sample container during irradiation and thereby forcing a portion of the iodine solution up a narrow tube and into isooctane. With this technique, the sample was stripped of I_2 only a few seconds after it left the irradiation zone. With initial iodide concentrations of 1×10^{-4} g-atom I^-/L, at pH 4.0 the measured fraction as I_2 was 38.9%, and the model calculation gave 72.6%. At pH 5.0, the measured value was 3.1%, and the calculated value was 17.9%. Thus, the model tends to overestimate the extent of conversion to I_2 at temperatures >30°C. The two equilibrium constants, K_1 and K_2, can be given for temperatures in excess of 30°C, but

Table 5. Constants for radiolytic conversion

Parameter	Value	Reference
k_1	0.012 L/mol·s	43
k_2	37 L/mol·s	44
k_3	$(6.6 \pm 2.0) \times 10^7$ L/mol·s	45
K_1	4.77×10^{-13}	39
K_2	2.31×10^{-11}	46
a	$(6.05 \pm 1.83) \times 10^{-14}$	Eq. (31)
b	1.47×10^{-9}	Eq. (31)

at this time, there is no good representation of the rate constants k_1, k_2, and k_3 at these temperatures; so it is recommended that the data for 25°C be used until such data are produced.

Table 6 gives measured values of the fraction of initial iodide that was converted to I_2 on irradiation, as well as the corresponding calculated values obtained from Eq. (24). Of the four sets of experimental data, the correspondence between calculated and experimental values is best for the data of Burns et al.[47] The worst model fit of experimental data was at pH 4.4 to 4.5 and an initial concentration of 1×10^{-5} g-atom I^-/L. In one case, Naritomi et al.[48] give 2.5% conversion at pH 4.4, and the calculated value was 18%. In the other case, the ORNL data give 42% conversion at pH 4.5, and the calculated value was 13.9%. It appears that the value of 2.5% at pH 4.4 and the 42% at pH 4.5 are not compatible with each other, and both may be somewhat in error. At a concentration of 5×10^{-5} g-atom I^-/L and pH 4.6, Burns et al. give a value of 30% conversion to I_2, and the calculated value is almost identical to this at 29.2%. Burns et al. noted that concentrations $<10^{-4}$ g-atom I^-/L gave scattered results. The comparison is also made in Fig. 7, where calculated values are plotted against data. Perfect correspondence is represented by the diagonal line. As seen in the figure, there is considerable scatter in the data, but the calculation fits as well as can be expected.

Table 6. Comparison of iodine radiolysis model with measured values at 25°C

Percent molecular iodine (I_2)				
pH	Concentration initial I^- g-atom/L	Measured	Calculated from Eq. (3)	Comments
4.6	1×10^{-4}	43.4 and 46.0	42.6	Burns et al.[47]
4.6	$\sim 5 \times 10^{-5}$	~30	29.2	(Data taken from curve in report)
5.6	1×10^{-4}	5.4 and 7.8	1.9	
6.6	1×10^{-4}	<0.01 and 0.017	0.021	0.2 *M* boric acid
3.0	1×10^{-4}	93.8	91.6	Lin[41] — pH not buffered
5.0	1×10^{-4}	8.0	17.9	and may have varied during
6.6	1×10^{-4}	1.7	0.021	irradiation. Initial value given 4.5 Mrad/h
4.4	1×10^{-5}	2.5	18.0	Naritomi et al.[48]
5.2	1×10^{-4}	12.3	9.4	
5.3	1×10^{-5}	0.33 and 0.63	0.73	
5.8	1×10^{-5}	0.16	0.08	
5.8	1×10^{-4}	1.2	0.79	
6.2	1×10^{-5}	0.038 and 0.15	0.013	
6.2	1×10^{-4}	0.49	0.13	
5.7	1×10^{-5}	0.16	0.13	
5.7	1×10^{-4}	3.7	1.2	
4.5	1×10^{-5}	42.0	13.9	ORNL data — 0.37 Mrad/h
4.7	6.67×10^{-5}	35.0	29.4	in 0.2 *M* boric acid
4.7	7.0×10^{-5}	34.0	30.2	
5.0	2×10^{-4}	18.8	27.8	

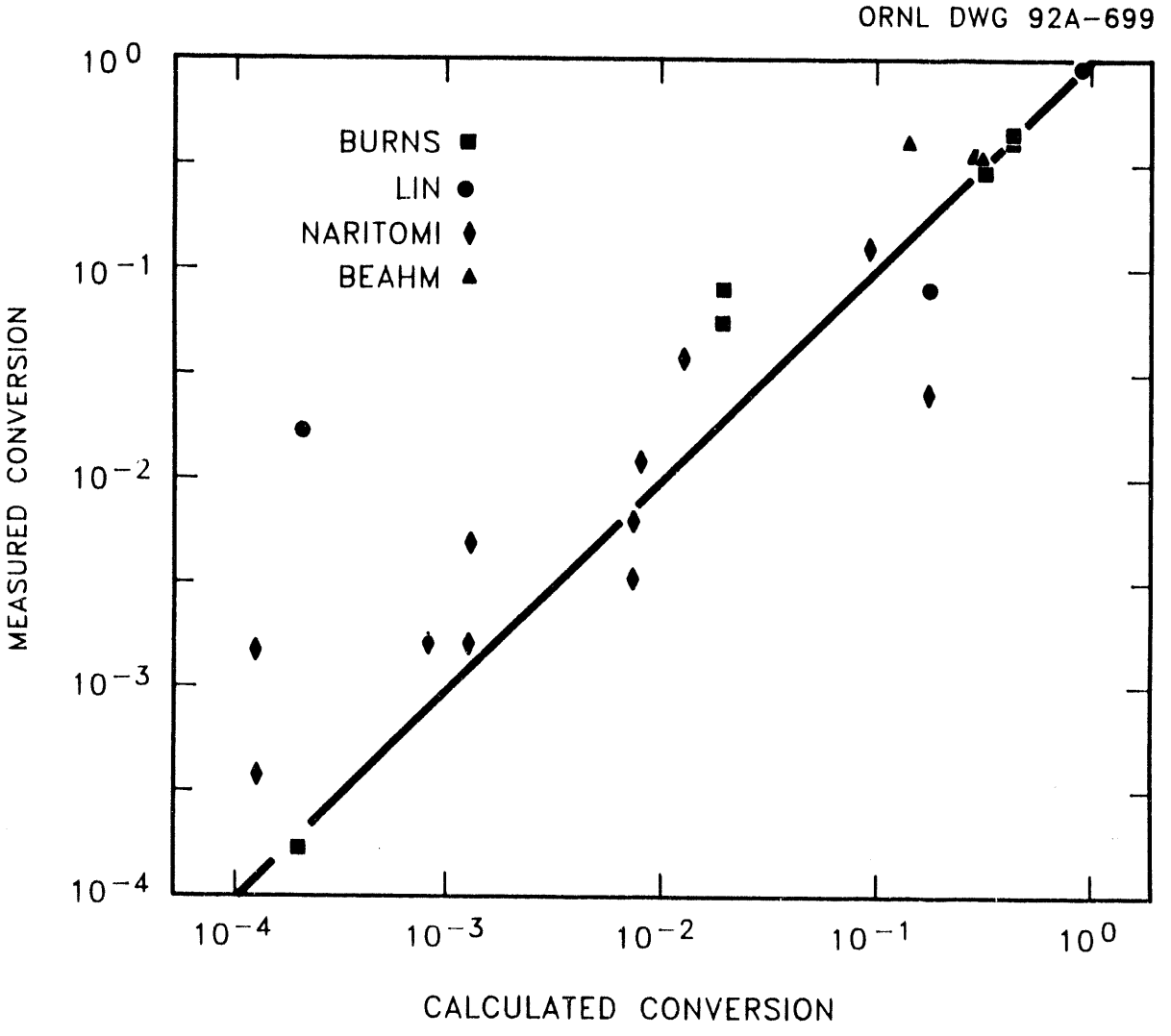

Fig. 7. Comparison of steady-state radiolysis model with data.

3.2.2 Transient Behavior

From Eqs. (30) and (31), it is possible to specify the equilibrium distribution of I_2 and I^-, given only the pH and the total iodine present:

$$[I_{TOT}] = 2[I_2] + [I^-]. \quad \text{(g-atom)}$$

As mentioned, the individual reaction steps depend on the presence of H_2O_2 to move toward equilibrium. In general, the equilibrium is attained quite rapidly, provided that H_2O_2 is present in sufficient excess, which is the case if irradiation occurs well before iodine addition. However, in many accident situations, iodine is likely to be the first fission product to enter water, and may even be its own primary radiation source. Hence, iodine conversion will occur as H_2O_2 is produced, creating a transient effect, depending solely on the production rate of H_2O_2.

The equations of Boyd, Carver, and Dixon[49] are widely accepted as the standard model for the simulation of water radiolysis. Using this set, the bulk H_2O_2 concentration was calculated under a variety of irradiation conditions, including a range of pH, dose rate, and dissolved O_2 concentration. The results of these calculations were then fit empirically to the following form:

$$[H_2O_2] = C_\infty(1 - e^{-\alpha \dot{d} t}), \tag{32}$$

where

$\dot{d}$ = dose rate (Mrad/h),

t = time (h),

$$\frac{1}{\alpha} = 9.549\text{E-}3 + 379.2\,[O_2] + \frac{[O_2]}{8.4E\text{-}4 + \exp(1.975\ \text{pH} - 13.87)},$$

$$C_\infty = 2.14\text{E-}4 + 46.1\,[O_2] + \left[\frac{1}{3E\text{-}4 + 201[O_2]} + \exp(3.02\ \text{pH} - 7.09)\right]^{-1},$$

$[O_2]$ = dissolved O_2 concentration (mol/L),

pH = $\log_{10}[H^+]$.

If not known exactly, the dissolved O_2 concentration can be estimated by assuming saturation in the liquid. Solubility data from *Lange's Handbook*[50] show a fairly linear relationship between 0 and 100°C, decreasing to 0 at 100°C. This relationship can be modeled by the regression

$$[O_2] = 1.863 \times 10^{-3} - 1.893 \times 10^{-5}\, T\,(°C), \tag{33}$$

which assumes 1 atm of pure O_2, and therefore should be adjusted proportionately for other O_2 pressures. The dose rate is determined from the inventory of radioactive species in the water as described in Weber.[51] The pH can be calculated using the model in Sect. 3.3. Thus, Eq. (32)

gives the time varying concentration of H_2O_2 under the irradiation conditions specified by pH, $\dot{d}$, and $[O_2]$. In this form, it does not reflect temperature dependence because many of the kinetic parameters in Boyd et al.[49] are known only at standard conditions.

We assume the steady state in Eq. (25) is reached instantly for sufficient concentration of H_2O_2. Every mole of I^- converted uses 2 mol of H_2O_2 [considering both forward and reverse steps in Eq. (25)], and produces 0.5 mol of I_2. Thus, the maximum conversion of iodide at any time is one-half of the available H_2O_2 (assuming that H_2O_2 is not involved in any competing processes). Then the distribution of iodine at any time t is given by

$$[I_2] = \min\{¼[H_2O_2], [I_2]_{eq}\} \qquad [I^-] = [I_{TOT}] - 2[I_2] ,$$

where $[H_2O_2]$ is calculated from Eq. (32) and $[I_2]_{eq}$ is the value calculated from Eq. (24).

3.3 DETERMINATION OF pH IN CONTAINMENT WATER POOLS

Results of various experiments have shown that solution pH is the major factor in determining the amount of I_2 and organic iodide formation in solution.[52] Numerous materials can influence pH in containment water pools during accident sequences, some of which are listed in Table 7. This list includes both acidic and basic materials, some present under normal operation, and some only occurring in accident conditions. For situations in which no chemical additives are present to control pH, the amounts of HI, cesium borate or hydroxide, and boron oxides reaching a sump will initially determine pH. In some sequences, the core-concrete interaction would produce aerosols that contain the basic oxides K_2O, Na_2O, and CaO. The influence of these oxides on pH will depend on the amount that has entered the water pool, the initial pH and buffering capacity of the solution, the quantity of water, and the extent of dissolution of the aerosol material. Further discussion of materials that could determine pH is given in ref. 53.

3.3.1 Nitric Acid Formation and pH Control

Water that is exposed to air absorbs CO_2 to form carbonic acid, which lowers pH to a limiting value of 5.65. In addition, irradiation of various organic materials (paints, cable insulation, lubricating oil, etc.) could create large quantities of HCl.[53] When deposited or washed into pools and sumps, it could significantly lower pH. Although it has not been investigated in great detail, this latter effect could be quite substantial.

An effect that has been measured is the creation of nitric acid by the irradiation of water and air. Table 8 shows the relationship between the formation of nitrate ions and hydrogen ions from the irradiation of an air-water system. Table 9 shows the decrease in pH for an irradiated solution that contained trisodium phosphate with an initial pH of 9.0. During the irradiation, nitric acid and atmospheric CO_2 decreased the pH as shown. Phosphate solutions have their

Table 7. Materials that affect pH in containment water pools

- Boron oxides (acidic)
- Basic fission-product compounds such as cesium hydroxide or cesium borates (basic)
- Iodine as HI (acidic)
- pH additives (basic)
- Atmospheric species such as carbon dioxide or nitric acid (acidic)
- Core-concentrate aerosols (basic)
- Pyrolysis products from organic materials (acidic)

Table 8. Concentrations of H^+ and NO_3^- in water due to irradiation[a]

Irradiation time (h)	$[H^+]$ from pH	$[NO_3^-]$ from ion electrode
6	3.2×10^{-5}	6.5×10^{-5}
12	6.3×10^{-5}	6.7×10^{-5}
22	1.0×10^{-4}	1.0×10^{-4}
65	2.5×10^{-4}	1.8×10^{-4}
114	5.0×10^{-4}	4.0×10^{-4}

[a]100 mL in closed 200-mL container at rate of 0.6 Mrad/h.

Table 9. Effects of irradiation dose[a] on pH in trisodium phosphate solution

Time (h)	pH
0	9.0
4	6.4
7	6.5
23	6.5
41	4.7
63	3.9

[a]Dose rate = 0.53 Mrad/h.

maximum pH buffer capacity at a pH near 7. This buffer capacity is reflected here in the length of time that the pH remained near 6.5. Once the buffer capacity was exceeded, the pH continually decreased.

In a reactor accident, if the pH level is not deliberately controlled using additives, it may decrease sufficiently through radiolytic generation of nitric acid to allow considerable conversion of I^- to I_2. If the pool is neutral initially, then this effect soon dominates, resulting in

$$[H^+] = 10^4\, g(HNO_3)\, \frac{E_{dep}}{V_L N_a}\,, \tag{34}$$

where

$[H^+]$ = concentration of H^+ (mol/L),
$g(HNO_3)$ = rate of HNO_3 production due to irradiation (molecules/100 eV),
E_{dep} = total energy deposition due to fission-product decay (MeV),
V_L = volume of water (L),
N_a = 6.022×10^{23} (molecules/mol).

The quantity E_{dep} can be determined (see Weber[51]) from inventories of fission products in the water, which must be calculated. The volume of water also must be available from accident sequence computations. The data in Table 8 indicate that at 30°C,

$$g(HNO_3) = 0.0068 \text{ molecules/100 eV}\,. \tag{35}$$

This relationship is based on radiation absorption by the aqueous phase. The actual mechanism for the formation of nitric acid is not known and may occur in the aqueous phase, in the gas

phase, or at the gas-surface interface. A comparison is made between experimental g-values for water and air in Appendix D.

3.3.2 Model for Calculation of pH

With knowledge of any additives and all species likely to be present, the solution pH at equilibrium can be determined by finding the minimum free energy. Such an approach assumes that all reactions that determine pH can be well characterized and proceed very rapidly. Within the range of interest for iodide conversion ($3 < pH < 7$), this assumption is generally the case, as shown later by verifying calculations.

Free energy minimization in water pools is performed using the principal subroutine of the SOLGASMIX code,[54] which has been extracted for use in accident sequence calculations. The species included in the calculation of pH are listed in Table 10, in the order that they are indexed in the calculational routine.

Data for the free energies of formation of the borate and phosphate species were obtained from refs. 55 and 56, respectively. Free energy information for other species was obtained from the FACT system.[57] All free energy data were cast into a linear form, with the regression constants a and b given in Table 10,

$$\frac{\Delta G^o}{R} = a + b \cdot T \qquad (T \text{ in Kelvin}) , \tag{36}$$

where

ΔG^o = the standard free energy of formation,

R = the universal gas constant in energy units consistent with ΔG^o.

Activity coefficients for the aqueous ions were calculated from the Debye-Hückel expression,[58]

$$- \log_{10} \gamma_i = \frac{A z_i^2 \sqrt{I}}{1 + a_i^0 B \sqrt{I}} .$$

The quantities A and B are properties of water, and within our range of interest can be described by:

$$A = 1.133 \times 10^{-3}\, T + 0.1733$$
$$B = 1.663 \times 10^{-4}\, T + 0.2794.$$

Table 10. Species in pH calculation

Phase	Species	Free energy constants $a \times 10^{-4}$	Free energy constants b	Activity constant[a] $a^0 \times 10^8$
Gas	1. Ar	0.0	0.0	
	2. H_2O	-2.911	5.435	
	3. CO_2	-4.745	0.0	
Aqueous solution	4. H_2O	-3.429	19.324	
	5. H_3BO_3	-12.94	43.478	
	6. K^+	-3.037	-12.077	3
	7. $B(OH)_4^-$	-16.29	81.119	4
	8. NO_3^-	-2.557	40.862	3
	9. H^+	0.0	0.0	9
	10. OH^-	-2.835	31.602	3
	11. $B_2(OH)_7^-$	-29.15	122.258	3
	12. $B_3(OH)_{10}^-$	-42.38	170.451	3
	13. $B_4(OH)_{14}^{-2}$	-58.99	260.052	3
	14. HCO_3^-	-8.355	43.478	4
	15. CO_3^{-2}	-8.335	66.425	5
	16. H_2CO_3	-8.374	29.589	
	17. PO_4^{-3}	-15.66	113.929	4
	18. HPO_4^{-2}	-15.71	87.359	4
	19. $H_2PO_4^-$	-15.66	69.303	4
	20. Ca^{+2}	-6.538	-4.026	6
Solid precipitate	21. $Ca_3(PO_4)_2$	-49.1	90.741	
	22. $CaHPO_4$	-21.61	51.564	
	23. $Ca(H_2PO_4)_2H_2O$	-40.6	137.721	
	24. $CaO \cdot B_2O_3$	-24.32	43.082	
	25. $CaCO_3$	-14.51	31.602	
	26. CaO	-7.643	12.681	

[a]*Source:* H. E. Barner and R. V. Scheuerman, *Handbook of Thermochemical Data for Compounds and Aqueous Species*, Wiley, New York, 1978.

The constants a_i^0 are given for each ion of interest in the last column of Table 10. The ionic strength is given by

$$I = \frac{1}{2} \Sigma\, m_i\, z_i^2 ,$$

where z_i and m_i are the charge and molal inventory of the i^{th} ion, respectively. These inventories must be supplied by the user, considering the presence and transport properties of various additives and fission products.

In PWR containments where pH control chemicals are used, borate buffers, phosphate buffers, or a combination of the two are formed. The direct calculation of pH in these complex solutions is difficult because of the low hydrogen-ion concentrations (10^{-9} to 10^{-3} M) that are expected in water pools during severe accidents. In the process of computer calculation of equilibrium, the contribution of the hydrogen ion to the total free energy is very small. For this reason, hydrogen ion concentrations in borate and/or phosphate buffer systems are calculated from equilibrium expressions for the borate or phosphate species, after the free energy minimization. A comparison of calculated and measured pH values in these systems, given in Table 11, shows that this technique is quite effective in yielding good calculated values of pH. Such a comparison does not encompass the entire range of pH expected in possible accident sequences. However, to lower the pH below 5, the buffering effect of various additives must be overcome by addition of strong acid (such as HNO_3 or HI), which will dominate the pH calculation. In such cases, it is fairly simple to calculate pH. Hence, the comparisons in Table 11 represent a comprehensive demonstration that the calculational model is quite robust under a variety of possible conditions. Additional description of the calculational procedure is provided in Appendix E, in conjunction with a listing of the necessary input which must be supplied.

3.4 IODINE REACTIONS WITH SILVER

Iodine in water pools may interact with impurities in the water to produce chemical compounds or oxidation states that can alter its volatility. The water pool may contain dissolved minerals, such as iron or copper as ions, organic compounds, and also fission product and structural material aerosols. Silver could play an important role in determining the ultimate chemical form of iodine following a light-water-reactor (LWR) accident, especially in PWRs, where silver is a major component of the control rod alloy.

Silver in the presence of radiation has proven to be very effective in converting dissolved iodine species into silver iodide, which precipitates out of solution. Silver readily reacts with elemental iodine, even in the absence of radiation. Irradiation of solutions containing predominantly iodide ion or methyl iodide has also resulted in substantial conversion to silver

Table 11. Comparison of measured and calculated pH values

Amounts of materials (mol/m^3)						pH values		
NaOH	H_3BO_3	H_3PO_4	$NaHCO_3$	$Ca(OH)_2$	$Na_2B_4O_7$	Calc.	Expt.	Reference
2.61	50.0					7.8	7.8	60
16.3	50.0					8.7	8.8	60
40.8	50.0					9.5	9.8	60
55.7		50.0				6.0	6.0	ORNL
79.63		50.0				6.9	7.0	ORNL
96.8		50.0				7.9	8.0	ORNL
45.5	45.5	45.5				5.0	5.0	ORNL
50.76	44.9	44.9				6.0	6.0	ORNL
69.7	43.0	43.0				7.0	7.0	ORNL
83.7	41.6	41.6				7.9	8.0	ORNL
98.4	40.2	40.2				8.9	9.0	ORNL
			50.0			8.1	8.15	ORNL
				20.87		12.3	12.26	ORNL
		10.0		16.7		11.6	11.4	ORNL
					10.0	9.0	9.2	61
					10.0	8.4	8.8	61, at 95°C

iodide. The mechanism is thought to be conversion of I^- or CH_3I to I_2, and subsequent reaction of I_2 with silver:[59]

$$I^- \xrightarrow{\gamma} I_2 \qquad CH_3I \xrightarrow{\gamma} I_2 \tag{37a,b}$$

$$\tfrac{1}{2} I_2 + Ag \rightharpoonup AgI \; . \tag{38}$$

The conversion of aqueous iodine species to silver iodide has received scant attention in the literature, in spite of its potential importance in severe accident sequences. Several studies by Furrer and coworkers[59,62,63] have provided a good qualitative framework. They also mention forward and reverse rate constants for reaction (38) of 1 and 10^{-10}, although there is considerable uncertainty in these values, and they do not specify the form of the reaction rate

expression. Consideration of AgI for long-term storage of radioactive waste has motivated study of radiolytic dissociation and regeneration of I_2.[64] While the rate is evidently measurable, it is quite low, with only about 10^{-3}% dissociation after an exposure of 1200 Mrad. The forward reaction in Eq. (37) overwhelms the reverse reaction; hence, for all practical purposes, reaction (38) can be considered irreversible for severe accident calculations.

3.4.1 Reactions with Elemental Iodine

To obtain more quantitative estimates, a number of experiments were performed to evaluate the forward reaction in Eq. (38). In the absence of radiation, I_2 in solution was reacted with suspended silver in the form of a fine powder (BET surface area, 800 cm^2/g) or as part of aerosol material from a fission product release test.

The silver powder was reduced before each test by heating to 350°C in a 4% hydrogen-96% argon atmosphere. Varying amounts were then suspended in a well-mixed solution containing 1.2×10^{-4} mol/L of I_2 at room temperature (23°C). After a specified time, the AgI was filtered out and the remaining I_2 was reduced to I^- by the addition of NaOH and measured using an iodide electrode. The results of eight such experiments are given in Table 12 and show increasing conversion with time and silver concentration.

Table 12. I_2 reaction with Ag particles

Time (min)	Silver (mg)	Final I_2 (mol/L· 10^5)
15	35.6	4.31
30	35.6	2.99
45	35.6	2.36
60	35.6	0.91
120	35.6	0.54
15	178.0	0.38
30	17.8	5.34
30	10.0	6.13

Consistent with these data, Eq. (38) is modeled as irreversible and first order in concentrations of both iodine and silver. Defining the variables

$$C_1 = [I_2] \ (\text{mol/L}), \ \tilde{C}_2 = [Ag] \ (\text{mol/cm}^2), \ C_3 = [AgI] \ (\text{mol/L}) ,$$

we have the reaction rate expression,

$$\text{rate of reaction} = k C_1 \tilde{C}_2 \left(\frac{A}{V}\right) ,$$

where A and V represent the total surface area of particles (cm^2) and volume of solution (L). The surface concentration $\tilde{C}_2$ can be replaced by a volumetric concentration

$$C_2 = \tilde{C}_2 \left(\frac{A}{V}\right) , \tag{39}$$

which represents mols/L of silver on the surface of the particles (i.e., available to react easily). The reaction rate then becomes

$$-2\dot{C}_1 = -\dot{C}_2 = \dot{C}_3 = k C_1 C_2 , \tag{40}$$

and the extent of reaction is

$$C_3 = C_{20} - C_2 = 2(C_{10} - C_1) ,$$

where C_{10} and C_{20} are the initial concentrations of I_2 and Ag. Rewriting Eq. (40) only in terms of C_1 gives

$$-2 \dot{C}_1 = k C_1(C_{20} - 2C_{10} + 2C_1) ,$$

which can be integrated exactly to yield

$$\ln\left[\frac{C_{20} - 2(C_{10} - C_1)}{C_1} \cdot \frac{C_{10}}{C_{20}}\right] = \frac{1}{2}(C_{20} - 2C_{10}) k t . \tag{41}$$

Letting m denote the mass (g) of silver particles used, Eq. (39) can be rewritten

$$C_2 = \tilde{C}_2\left(\frac{\tilde{A}m}{V}\right),$$

where $\tilde{A}$ = 800 cm^2/g = BET surface area of particles. Substitution into Eq. (41) and rearrangement then gives

$$y = k\,x + \beta\,, \tag{42}$$

where $y \equiv \ln\left[\frac{C_{20} - 2(C_{10} - C_1)}{m\,C_1}\right]$, $x \equiv \frac{1}{2}(C_{20} - 2\,C_{10})t$, $\beta \equiv \ln\left(\frac{\tilde{C}_{20}\tilde{A}}{V C_{10}}\right)$.

The rate constant k is obtained from the slope of a linear regression of Eq. (42). The quantity $\tilde{C}_{20}$, representing surface concentration of reaction sites (mol/cm^2), is also obtained from the regression. However, since it is also required to calculate each y and x value, it must be obtained by trial and error. That is, successive values of $\tilde{C}_{20}$ are guessed and the regression performed. The initial value $\tilde{C}_{20}$ is then compared with $(V C_{10}/\tilde{A})e^{\beta}$; when they match, the calculation is complete. This procedure was performed for the data in Table 12, resulting in

$$k = 178.1\ min^{-1}\ M^{-1} = 2.969\ s^{-1}\ M^{-1}, \qquad \tilde{C}_{20} = 2.78 \times 10^{-6}\ mol/cm^2\,.$$

The regression line is plotted with the data in Fig. 8, showing a reasonable fit through most of its range. Furrer[59] notes that conversion changes very little with temperature, so the activation energy for reaction (38) is assumed negligible.

3.4.2 Radiolytic Conversion of Cesium Iodide

A number of tests were conducted in which a predominantly iodide solution was irradiated, using the silver powder described in the previous section.[65] In addition, a few experiments were performed using actual aerosol material with a high silver content. The experimental conditions and conversions achieved are shown in Table 13. This study was not as useful for mechanistic model development, because the radiolytic conversion to I_2 [cf. Eq. (37)] was also involved. However, it does give some indication of the applicability of mechanistic models in more realistic situations.

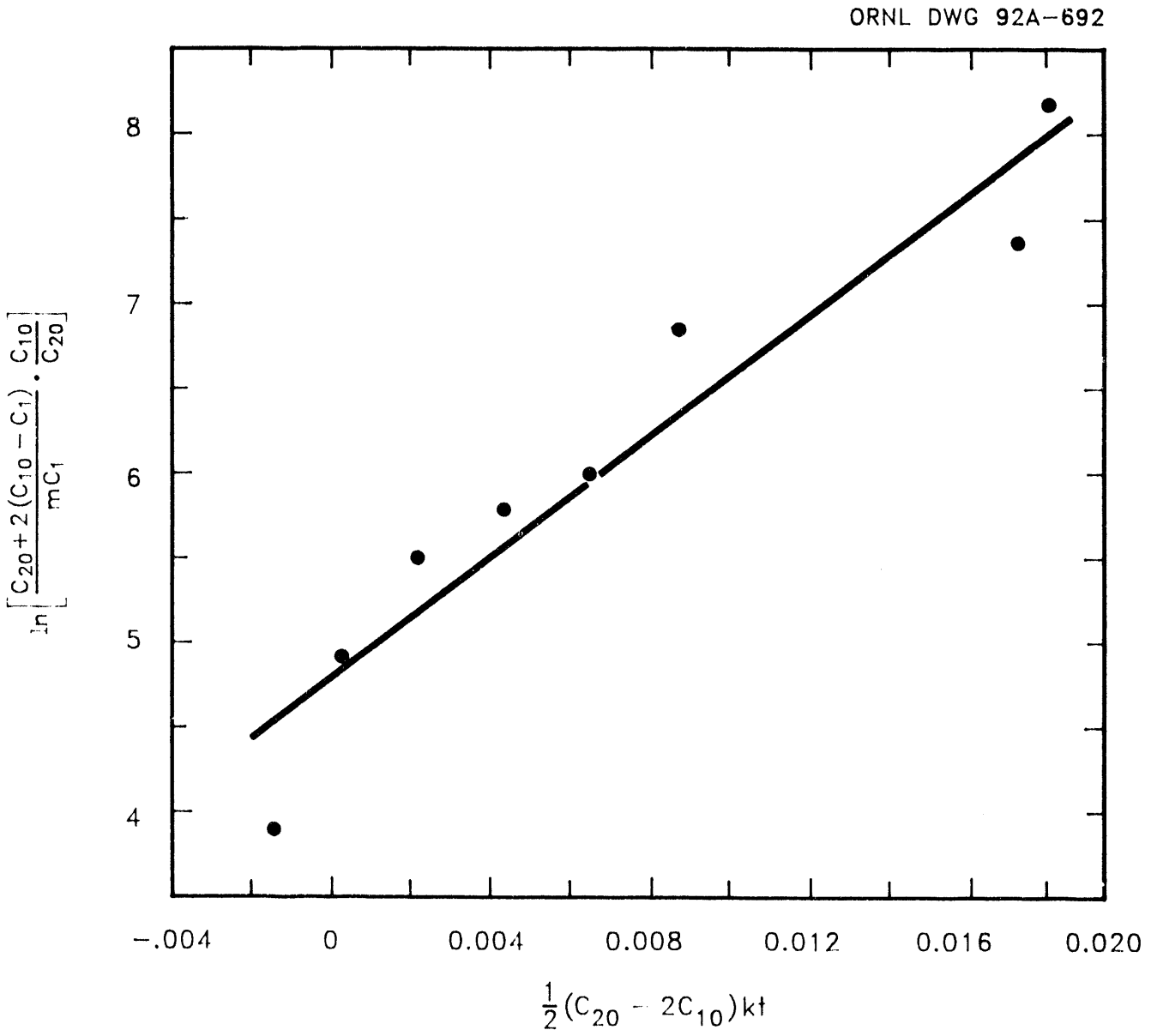

Fig. 8. I_2 conversion to AgI.

Table 13. Radiolytic conversion of I^-/I_2 to AgI[a]

Time (h)	Ag (mg)	Conversion (%)
1.2	3	14.9
1.2	5	19
1.2	5	19.8
1.2	10	23
1.2	10	20.5
1.2	10	42
20	10	82.7
1.2	22	58.8
1.2	28.5	56.2
1.2	35	99
1.2	50	91.7
1.25	30[b]	98

[a]Conditions: 50°C, pH = 6.0, dose rate = 0.83 Mrad/h; Volume = 10.2 ml, initial $[I^-] = 10^{-4}$ mol/L, initial $[I_2] = 10^{-6}$ mol/L.

[b]Material used is actual control rod aerosol from test HS-4. For further description, see M. F. Osborne, J. L. Collins, and R. A. Lorenz, *Highlights Report for Fission Product Release Tests of Simulated LWR Fuel,* ORNL/NRC/LTR-85/1, Martin Marietta Energy Systems, Inc., Oak Ridge Natl. Lab., Technical Letter Report to U.S. Nuclear Regulatory Commission, February 1985.

In order to simulate this situation, it is necessary to model both Eqs. (37) and (38). Even though the treatment of Eq. (38) is straightforward and simple (as done in the previous section), the radiolysis process in Eq. (37) involves many elementary reactions. These include the interactions of water radiolysis products with each other and with various iodine species, in addition to the thermal (hydrolysis) reactions of iodine in water. Some calculation schemes use empirical models to simulate the actual chemistry (e.g., the treatment in Sect. 3.2 and that of ref. 62), while others have proposed reaction sets which include over 100 reactions.[66-67] In the latter case, many of the intermediate species and their reactions are known very poorly and their rate constants must be estimated (or guessed!). Nevertheless, such models have been somewhat successful in estimating the macroscopic behavior of aqueous iodine/iodide solutions under

radiation. However, this is generally the case only at room temperature. Few of the activation energies in use are derived directly from experimental data; hence, at higher temperatures the performance of such models is unreliable.

In spite of the aforementioned uncertainties, one of the models[66] has been appropriated to compute the conversion of Eq. (37). This set of 120 reactions was solved simultaneously with the single reaction (38) in order to simulate each of the experiments in Table 13. The results are shown in Fig. 9, where the computed results are plotted against the corresponding experimental values. (A perfect match would lie on the diagonal line.) For a temperature input to the computations of 30°C, the computed solutions do match the experimental values quite well. However, at 20°C, the conversion is considerably overpredicted, and at 40°C it is underpredicted. At 50°C (the actual temperature of the experiments), the computed solution underpredicts conversion to AgI even further. This well illustrates the sensitivity of conversion to small concentration differences of I_2, as well as the difficulty of mechanistic models in simulating realistic scenarios. Similar sensitivities (and computational difficulties) are also encountered by varying pH or dissolved oxygen concentration.

In addition to the silver powder, iodide/iodine reactions with actual aerosol samples were investigated. The aerosol material was obtained from fission product release test HS-4, which was conducted on October 18, 1984, at ORNL.[68] This material contained 67% silver (by weight), along with other metals, including tin, iron, nickel, and chromium. It consisted of a fine black powder that remained suspended in the water during the test.

Because the reaction occurs on the particle surface, it is important to know the surface characteristics. Electron diffraction studies (see Fig. 10) indicated that most of the surface was silver, that is, the silver tended to condense on the surface or migrate to the surface, and is therefore available for reaction. It would be generally conservative to assume that silver was represented on the surface according to its mass fraction within the aerosol.

The experimental procedures and conditions using the HS-4 aerosol were the same as those employed for the silver powder, except that the aerosol was not reduced beforehand. As shown on the last line of Table 12, conversion to AgI was nearly complete in a very short time, exceeding the conversion using reduced silver powder. This is most likely due to the presence of oxide on the surface, since reaction of iodine with oxidized silver is much faster than the measured rate for Eq. (38).

3.4.3 Overall Model

Iodine in solution will react with any silver-containing aerosols that are washed into the reactor pool or sump. It is conservative (i.e., yields lower conversion of volatile I_2 to involatile AgI) to assume that (1) all silver is completely reduced, and (2) silver is represented on the surface according to its overall mass fraction in the aerosol. Then the conversion can be modeled by Eq. (38), with reaction rate in Eq. (40) and replacing A with Ax, where x is the mass

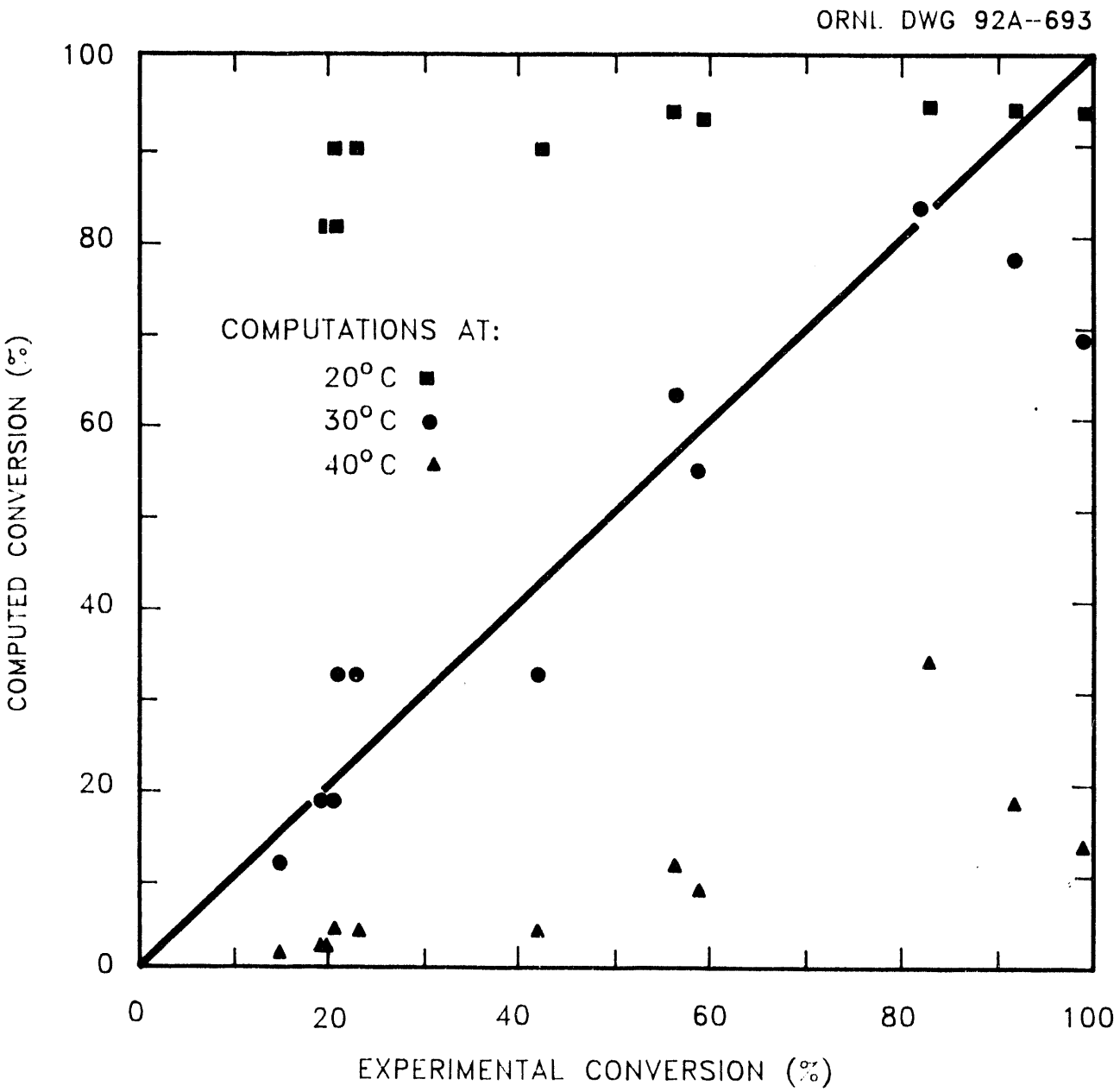

Fig. 9. Radiolytic conversion of I^- to AgI.

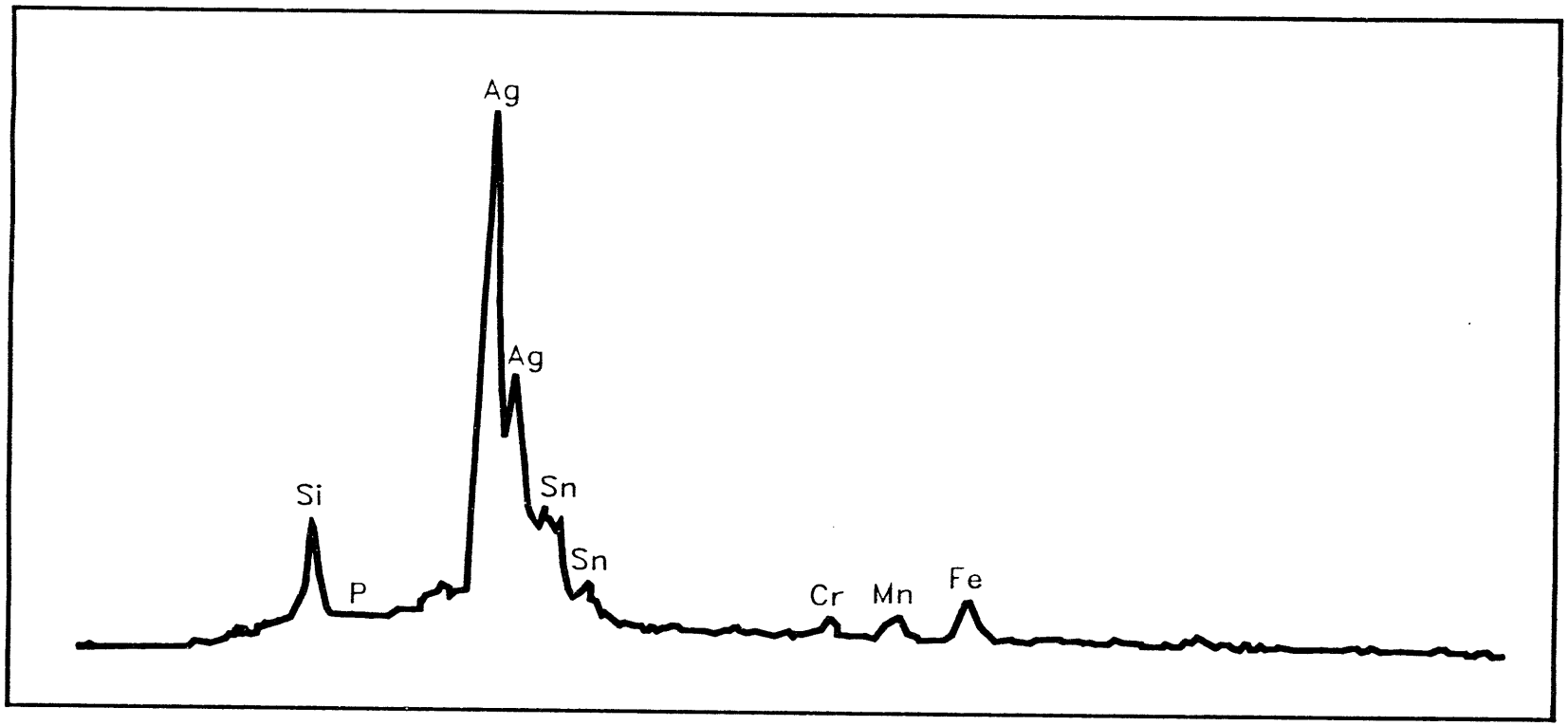

Fig. 10. Small particle overall surface.

fraction of silver in the aerosol. If other iodine species are present, it will also be necessary to simultaneously model their conversion to I_2 either by radiolysis [i.e., Eq. (37)], or hydrolysis in the absence of radiation (see Sect. 3.1).

3.5 ORGANIC IODIDE IN AQUEOUS SOLUTION

The model for the formation of organic iodides in aqueous solution will be based on methane as the initial organic material. The reactions to form methyl iodide are

$$CH_4\ (aq) + OH\ (aq) \xrightarrow{k_1} CH_3\ (aq) + H_2O\ , \tag{43}$$

$$CH_3 + I_2 \xrightarrow{k_2} CH_3I + I\ . \tag{44}$$

The hydroxyl radicals are also consumed by the side reaction:

$$OH + I^- \xrightarrow{k_3} I + OH^-\ .$$

If additional side reactions occur, then less OH is available for reaction (43), which implies less CH_3 is created. This in turn reduces the production of CH_3I in Eq. (44). Thus, it is conservative to assume no other significant side reactions are involved. Assuming also that the concentrations of the radical intermediates OH and CH_3 quickly reach their steady-state values, the concentration of CH_3 is then given by

$$[CH_3] = \frac{k_1[CH_4]}{k_2[I_2]} \cdot \frac{G(OH)}{k_1[CH_4] + k_3[I^-]}\ , \tag{45}$$

where G(OH) is the formation rate of OH radicals in the bulk liquid (molecules/100 eV). This quantity is largely independent of temperature and pH (within our ranges of interest). Values for this and other quantities appearing in Eq. (45) are given in Table 14.

The aqueous methane concentration is more difficult to obtain. The main source of aqueous methane is that produced in the gas phase by irradiation of organic materials (e.g., paint and cable insulation), and subsequently dissolved in water. For simplicity, equilibrium solubility between methane gas and aqueous methane is assumed and is given by

$$[CH_4] = P_{CH_4} \exp\left(\frac{847}{T} - 9.46\right)\ , \tag{46}$$

where P_{CH_4} is the methane pressure (atm).

Table 14. Constants for the aqueous formation of methyl iodide

Parameter	Value	Reference
k_1	1.1×10^8 $M^{-1}s^{-1}$	69
k_2	6.0×10^7 $M^{-1}s^{-1}$	70
k_3	1.1×10^{10} $M^{-1}s^{-1}$	69
G(OH)	2.70	69

Under high radiation fields, the value of P_{CH_4} will exceed the minimal value noted in Sect. 2, due to the formation of organic gases from the radiolysis of paints, cable insulation, and other organic materials in containments. Wing[71] has estimated the gas generation rate for generic conditions often found in commercial LWRs. Assuming that all paint is epoxy based (conservative, since other types do not produce gases as readily), and all cable has layers of Hypalon and ethylene propylene rubber as insulation, then the gas generation is determined by

$$R = \frac{10^6 \dot{E}_\gamma}{VN_A}[1 - \exp(-3.74 \times 10^{-5} r)](2.21\ G_P S_P + 4.79\ G_H S_H + 4.60\ G_R S_R)$$

$$+ \frac{10^5 \dot{E}_\beta}{VN_A}(4.98\ G_P S_P + 2.53\ G_H S_H + 1.83 \times 10^{-4}\ G_R S_R)\ , \qquad (47)$$

where

R = organic gas generation rate (mol/s),

$\dot{E}_\gamma, \dot{E}_\beta$ = energy release rates from γ and β radiation sources (MeV/s),

V = bulk gas volume (cm^3),

G_P, G_H, G_R = gas yield from radiation absorbed in paint, Hypalon, and rubber (molecules/100 eV),

S_P, S_H, S_R = total external surface areas of paint, Hypalon, and rubber (cm^2),

r = average distance from radiation source to absorbing organic material (cm),

N_A = 6.02×10^{23} molecules/mol.

The energy release rates, $\dot{E}_\gamma$ and $\dot{E}_\beta$, can be determined from the total fission-product inventories released into containment, as described in Weber.[51] The volume and surface areas must be determined or estimated from reactor data. The distance r can be approximated by the radius of a sphere whose volume equals that of the containment. Wing[71] estimates gas yields as follows:

$$G_P = 1.1 \qquad G_H = 0.15 \qquad G_R = 0.8 .$$

Assuming the methane is the only gas generated (conservative, since some of the gases will likely be nonvolatile), then Eqs. (45), (46), and (47) yield the concentration of CH_3, which forms CH_3I according to Eq. (44), with the following:

$$\text{Rate of aqueous } CH_3I \text{ formation} = k_2[CH_3][I_2] . \tag{48}$$

4. GAS-LIQUID INTERFACE TRANSPORT

4.1 IODINE TRANSFER RATES TO SURFACE WATER

Two models are used for the removal of gaseous iodine by dissolution in water, one of which dominates under conditions of heavy steam condensation, while the other (based on a mass-transfer analogy to heat transfer) applies to wetted wall conditions regardless of steam condensation rates. It is recommended that whichever model produces the highest transfer rate should be used.

4.1.1 Diffusiophoresis in Condensing Steam

Under condensing steam conditions, a strong mass flux toward surfaces is expected to enhance the removal of iodine vapor species into surface liquid. This phenomenon (diffusiophoresis) is modeled by the following equation:

$$\frac{dC_i}{dt} = - \frac{X_s}{X_s + X_a\sqrt{M_a/M_s}} \frac{QC_i}{V} , \tag{49}$$

where

C_i = concentration of depositing iodine specie (mol/cm^3),
X_s = mole fraction of steam in the containment atmosphere,
X_a = mole fraction of noncondensibles in the containment atmosphere,
M_s = molecular weight of steam,
M_a = average molecular weight of noncondensibles,
V = containment cell volume (cm^3),
Q = volumetric steam condensation rate onto surfaces (cm^3/s).

To derive this model, consider a solitary gas molecule (e.g., I_2) of radius R moving at constant velocity v_p through a stationary gas consisting of N moles/unit volume. In time Δt, the average number of collisions of the "moving" molecule with the "stationary" gas molecule would be expected to follow an expression like

$$\text{average number of collisions} \approx v\, \Delta t\, \pi R^2 N A_v , \tag{50}$$

where A_v is Avagadro's Number. We now assume that the stationary gas possesses a Maxwellian velocity distribution so that the average molecular velocity is given by

$$v = \sqrt{\frac{8kT}{\pi m}} ,$$

where m is the mass of the molecule. For each collision above, assume the change in momentum is given by

$$mv = m\sqrt{\frac{8kT}{\pi m}} ,$$

and, given the average number of collisions in Eq. (50), the total momentum exchange in time Δt is

$$\Delta(mv) \approx v\Delta t\pi R^2 N A_v m\sqrt{\frac{8kT}{\pi m}} = v\Delta t N R^2\sqrt{8kT\pi M A_v} ,$$

where M is the molecular weight of the stationary gas species. By Newton's Law, the average force experienced by the molecule as it moves through the stationary gas is given by

$$F = \frac{\Delta(mv)}{\Delta t} = vNR^2\sqrt{8kT\pi M A_v} .$$

In the case of steam condensation onto surfaces, the situation can be imagined to be as follows. The "flux" of steam carries noncondensible gases (air) with it toward the surface until a concentration gradient of the air is built up causing back diffusion of the air at a rate that exactly balances the amount of air carried by the steam flux so that, in actuality, the air is stationary. The steam also carries the third gas molecule (I_2) toward the surface by collisions between the steam and the molecule. However, the molecule also experiences collisions with the air tending to slow its motion down so that there is some net slip between the molecule velocity v_p and the steam velocity v_s. Therefore, the average force on the molecule due to collisions with the steam molecules is given by

$$F_s = N_s R^2(v_s - v_p)\sqrt{8kT\pi M_s A_v} .$$

In equilibrium, the force due to collision with air molecules will equal the force due to collision with the steam molecules so that

$$N_s R^2 (v_s - v_p)\sqrt{8kT\pi M_s A_v} = N_a R^2 v_p \sqrt{8kT\pi M_a A_v} ,$$

which is rearranged to get

$$v_p = \left[\frac{\sqrt{M_s}N_s}{\sqrt{M_a}N_a + \sqrt{M_s}N_s}\right] v_s . \tag{51}$$

Equation (51) represents the velocity at which iodine species are transported to the condensing surface relative to the steam condensation velocity. If all iodine is absorbed at the surface and no desorption takes place, then v_p represents a "deposition velocity" in the usual sense (i.e., as a first-order removal rate coefficient):

$$-\frac{dC_i}{dt} = \frac{v_p A C_i}{V} = \left[\frac{\sqrt{M_s}N_s}{\sqrt{M_a}N_a + \sqrt{M_s}N_s}\right]\frac{QC_i}{V} ,$$

which is equivalent to Eq. (49).

4.1.2 Natural Convection Mass Transfer

In the absence of diffusiophoretic forces, natural convection within each control volume should still promote considerable transfer of vapor species to surface water. Such a model would be in the form:

$$\frac{dC_t}{dt} = h_w (C_g - C_g^*) ,$$

where C_g^* is the equilibrium concentration, determined using the partition coefficient $P = C_g^*/C_l^* = C_g^*/(C_{TOT} - C_g^*)$. This implies that $C_g^* = C_{TOT}P/(P + 1)$, where $C_{TOT} = C_g + C_l$ is the total in both phases. The mass-transfer coefficient h_w is generally expressed in terms of the Sherwood number $Sh = h_w L/D$. A correlation in wide use has been derived by evaluating heat-transfer data and appropriating the mass-transfer analogy[72] to get

$$Sh = \begin{cases} 0.54\ (Sc\ Gr)^{1/4}, & Sc\ Gr < 10^8 \\ 0.14\ (Sc\ Gr)^{1/3}, & Sc\ Gr > 10^8 \end{cases} , \tag{52}$$

where

L = characteristic length of the surface,
D = binary diffusion coefficient,
Sc = $\mu/\rho D$ = Schmidt number,
μ = viscosity of containment atmosphere,
ρ = density of containment atmosphere,
Gr = $g\,\Delta\,T\,L^3\,\rho^2\,/T\,\mu^2$ = Grashof number,
ΔT = temperature difference between gas and wall,
g = acceleration of gravity.

All experimental surfaces were suspended in a free volume of much larger dimensions. Slight variations in the leading coefficients of Eq. (52) were noted in ref. 72 for different transfer geometries, although Lloyd and Moran[73] use it to correlate mass-transfer data for a number of geometrical shapes (their work suggests 0.16 as the leading coefficient for turbulent flow). They also mention data for horizontal surfaces surrounded by walls and point out that Eq. (52) remains a good prediction. These authors also indicate that the characteristic length can be represented in Eq. (52) by $L = A/p$, where A is the surface area and p is the perimeter. Note that Eq. (52) is used in the CONTAIN code[4] to describe natural convection heat transfer.

4.2 EVAPORATION OF VOLATILE IODINE SPECIES FROM WATER

Consider the problem of I_2 (and CH_3I) evaporation from a containment pool or sump to a gas space. This is generally modeled by assuming a two-film model:

$$\text{Flux across interface} = K(C_\ell - PC_g), \qquad \frac{1}{K} = \frac{1}{k_\ell} + \frac{P}{k_g}, \tag{53a,b}$$

where

k_ℓ, k_g = liquid and gas-phase film transfer coefficients (cm/s),
C_ℓ, C_g = bulk concentrations (mol/cm^3),
P = the equilibrium partition coefficient (inverse of Henry's Law Constant).

Hewison and Rodliffe[74] give a thorough discussion of the assumptions implicit in interphase transport modeling in general, and the two-film model applied to reactor accident situations.

The partition coefficient as used here pertains to mechanistic mass transport of individual species and is the inverse of the Henry's Law Constant. It should not be confused with the

overall partition coefficient representing all iodine species together, which is often used in safety studies. For the two principal volatile species, the following empirical forms have been determined:[75,76]

$$\text{(for } I_2\text{)} \qquad \log_{10} P = 6.29 - 0.0149\,T \qquad (T \text{ in Kelvin}).$$

$$\text{(for } CH_3I\text{)} \qquad \log_{10} P = -4.82 + 1597/T$$

For transfer in the gas film, Yuill et al.[77] suggest the following coefficients, derived for forced convection parallel flow over an immovable flat surface:

$$\frac{k_g L}{D} = \begin{cases} 0.664\ Re^{0.5}\ Sc^{0.33} & Re \le 2 \times 10^4 \\ 0.036\ Re^{0.8}\ Sc^{0.33} & Re > 2 \times 10^4 \end{cases}, \tag{54}$$

and assume no transfer resistance in the liquid (i.e., k_ℓ=0). The quantity $Re = Lv/T$ in Eq. (54) is the Reynolds number, where v is the velocity of one phase with respect to the other. Hewison and Rodliffe[74] also use Eq. (54) in the gas film and suggest Eq. (52) for the liquid-phase coefficient, which was derived from a natural convection correlation, driven by a temperature gradient in the liquid. One problem with this approach is that use of a forced convection correlation presupposes one-dimensional semi-infinite plane flow of known velocity. In situations where forced convective flow is known, Eq. (54) is appropriate, combined with an analagous correlation for the liquid, such as that of Cohen.[78] Otherwise, the natural convection correlations in Eq. (52) should be used for both air and water, as done for heat transfer in the CONTAIN code when water is warmer than air.

When air is warmer than water, natural convection should not occur, although other forces (e.g., venting) may still induce circulating flows. Without such flows, molecular diffusion would be the mechanism of equilibration. The CONTAIN code[4] uses a correlation for heat transfer in this situation and mass transfer analogy could be employed here as well:

$$Sh = 0.27(Gr\ Pr)^{0.25}\ . \tag{55}$$

This equation should be used with caution, however, since it is not well documented or compared with data.

Natural convection correlations [such as Eq. (52)] are usually derived for semi-infinite surfaces totally suspended in a large free volume. Even though considerable studies of natural convection in closed compartments have been made, we have not seen any geometry that matches the general situation expected in a containment, which should include (1) completely closed square or circular cylinder and (2) heated floor or cooled ceiling. Furthermore, the fluid-

fluid interface presents a different situation, since Eq. (52) was derived from experiments using a fluid-solid interface. And finally, all correlations (including those that assume a heat-mass transfer analogy) and almost all experiments concerning mass transfer assume that the driving force is a concentration gradient. In our situation, concentrations of fission-product species are expected to be so small (10^{-4} to 10^{-6} M) that negligible contributions to fluid circulation should result. Thus, we actually have *mass transfer* in natural convection driven by a *temperature* gradient. Very few studies have touched on this phenomenon, although Khair and Bejan[79] showed smaller mass transfer by an order of magnitude in a computer calculation of flow near a semi-infinite heated vertical surface. Thus, Eq. (52) is likely to be conservative, indicating much more evaporation than might actually occur.

4.3. ABSORPTION OF GASEOUS IODINE IN WATER SPRAYS

Numerous tests have indicated that containment sprays could significantly deplete airborne iodine concentrations during accident situations. However, the modeling of flow patterns, diffusion and reactions, is not well characterized even for a single droplet. Obviously then, the treatment of entire sprays systems will involve considerable assumptions and heuristics.

Virtually all modeling of iodine uptake in containment sprays has used the first-order rate equation

$$-\frac{dC}{dt} = \lambda C \,, \tag{56}$$

where C is the concentration of airborne iodine (all species), and λ is a removal rate coefficient, which has evolved through various semi-empirical forms. Postma and Pasadag[80] give a good review of early uses and provide a thorough assessment of the assumptions upon which Eq. (56) is based. Nearly half of these assumptions relate to the identifiability of conditions in containment (well mixed with known volume, density, viscosity, diffusivities, etc.) or to the characterization of spray operation itself (drops are well characterized by some average size and fall vertically a known (constant) distance at their terminal velocity). Obviously, such assumptions, based on reliable understanding of spray operations, need to be made by any model. A few of the assumptions deal with the applicability of certain correlations in establishing mass transfer coefficients which, again, must be done intelligently by any modeler. The remaining assumptions (nearly half of those listed in ref. 80) regard the heuristic treatment of iodine chemistry, particularly in regard to the partition coefficient. Their approach does not easily allow variation with temperature, concentration in gas and liquid, or the distribution of iodine species present. Although various improvements have been performed,[81] the treatment of iodine

chemistry in models widely employed (e.g., the CONTAIN code[4]) is still based predominantly on Eq. (56) as described above.

In calculating the removal rate constant λ, an overall partition coefficient is used to describe all iodine species simultaneously (not to be confused with the individual species partition coefficients used in Sects. 4.2 and 4.3.1), and thus is an empirical variable. For most applications, a value of 10^3 to 10^5 is suggested, depending on conditions in the spray water. A value of 10^5 gave excellent agreement with the Containment Systems Experiments (CSE),[80] although it was apparently chosen to achieve that result, rather than for mechanistic reasons. If conditions vary from those of the CSE, then predictions could be seriously in error. For example, safety studies on Browns Ferry identified fire sprinklers in the reactor building as a non-safety system, with possible implications in severe accidents.[82] These sprinklers use river water and produce larger droplets than typical reactor containment sprays. Foreign reactors also may vary, and even certain aspects of American reactors will produce departure from the basic patterns of the CSE.

It is possible to overcome many of the deficiencies described above with more rigorous treatment of iodine chemistry in both the droplets and the entire containment system. Albert et al.[83] suggested a model which retained some of the basic system assumptions of earlier work, but which treated iodine species individually and considered hydrolysis chemistry within the droplets. The present work builds on their effort, with improved aqueous chemistry models and the capability of calculating at any temperature. In contrast to Eq. (56), different iodine species are now treated separately, and the behavior of each is treated as simultaneous mass transfer with chemical reaction.

4.3.1 Mass Transfer to Droplets

The mass transfer of any individual specie from gas to liquid is described by the two-film model, as described in Sect. 4.2. To estimate the gas transfer coefficient, Postma et al.[81] have appropriated the correlation of Rantz and Marshall,[84] which was derived for heat transfer in flow past a single sphere.[85] Using a mass transfer analogy gives the following correlation, which is consistent with the heat transfer models in CONTAIN:[4]

$$Sh = \frac{k_g d}{D} = 2.0 + 0.60\, Re^{0.5} Pr^{0.33} , \qquad (57)$$

where

d = drop diameter,
D = diffusion coefficient for iodine specie in gas,
Re = dv/υ = drop Reynolds number,
Pr = υ/α = Prandtl number,

υ = kinematic viscosity of gas,
α = thermal diffusivity of gas,
ν = velocity of gas with respect to droplet.

Albert et al.[83] prefer a correlation by Clift et al.[86] which was derived specifically for freely falling droplets in air,

$$k_g = 0.83\left(\frac{\Delta\rho g}{\rho d}\right)^{0.25} \nu^{0.167} D^{0.67} , \tag{58}$$

where

g = acceleration of gravity,
ρ = density of gas,
$\Delta\rho$ = density difference between liquid and gas.

For the liquid transfer coefficient, Postma and Pasadag[80] describe the model of Griffiths[87] as the truncation of an infinite series for diffusion (the only mechanism) within a rigid spherical drop:

$$k_l = \frac{2\pi^2}{3}\frac{D_l}{d} , \tag{59}$$

where D_l is the liquid-phase diffusion coefficient for the iodine specie. This equation is reasonable for very small droplets, but is quite conservative for larger ones, where fluid circulation and drop deformation mix the fluid more quickly.[28]

In an effort to provide a more realistic model for the larger droplets usually encountered in containment sprays, Albert et al.[83] suggest

$$\frac{k_l d}{D_l} = \sqrt{\frac{4d\nu}{\pi D_l}} , \tag{60}$$

based on the penetration theory.

Both Eqs. (57) and (60) depend on the velocity of the gas with respect to the droplets, generally assumed to be the terminal velocity (see ref. 80, page 22, for a good discussion of the justifications and implications). Sherwood et al.[28] claim that as a first approximation, the terminal velocity can be represented by a correlation for hard spheres, up to drop diameters of 1 to 2 mm. Albert et al.[83] uses an empirical formulation from Clift[86] to estimate the drop Reynolds number, from which the terminal velocity is then obtained. The CONTAIN code[4] does much the same thing, although the Reynolds number formula is different.

To estimate the remaining material and transport properties, it is necessary to make standard assumptions. Diffusion coefficients can be obtained from well-known correlations by assuming pure binary systems of I_2, HI, or CH_3I in water and air (see ref. 28 or 85). Basic fluid properties can also be obtained from texts or reference materials for water and air.

4.3.2 Chemical Reactions Involving I_2

Most containment sprays are designed to be slightly basic because of the addition of NaOH; hence, considerable hydrolysis of I_2 is expected to occur. In some cases, water droplets may be neutral or acidic, as, for example, in fire spray systems or recirculating systems that have been neutralized over time. Thus, the thermal reactions of I_2 in water (hydrolysis) are important and must be modeled within droplets. The procedure is identical to that described in Sect. 3.1 for larger bodies of water and, hence, will not be repeated here.

During an accident, the containment may also be subject to considerable radiation doses. The effect on iodine speciation within droplets is not expected to be very great, however, because the average drop fall time (10 to 20 s) is much less than the time usually required for the buildup of H_2O_2, the primary reactant in iodine radiolysis. In situations where spray water is recirculated, this effect may be more important. If this is the case, the radiolysis model of Sect. 3.2 should be employed to give a nonzero H_2O_2 concentration, and subsequent reaction within droplets is modeled analogous to this phenomenon in a pool or sump.

4.3.3 Chemical Reactions Involving CH_3I

As with many organic compounds, organic iodides (of which CH_3I is the most likely airborne specie) are only slightly soluble in water. Certain additives have been used which can react with the CH_3I that does dissolve, enhancing the overall uptake. Even though sodium thiosulfate has been used in the past, it is no longer advisable because of a number of other complications. Hydrazine in basic solution is used in a few locations and should have some effect on gaseous CH_3I concentration.

Reactions with methyl iodide generally take the form

$$CH_3I + A \xrightarrow{k} I^- + \text{organic} ,$$

and thus are first order in the concentrations of both reactants. Hasty and his colleagues at Pacific Northwest Laboratory have measured and compiled the bimolecular reaction rate constants for several possible additives and impurities.[88-90] In particular, for reaction with hydrazine, they give

$$k = 0.0011 \ M^{-1}s^{-1} \text{ at } 25°C, \qquad E_a = 84.4 \text{ kJ/mol} .$$

5. SUMMARY AND APPLICATION

The models described in this work have been developed over nearly ten years, utilizing considerable experimental data from ORNL and elsewhere. The purpose has been to solidify understanding of iodine behavior in containments during reactor accidents to more accurately predict releases and consequences of severe accidents. In particular, the speciation of iodine in both gas and liquid phases has been addressed. Significant mechanisms of both volatilization and retention have been included.

As with any scientific endeavor, answers to old questions often pose new questions. Many uncertainties in iodine behavior still exist. Some of the rate coefficients given in this study represent only order-of-magnitude estimates. Some of the models are necessarily vague or overly dependent on empiricism, since underlying processes are still poorly understood. However, probably the greatest source of uncertainty lies in the assumptions and circumstances of the accident sequence itself. Given perfect information concerning reactor geometry, additives, event timing, operator action, etc., the underlying chemical processes can be reasonably calculated and iodine behavior predicted. But where can one expect a perfect description of chemical conditions within each control volume?

The purpose of this study has not been to predict what would happen in an accident, but rather to resolve many of the questions regarding chemical processes that might be influential. The assumptions and events of postulated accidents are not considered here. Neither are actual calculations or simulations of iodine behavior. Such computation would require considerable input from existing accident analysis codes (see refs. 2-4) in the form of temperatures, pressures, flow rates, sources released from primary system or fuel rubble, aerosol transport, and other parameters. Iodine transport models in various stages of development have been used selectively in this way for LWR studies,[91] experimental evaluation,[92] and a recent evaluation of accident sequences for the High Flux Isotope Reactor at ORNL.[93] In addition, there is some effort underway to include most, if not all, of these models as an iodine transport option in the CONTAIN code.[4] However, there has been no move to construct a comprehensive and readily accessible code containing all of these models for general safety applications.

REFERENCES

1. *Reactor Safety Study*, WASH-1400, U.S. Nuclear Regulatory Commission, October 1975.

2. R. O. Wooten, P. Cybulskis, and S. F. Quayle, *March 2 Meltdown Accident Response Characteristic Code Description and User's Manual*, NUREG/CR-3988 (BMI-2115), Battelle Columbus Laboratories, 1984.

3. R. M. Summers et al., *MELCOR 1.8.0: A Computer Code for Nuclear Reactor Severe Accident Source Term and Risk Assessment Analyses*, NUREG/CR-55341 (SAND90-0364), Sandia Natl. Lab., January 1991.

4. K. E. Washington et al., *Reference Manual for the CONTAIN 1.1 Code for Containment Severe Accident Analysis*, NUREG/CR-5715, Sandia Natl. Lab., July 1991.

5. H. S. Rosenberg, J. M. Genco, and D. L. Morrison, *Fission-Product Deposition and Its Enhancement Under Reactor Accident Conditions: Deposition on Containment-System Surfaces*, BMI-1865, Battelle Memorial Inst., 1969.

6. R. L. Bennett, R. Slusher, and R. E. Adams, *Reactions of Iodine Vapor with Organic Paint Coatings*, ORNL/TM-2760, Union Carbide Corp., Nucl. Div., Oak Ridge Natl. Lab., 1970.

7. A. K. Postma and R. W. Zavadoski, *Review of Organic Iodide Formation Under Accident Conditions in Water-Cooled Reactors*, WASH-1233, U.S. Atomic Energy Commission, 1972.

8. W. S. Durant, R. C. Milham, D. R. Muhlbaier, and A. H. Peters, *Activity Confinement System of the Savannah River Plant Reactors*, DP-1071, E. I. duPont de Nemours & Co., 1966.

9. R. L. Lemire, J. Paquette, D. F. Torgerson, D. J. Wren, and J. W. Fletcher, *Assessment of Iodine Behavior in Reactor Containment Buildings from a Chemical Perspective*, AECL-6812, Atomic Energy of Canada, Ltd., 1981.

10. D. Lillian, H. B. Singh, A. Appelby, L. Lobban, R. Arnts, R. Gumpert, R. Hogue, J. Toamey, K. Kananis, M. Antell, D. Hansen, and B. Scott, "Atmospheric Fates of Halogenated Compounds," *Environ. Sci. Technol.* **12**, 1042 (1975).

11. H. Behrens and A. G. Maddock, "The Exchange Reaction Between Iodine and Methyl Iodide," *J. Chem. Phys.* **22**, 1139 (1954).

12. E. C. Beahm, W. E. Shockley, and O. L. Culbertson, *Organic Iodide Formation Following Nuclear Reactor Accidents*, NUREG/CR-4327 (ORNL/TM-9627), Martin Marietta Energy Systems, Inc., Oak Ridge Natl. Lab., 1985.

13. R. P. Wichner et al., *SBLOCA Outside Containment at Browns Ferry Unit One*, NUREG/CR-2672, Vol. 2 (ORNL/TM-8119/V2), Union Carbide Corp., Nucl. Div., Oak Ridge Natl. Lab., 1983.

14. R. K. Hilliard and L. F. Coleman, *Natural Transport Effects on Fission Product Behavior in the Containment Systems Experiment*, BNWL-1457, Battelle-Pacific Northwest Lab., 1970.

15. R. Borkowski, *A Study of the Chemical Behavior of Methyl Iodide in Severe PWR Accidents*, Ph.D. Dissertation, University of Karlsruhe, November 7, 1985.

16. M. L. Brown, E. C. Beahm, and W. E. Shockley, *The Oxidation of Cesium Iodide in Stationary, Premixed Hydrogen Flames*, ACE-TR-B6 (ORNL/TM-1080), Martin Marietta Energy Systems, Inc., Oak Ridge Natl. Lab., June 1990.

17. W. C. H. Kupferschmidt et al., *The Effects of Steam on the Oxidation of Cesium Iodide Aerosol During Hydrogen Combustion*, ACE-TR-B8, AECL Research-Whiteshell Laboratories, October 1990.

18. A. C. Chamberlain, A. E. J. Eggleton, W. J. Megaw, and J. B. Morris, "Physical Chemistry of Iodine and Removal of Iodine from Gas Streams," *J. Nucl. Energy Parts A/B* **17**, 519-550 (1963).

19. W. J. Megaw and F. G. May, "The Behavior of Iodine Released in Reactor Containers," *J. Nucl. Energy Parts A/B* **19**, 585-595 (1965).

20. W. J. Megaw, "The Adsorption of Iodine on Atmospheric Particles," *J. Nucl. Energy Parts A/B* **19**, 585-595 (1965).

21. R. D. Spence and A. L. Wright, "The Importance of Fission Production/Aerosol Interactions in Reactor Accident Calculations," *Nucl. Technol.* **77**, 150 (1987).

22. A. M. Beard, C. G. Benson, B. R. Bowsher, *Fission Product Vapor-Aerosol Interactions in the Containment: Simulant Fuel Studies*, AEEW-R-2449, United Kingdom Atomic Energy Authority, Winfrith Technology Center, Dorchester, U.K., December 1988.

23. A. M. Beard, C. G. Benson, B. R. Bowsher, *The Interaction of Simulant Fission Product Vapours with Control Rod Aerosols in a Flowing System*, AEEW-R-2470, United Kingdom Atomic Energy Authority, Winfrith Technology Center, Dorchester, U.K., December 1988.

24. E. C. Beahm, M. L. Brown, and W. E. Shockley, *Adsorption of Iodine on Aerosols*, ORNL/TM-1079, Martin Marietta Energy Systems, Inc., Oak Ridge Natl. Lab., November 1990.

25. R. P. Wichner and R. O. Spence, "A Chemical Equilibrium Estimate of the Aerosols Produced in an Overheated Light Water Reactor Core," *Nucl. Technol.* **70**, 376 (1985).

26. D. A. Powers, J. E. Brockmann, and A. W. Shiver, *VANESA — A Mechanistic Model of Radionuclide Release and Aerosol Generation During Core Debris Interactions with Concrete*," NUREG/CR-4308 (SAND85-1370), Sandia Natl. Lab., Albuquerque, N.M., May 1985.

27. C. F. Weber, E. C. Beahm, and J. S. Watson, "Optimal Determination of Rate Coefficients in Multiple Reaction Systems," accepted for publication in *Comp. Chem.* (April 1992).

28. T. K. Sherwood, R. L. Pigford, and C. R. Wilke, *Mass Transfer*, McGraw, New York, 1975, p. 215.

29. J. B. Morris and B. Nicholls, *The Deposition of Iodine Vapour on Surfaces*, AERE-R4502, Atomic Energy Research Establishment, Harwell, U.K., March 1965.

30. J. F. Croft, R. S. Isles, and R. E. Davis, *Experiments on the Surface Deposition of Airborne Iodine of High Concentration*, AEEW-R265, Atomic Energy Research Establishment, Winfrith, U.K., June 1963.

31. J. M. Genco et al., *Fission Product Deposition and Its Enhancement Under Reactor Accident Conditions*, BMI-X-10186, Battelle Columbus Laboratories, Columbus, Ohio, January 1967.

32. F. H. Neill, *Adsorption and Desorption of Iodine on Mild Steel*, ORNL/TM-2763, Union Carbide Corp., Nucl. Div., Oak Ridge Natl. Lab., April 1970.

33. C. C. Lin, "Volatility of Iodine in Dilute Aqueous Solutions," *J. Inorg. Nucl. Chem.* **43**, 3229-3238 (1981).

34. T. R. Thomas, D. T. Pence, and R. A. Hasty, "The Disproportionation of Hypoiodous Acid," *J. Inorg. Nucl. Chem.* **42**, 183 (1980).

35. J. T. Bell, M. H. Lietzke, and D. A. Palmer, *Predicted Rates of Formation of Iodine Hydrolysis Species at pH Levels, Concentrations, and Temperatures Anticipated in LWR Accidents*, NUREG/CR-2900 (ORNL-5876), Union Carbide Corp., Nucl. Div., Oak Ridge Natl. Lab., 1982.

36. L. M. Toth, K. D. Pannell, and O. L. Kirkland, *The Chemical Behavior of Iodine in Aqueous Solutions up to 150°C*, NUREG/CR-3513 (ORNL/TM-8664), Martin Marietta Energy Systems, Inc., Oak Ridge Natl. Lab., 1984.

37. A. M. Deane, "Iodine Hydrolysis Reactions: Preliminary Species Identification and Rate Measurements," in *Proceedings of the Specialists' Workshop on Iodine Chemistry in Reactor Safety*, September 11-12, 1985, Harwell, U.K., AERE-R-11974, 1985.

38. D. J. Wren and J. Paquette, "The Kinetics of Iodine Release from Aqueous Solutions," in *Proceedings of the Specialists' Workshop on Iodine Chemistry in Reactor Safety*, September 11-12, 1985, Harwell, U.K., AERE-R-11974, 1985.

39. D. A. Palmer, R. W. Ramette, and R. E. Mesmer, "The Hydrolysis of Iodine: Equilibria at High Temperatures," *J. Nucl. Materials* **130**, 280-286 (1985).

40. D. H. Turner, G. W. Flynn, N. Sutin, J. V. Beitz, "Laster Raman Temperature-Jump Study of the Kinetics of the Triodide Equilibrium," *J. Amer. Chem. Soc.* **94(5)**, 1554-1559 (1972).

41. C. C. Lin, "Chemical Effects of Gamma Radiation on Iodine in Aqueous Solutions," *J. Inorg. Nucl. Chem.* **42**, 1101 (1980).

42. E. Abel, "Über das Reaktionspiel Zwischen Wasserstoffsuperoxyd, Jod und Jodion," *Z. Physik. Chim.* **136**, 161 (1928).

43. H. A. Liebhafsky, "The Catalytic Decomposition of Hydrogen Peroxide by the Iodine-Iodide Couple at 25°C," *J. Am. Chem. Soc.* **54**, 1792 (1932).

44. H. A. Liebhafsky, "The Catalytic Decomposition of Hydrogen Peroxide by the Iodine-Iodide Couple. II. The Rate of Oxidation, in Neutral Solution, of Hydrogen Peroxide by Iodine," *J. Am. Chem. Soc.* **54**, 3499 (1932).

45. H. Shiraishi et al., "Measurement of the Rate of Some Reactions Relevant to Iodine Chemistry in the Aqueous Phase," in *Proceedings of the Third CSNI Workshop on Iodine Chemistry in Reactor Safety*, Tokai-mura, Japan, September 11-13, 1991, NEA/CSNI/R(91)15, Japan Atomic Energy Research Institute, March 1992.

46. M. Eigen and K. Kusten, "The Kinetics of Halogen Hydrolysis," *J. Am. Chem. Soc.* **84**, 1355 (1962).

47. W. G. Burns, M. C. Kent, W. R. Marsh, and H. E. Sims, "The Radiolysis of Aqueous Solutions of Caesium Iodide and Caesium Iodate," AERE-R-13520, ACE-TR-B17, March 1990.

48. M. Naritomi, H. Nagai, S. Okagawa, and N. Ishiwatari, "Batch-Type Tests on Formations of Volatile Iodine Species from Aqueous Iodide Solution Under ^{60}Co γ-Rays Irradiation," *Proceedings of the Third CSNI Workshop on Iodine Chemistry in Reactor Safety*, Tokai-mura, Japan, September 11-13, 1991, NEA/CSNI/R(91)15, Japan Atomic Energy Research Institute, March 1992.

49. A. W. Boyd, M. V. Carver, and R. S. Dixon, "Computed and Experimental Product Concentrations in the Radiolysis of Water," *Radiat. Phys. Chem.* **15**, 177-185 (1980).

50. *Lange's Handbook of Chemistry*, 13th Edition, McGraw, 1985, p. 10-5.

51. C. F. Weber, *Calculation of Absorbed Doses to Water Pools in Severe Accident Sequences*, NUREG/CR-5808 (ORNL/TM-11970), Martin Marietta Energy Systems, Inc., Oak Ridge Natl. Lab., December 1991.

52. S. J. Wisbey, E. C. Beahm, W. E. Shockley, and Y. M. Wang, "Iodine Behavior in Containment Under LWR Accident Conditions," pp. 6-29 in *Proceedings of the Symposium on Chemical Phenomena Associated with Radioactivity Releases During Severe Nuclear Plant Accidents*, Anaheim, Calif., September 1986.

53. E. C. Beahm, *Iodine Evolution and pH Control*, ORNL/NRC/LTR-92/2, Martin Marietta Energy Systems, Oak Ridge Natl. Lab., February 1992.

54. G. Eriksson, "Thermodynamic Studies of High-Temperature Equilibriums. XII SOLGASMIX, A Computer Program for Calculation of Equilibrium Compositions in Multiphase Systems," *Chemica Scripta* **8**, 3 (1975).

55. R. E. Mesmer, C. F. Baes, Jr., and F. H. Sweeton, "Acidity Measurements at Elevated Temperatures. VI Boric Acid Equilibriums," *Inorg. Chem.* **11(3)**, 537 (1972).

56. R. E. Mesmer and C. F. Baes, Jr., "Phosphoric Acid Dissociation Equilibria in Aqueous Solutions to 300°C," *J. Solution Chem.* **3(4)**, 307 (1974).

57. FACT, a copyrighted product of THERMFACT Ltd., 447 Berwich Ave., Mount-Royal, Quebec, Canada, H3R 1Z8.

58. H. E. Barner and R. V. Scheuerman, *Handbook of Thermochemical Data for Compounds and Aqueous Species*, Wiley, New York, 1978.

59. M. Furrer and T. Gloor, *Einfluss von metallischem Silber und Sauerstoff auf die Radiolyse von Cäsiumiodidlösungen*, EIR-Bericht Nr. 620, Swiss Federal Institute for Reactor Research, Würlingen, May 1987.

60. *Lange's Handbook of Chemistry*, 13th Edition, McGraw, New York, 1985.

61. *Handbook of Chemistry and Physics*, 66th Ed., CRC Press, Boca Raton, Fla., 1985.

62. M. Furrer, R. C. Cripps, and E. Frick, *Iodine Severe Accident Behavior Code IMPAIR-2*, PSI-Ber, Paul Scherrer Inst., Villigen, Switzerland, 1989.

63. M. Furrer and T. Gloor, "Effects of β^-, γ Radiolysis on Cesium Iodide Solutions in Contact with Simulated Silver Metal Aerosol," pp. 193-199 in *Proceedings of the Specialists' Workshop on Iodine Chemistry in Reactor Safety*, September 11-12, 1985, Harwell, U.K., AERE-R-11974, Harwell Laboratory, January 1986.

64. K. H. Lieser, P. O. Coetzee, and M. Forster, "Liberation of Iodine from AgI During Radiolysis," *Radiochim. Acta.* **38**, 33-35 (1985).

65. E. C. Beahm, W. E. Shockley, C. F. Weber, S. J. Wisbey, and Y.-M. Wang, *Chemistry and Transport of Iodine in Containment*, NUREG/CR-4697 (ORNL/TM-10135), Martin Mariette Energy Systems, Inc., Oak Ridge Natl. Lab., October 1986.

66. R. A. Barton and H. E. Sims, "A Comparison of the Predictions of the INSPECT Reaction Set with Experimental Data," pp. 346-361 in *Proceedings of the Third CSNI Workshop on Iodine Chemistry in Reactor Safety*, Tokai-mura, Japan, September 11-13, 1991, ed. K. Ishigure, NEA/CSNI/R(91)15, Japan Atomic Energy Research Institute, March 1992.

67. J. C. Wren, N. H. Sagert, and H. E. Sims, "Modeling of Iodine Chemistry: The LIRIC Database," pp. 381-394 in *Proceedings of the Third CSNI Workshop on Iodine Chemistry in Reactor Safety*, Tokai-mura, Japan, September 11-13, 1991, ed. K. Ishigure, NEA/CSNI/R(91)15, Japan Atomic Energy Research Institute, March 1992.

68. M. F. Osborne, J. L. Collins, and R. A. Lorenz, *Highlights Report for Fission Product Release Tests of Simulated LWR Fuel*, ORNL/NRC/LTR-85/1, Martin Marietta Energy Systems, Inc., Oak Ridge Natl. Lab., Technical Letter Report to U.S. Nuclear Regulatory Commission, February 1985.

69. D. G. V. Buxton, C. L. Greenstock, W. P. Helman, and A. B. Ross, "Critical Review of Rate Constants for Reactions of Hydrated Electrons, Hydrogen Atoms, and Hydroxyl Radicals ($\cdot OH/\cdot O^-$) in Aqueous Solutions," *J. Phys. Chem. Ref. Data* **17**, 513 (1988).

70. J. K. Thomas, "Pulse Radiolysis of Aqueous Solutions of Methyl Iodide and Methyl Bromide. The Reactions of Iodine Atoms and Methyl Radicals in Water," *J. Phys. Chem.* **71**, 1919 (1967).

71. J. Wing, *Post-Accident Gas Generation From Radiolysis of Orgnaic Materials*, NUREG-1081, U.S. Nuclear Regulatory Commission, September 1984.

72. M. Fishenden and O. A. Saunders, *An Introduction to Heat Transfer*, Oxford University Press, London, 1950.

73. J. R. Lloyd and W. R. Moran, "Natural Convection Adjacent to Horizontal Surface of Various Planforms," *J. Heat Transfer* **96**, 443-447 (1974).

74. R. C. Hewison and R. S. Rodliffe, *Transfer of Volatile Species From a Pool of Water Into Air*, CEGB-TPRD/B/0889/R87, Berkeley Nuclear Laboratories, U.K.

75. E. C. Beahm, C. F. Weber, and T. S. Kress, *Iodine Chemical Forms in LWR Severe Accidents*, NUREG/CR-5732 (ORNL/TM-11861), Martin Marietta Energy Systems, Inc., Oak Ridge Natl. Lab., July 1991.

76. R. A. Hasty, "Partition Coefficient of Methyl Iodide Between Vapor and Water," *Can. J. Chem.* **46**, 1643 (1968).

77. W. A. Yuill, V. F. Barton, O. L. Condes, *Release of Radioiodine From Open Pools,* IN-1449, Idaho Nuclear Corp., December 1970.

78. Y. Cohen, "Mass Transfer Across a Sheared, Wavy, Air-Water Interface," *Int. J. Heat Mass Transfer* **26(9)**, 1289-1297 (1983).

79. K. R. Khair and A. Bejan, *J. Heat Transfer* **107**, 979-81 (1985).

80. A. K. Postma and W. F. Pasadag, *A Review of Mathematical Models for Predicting Spray Removal of Fission Products in Reactor Containment Vessels*, WASH-1329 (also UC-78 and BNWL-B-268), Battelle Pacific Northwest Laboratories, Richland, Wash. 99352, June 1973.

81. A. K. Postma, R. R. Sherry, and P. S. Tam, *Technological Bases for Models of Spray Washout of Airborne Contaminants in Containment Vessels*, NUREG/CR-0009 (PB288394), Benton City Technology, Benton City, Wash., October 1978.

82. S. A. Hodge et al., *Loss of DHR Sequences at Browns Ferry Unit 1—Accident Sequence Analysis*, NUREG/CR-2973 (ORNL/TM-8532), Union Carbide Corp., Nucl. Div., Oak Ridge Natl. Lab., May 1983; see also, R. P. Wichner et al., *Noble Gas, Iodine, and Cesium Transport in a Postulated Loss of Decay Heat Removal Accident at Browns Ferry*, NUREG/CR-3617 (ORNL/TM-9028), Martin Marietta Energy Systems, Inc., Oak Ridge Natl. Lab., August 1984.

83. M. F. Albert, J. S. Watson, and R. P. Wichner, "The Absorption of Gaseous Iodine by Water Droplets," *Nucl. Tech.* **77**, 161-174 (1987).

84. W. E. Ranz and W. R. Marshall, Jr., "Evaporation from Drops," *Chem. Eng. Prog.* **41**, 141-146, 173-180 (1952).

85. R. B. Bird, W. E. Stewart, E. N. Lightfoot, *Transport Phenomena*, Wiley, New York, 1960, p. 409-413.

86. R. Clift, J. R. Grace, and M. E. Weber, *Bubbles, Drops, and Particles*, Academic Press, New York, 1978.

87. V. Griffiths, *The Removal of Iodine from the Atmosphere by Sprays*, AHSB(S)R45, United Kingdom Atomic Energy Authority, London, 1963.

88. R. A. Hasty and S. L. Sutter, "Kinetics of the Reaction of Methyl Iodide with Sulfite and Thiosulfate Ions in Aqueous Solution," *Can. J. of Chem.* **47**, 4537 (1969).

89. R. A. Hasty, "The Rate of Reaction of Methyl Iodide and Hydrazine in Aqueous Solution," *J. Phys. Chem.* **73(2)**, 317 (1969).

90. L. C. Schwendiman, R. A. Hasty, and A. K. Postma, *The Washout of Methyl Iodide by Hydrazine Sprays*, BNWL-935, Battelle Memorial Institute, Richland, Wash., November 1968.

91. E. C. Beahm et al., *Calculations of Iodine Source Terms in Support of NUREG-0956*, ORNL/NRC/LTR-86/17, Martin Marietta Energy Systems, Inc., Oak Ridge Natl. Lab., Technical Letter Report to L. K. Chan (NRC), January 1987.

92. C. F. Weber and E. C. Beahm, *Pretest Calculations for the Radioiodine Test Facility in Support of the ACE Program*, ORNL/NRC/LTR-89/10, Martin Marietta Energy Systems, Inc., Oak Ridge Natl. Lab., Technical Letter Report to T. J. Walker (NRC), June 1989.

93. C. F. Weber and E. C. Beahm, *Iodine Transport During a Large Break LOCA in the Pipe Tunnel With Drainage Outside Confinement, Research Reactors Division*, C-HFIR-92-032, Martin Marietta Energy Systems, Inc., Oak Ridge Natl. Lab., October 1992.

94. J. H. Barrett and J. S. Bradley, *Ordinary Differential Equations*, Intext Educational Publishers, Scranton, Pa., pp. 209-257, 1972.

95. J. M. Genco et al., *Fission Product Deposition and Its Enhancement Under Reactor Accident Conditions*, BMI-X-10179, Battelle Columbus Laboratories, Columbus, Ohio, October 1966.

96. J. M. Genco et al., *Fission Product Deposition and Its Enhancement Under Reactor Accident Conditions*, BMI-X-10193, Battelle Columbus Laboratories, Columbus, Ohio, April 1967.

97. J. M. Genco et al., *Fission Product Deposition and Its Enhancement Under Reactor Accident Conditions*, BMI-X-10222, Battelle Columbus Laboratories, Columbus, Ohio, January 1968.

98. K. J. Laidler, *Chemical Kinetics*, Harper & Row, New York, 1987.

99. J. K. Linacre and W. R. Marsh, *The Radiation Chemistry of Heterogeneous and Homogeneous Nitrogen and Water Systems*, AERE-R10027, U.K. Atomic Energy Authority, Harwell, U.K., June 1981.

100. R. May, D. Stinchcombe, and H. P. White, *The Radiolytic Formation of Nitric Acid in Argon/Air/Water Systems*, AERE-R8176 (Rev. 1), U.K. Atomic Energy Authority, Harwell, U.K. (no date).

101. A. B. Chilton, J. K. Shultis, and R. E. Faw, *Principles of Radiation Shielding*, Prentice Hall, Englewood Cliffs, N.J., 1984.

APPENDIX A

KINETIC PARAMETERS FOR I_2 DEPOSITION ONTO STEEL SURFACES

Numerous studies have been performed to determine I_2 deposition onto steels, although the data are not always amenable to re-evaluation. Furthermore, most early experiments were designed to perform qualitative analyses, and are therefore not well suited for the quantitative determination of parameters for use in accident sequence simulations. In addition, there has been considerable variation in the approaches and assumptions, requiring that re-evaluation treat each set of data individually. Nevertheless, it is possible to glean sufficient information from previous work to supply reasonable values to the reaction parameters in Eq. (18).

A.1 DATA OF CROFT, ILES, AND DAVIS[30]

These researchers performed three adsorption experiments (with respective humidities of 85%, 65%, and 100%), each involving simultaneous deposition onto mild steel, concrete, paint, and other materials. A single gas-phase iodine release occurred within the first few minutes and was allowed to deposit while the gas concentration (and occasionally surface values) were measured at various time points. Desorption experiments were also performed by placing various samples in a well-ventilated room for several days. All experiments occurred at room temperature (20°C).

In order to model the reactions (18), we first assume (consistent with these data and others) that the chemisorbed iodine is irreversibly bound [i.e., $k_4 = 0$ in Eq. (18)]. Defining the variables

$$C_g = [I_2(g)], \qquad C_{pi} = [I_2(\text{physisorbed})], \qquad C_{ci} = [I_2(\text{chemisorbed})], \qquad i = 1,\ldots,N,$$

where the subscript i ranges over the different surface materials, Eq. (18) can be described by the equations

$$\dot{C}_g = -\left(\sum_{i=1}^{N} k_{1i}\right) C_g + \sum_{i=1}^{N} r_i k_{2i} C_{pi} \tag{A.1}$$

$$\dot{C}_{pi} = \frac{1}{r_i} k_{1i} C_g - k_{2i} C_{pi} - k_{3i} C_{pi} \qquad i = 1,\ldots,N, \tag{A.2}$$

$$\dot{C}_{ci} = k_{3i} C_{pi} \tag{A.3}$$

where k_{1i}, k_{2i}, and k_{3i} represent rate constants in Eq. (18) corresponding to surface material i. Note that the surface reaction rate does not depend on the concentration of deposited iodine or the number of surface sites available; this has been verified qualitatively in many experimental efforts. The quantity $r_i \equiv$ surface area/gas volume had a value for the current experiments on steel of $r_i = 3.026\ \text{cm}^2/\text{m}^3$.

A.1.1 Adsorption Step

Data for the adsorption at 85% humidity is given in Table A.1, calculated from Figs. 2 and 4 and Table 4 of ref. 30. The authors note that gas-phase concentration of I_2 is well described by the form

$$C_g(t) = A\,e^{-Bt}, \quad A = 3.54 \times 10^{-4}\ \text{mol/m}^3, \quad B = 5.33 \times 10^{-3}\ \text{min}^{-1}\ . \tag{A.4}$$

Using Eq. (A.4) allows exact integration of Eq. (A.2) for i = steel, which, in turn, allows integration of Eq. (A.3); dropping the subscript i, the resulting solutions are

$$C_p(t) = \frac{k_1}{r}\int_o^t C_g(\tau)\, e^{(k_2+k_3)(\tau - t)}\, d\tau = \frac{k_1 A}{r(k_2 + k_3 - B)}\left[e^{-Bt} - e^{-(k_2+k_3)t}\right] \tag{A.5}$$

$$C_c(t) = k_3\int_o^t C_p(\tau)\, d\tau = \frac{k_1 k_3 A}{r(k_2 + k_3 - B)}\left[\frac{(1 - e^{-Bt})}{B} - \frac{(1 - e^{-(k_2+k_3)t}}{k_2 + k_3}\right] \tag{A.6}$$

The sum of these two quantities represents the total surface iodine, corresponding to column 3 of Table A.1.

Table A.1. Data of Croft, Iles, and Davis[a] - adsorption of I_2 onto mild steel at 20°C

Time (min)	C_g (mol/m^3) × 10^4	C_s (mol/cm^2) × 10^6	P (min-mol/cm^2) × 10^3	k_1 (min^{-1}) × 10^5
0	4.4488	0	-	
20	3.1496	0.2197	2.215	9.916
100	2.0079	0.3638	8.981	4.050
500	0.2441	0.4538	19.21	2.362
1500	0.0031	0.4757	17.52	2.714
				Avg = 4.761

[a]*Source*: J. F. Croft, R. S. Isles, and R. E. Davis, *Experiments on the Surface Deposition of Airborne Iodine of High Concentration*, AEEW-R265, Atomic Energy Establishment, Winfrith, U.K., June 1963.

A.1.2 Desorption Modeling

Concerning desorption, the author's treatment is somewhat vague and inadequate for modeling purposes. The results are stated in terms of a mean desorption factor $\bar{\varphi}$, which is the average over a four-day period of the desorption factor

$$\varphi(t) = \frac{1}{C_s(0)} \frac{[C_s(0) - C_s(t)]}{t} . \qquad \text{(A.7)}$$

They state that this quantity undergoes a fourfold decrease over the four-day interval, which implies a decreasing trend not reflected in the average $\bar{\varphi}$. A desorption curve reflecting this behavior can be constructed at N time points by the form

$$\varphi(t_i) = f_i \, \varphi(t_N) \qquad i=1,...,N. \qquad \text{(A.8)}$$

The fractions f_i must satisfy

$$4 \geq f_1 > f_2 > \ldots > f_N = 1,$$

$$f_i t_i < f_{i+1} t_{i+1},$$

which can be combined to give

$$f_{i+1} < f_i < f_{i+1}\left(\frac{t_{i+1}}{t_i}\right) .$$

We now seek specific values for these fractions which satisfy the above restrictions. For $0 \leq \alpha \leq 1$, we have

$$f_i = \alpha f_{i+1} + (1 - \alpha) f_{i+1}\left(\frac{t_{i+1}}{t_i}\right) ,$$

which are rearranged to get

$$\frac{f_{i+1} - f_i}{t_{i+1} - t_i} = (\alpha - 1)\frac{f_{i+1}}{t_i} .$$

As the number of points N increases, then the fractions become a continuous function determined by

$$\frac{df}{dt} = (\alpha - 1)\frac{f}{t} ,$$

which has solution $f(t) = f(t_0)\ (t/t_0)^{\alpha-1}$. If we take $f_0 = 4$ at $t_0 = 1$ h, then at $t = 96$ h (4 d), a fraction of $f = 1$ implies $\alpha = 1 - \dfrac{\ln 4}{\ln 96} = 0.6963$. We then have the desorption factors

$$\varphi(t) = \left(\frac{t}{4}\right)^{\alpha-1} \varphi(4) \qquad \text{(time in days)} . \tag{A.9}$$

The average factor for steel is given as

$$\bar{\varphi} = 0.04 \text{ days}^{-1} = \frac{1}{4}\int_0^4 \varphi(t)\, dt = \varphi(4) \cdot \frac{1}{\alpha} . \tag{A.10}$$

Substituting Eq. (A.9) into Eq. (A.10) yields the revised desorption factor

$$\varphi(t) = \alpha\, \bar{\varphi}\left(\frac{t}{4}\right)^{\alpha-1} = 0.028\left(\frac{t}{4}\right)^{-0.3037} . \tag{A.11}$$

Use of Eq. (A.7) implies the general solution

$$\hat{C}_s(t) = \hat{C}_s(0)\, e^{-\gamma t}, \tag{A.12}$$

which assumes no irreversible desorption. However, analytic treatment of Eqs. (A.2) and (A.3) when $C_g = 0$ yields

$$C_p(t) = C_p(0)\, e^{-(k_2 + k_3)t}$$
$$C_c(t) = C_c(0) + \frac{k_3 C_p(0)}{k_2 + k_3}\left[1 - e^{-(k_2 + k_3)t}\right],$$

where $t = 0$ denotes the start of the desorption phase. Summing these two yields the total surface concentration, C_s, which can be expressed as

$$\frac{C_s(t) - C_{s\infty}}{C_s(0) - C_{s\infty}} = e^{-\gamma t}, \tag{A.13}$$

where

$$\gamma = k_2 + k_3, \quad C_{s\infty} = C_c(0) + C_p(0)k_3/\gamma, \quad \text{and } C_s(t) = C_c(t) + C_p(t). \tag{A.14a,b,c}$$

A.1.3 Parameter Estimation

Using Eq. (A.11), the desorption concentration in Eq. (A.12) can be reconstructed. The form of Eq. (A.13) is obtained by optimizing the choice of $C_{s\infty}$ and γ to minimize the integral squared error

$$\min_{\gamma, C_{s\infty}} \int_0^4 \left[C_s(t) - \hat{C}_s(t)\right]^2 dt. \qquad \text{(time in days)}$$

This optimization was done numerically using the final value in Table A.1 for initial input (i.e., concentration of adsorption time 1500 min = $C_s(0)$ = concentration at desorption time 0), resulting in the values

$$C_s(0) = 4.757 \times 10^{-7}\ \text{mol/cm}^2, \quad C_{s\infty} = 4.042 \times 10^{-7}\ \text{mol/cm}^2, \quad \gamma = 2.20 \times 10^{-4}\ \text{min}^{-1}. \tag{A.15}$$

Combining Eqs. (A.14)-(A.15) gives three relations from which the four quantities k_2, k_3, $C_p(0)$, and $C_c(0)$ must be calculated. A fourth relation can be obtained by dividing Eq. (A.6) by Eq. (A.5), evaluated at adsorption time 1500 min (which corresponds to desorption time zero),

$$\frac{C_c(0)}{C_p(0)} = k_3 Q, \quad Q = \left.\frac{\frac{1-e^{-Bt}}{B} - \frac{(1-e^{-\gamma t})}{\gamma}}{e^{-Bt} - e^{-\gamma t}}\right|_{t = \substack{\text{ads. time} \\ 1500\,\text{min}}} = 1517 \text{ (min)} .$$

These four relations can be combined and rearranged to obtain values for the desired unknowns:

$$\frac{C_s(0)}{C_{s\infty}} = \frac{C_s(0)/C_p(0)}{C_{s\infty}/C_p(0)} = \frac{k_3 Q + 1}{k_3(Q + \frac{1}{\gamma})} \rightarrow k_3 = \frac{C_{s\infty}}{Q(C_s(0) - C_{s\infty}) + C_s(0)/\gamma} = 1.768 \times 10^{-4} \text{ min}^{-1}$$

$$k_2 = \gamma - k_3 = 4.165 \times 10^{-5} \text{ min}^{-1}$$

$$C_s(0) = C_p(0) + C_c(0) = C_p(0)(1 + k_3 Q) \rightarrow C_p(0) = C_s(0)/(1 + k_3 Q) = 3.751 \times 10^{-7} \text{ mol/cm}^2$$

$$C_{s\infty} = C_c(0) + C_p(0)k_3/\gamma = C_c(0)\left(1 + \frac{1}{\gamma Q}\right) \rightarrow C_c(0) = \frac{C_{s\infty}}{1 + \frac{1}{\gamma Q}} = 1.006 \times 10^{-7} \text{ mol/cm}^2 .$$

From the above, it appears that only about 21% $[C_c(0)/C_s(0)]$ of the surface iodine is irreversibly bound at the end (1500 min) of the adsorption step. The surface reaction continues even during the desorption phase, until about 85% $[C_{s\infty}/C_s(0)]$ of the possible maximum is reacted.

The remaining parameter to be determined is the adsorption rate constant k_1, which is obtained by adding together Eqs. (A.5) and (A.6) to get the total surface inventory during adsorption:

$$C_s(t) = k_1 P ,$$

where

$$P = \frac{A}{r(k_2 + k_3 - B)}\left[\frac{k_3}{B} - \frac{k_3}{\gamma} + \left(1 - \frac{k_3}{B}\right)e^{-Bt} - \frac{k_2}{\gamma}e^{-\gamma t}\right] .$$

The quantity P can be calculated at each adsorption time point where C_s is known, and the ratio C_s/P used as an estimate for k_1. These values are shown in Table A.1, along with the average rate constant value of $k_1 = 4.761 \times 10^{-5}$ min^{-1}.

A.2 DATA OF ROSENBERG, GENCO, AND MORRISON[5]

A number of tracer experiments were performed with a continuous flow of iodine through a test chamber containing a single material sample. Excellent results are presented for both adsorption and desorption on stainless steel at 115°C. Additional results are given for deposition only at other temperatures and for experiments involving multiple samples. The effects of various humidity levels are also included.

A.2.1 Adsorption Modeling

Since the depletion of gaseous iodine is due only to deposition onto a single sample, Eqs. (A.1)-(A.3) reduce to

$$\dot{C}_g = - k_1 C_g + r k_2 C_p + f(C_{gi} - C_g) , \tag{A.16}$$

$$\dot{C}_p = \frac{1}{r} k_1 C_g - k_2 C_p - k_3 C_p , \tag{A.17}$$

$$\dot{C}_c = k_3 C_p , \tag{A.18}$$

where f is the volume fractional flow rate of ventilating air, and C_{gi} is the inlet iodine concentration. The last term in Eq. (A.16) did not appear in Eq. (A.1) because that experiment included a single initial source, whereas this system includes a continuous inlet (and outlet) flow. Equations (A.16) and (A.17) constitute a coupled set of ordinary differential equations with constant coefficients. An analytic solution is obtained by the procedure in ref. 94 for zero initial conditions:

$$C_g(t) = \frac{f C_{gi}}{m_2 - m_1} \left[\frac{m_2 + k_1 + f}{m_1} (e^{m_1 t} - 1) - \frac{m_1 + k_1 + f}{m_2} (e^{m_2 t} - 1) \right] , \tag{A.19}$$

$$C_p(t) = \frac{f k_1 C_{gi}}{r(m_1 - m_2)} \left[\frac{e^{m_1 t} - 1}{m_1} - \frac{e^{m_2 t} - 1}{m_2} \right] . \tag{A.20}$$

The chemisorbed concentration is obtained by substituting Eq. (A.20) into (A.18) and integrating:

$$C_c(t) = \frac{k_1 k_3 f C_{gi}}{r(m_1 - m_2)}\left[\frac{1}{m_1^2}(e^{m_1 t} - m_1 t - 1) - \frac{1}{m_2^2}(e^{m_2 t} - m_2 t - 1)\right] \qquad \text{(A.21)}$$

In the above equations, m_1 and m_2 are eigenvalues of the ODE system, given by

$$m_1 = -\beta + \sqrt{\beta^2 - \gamma}\,, \qquad m_2 = -\beta - \sqrt{\beta^2 - \gamma}\,,$$

$$\beta \equiv \frac{1}{2}(k_1 + k_2 + k_3 + f)\,, \qquad \gamma = k_1 k_3 + f(k_2 + k_3)$$

Note that both m_1 and m_2 are real and negative, indicating that all exponential terms decay as t increases. Thus, the iodine concentrations exhibit limiting behavior as follows:

$$\lim_{t\to\infty} C_g(t) = \frac{f C_{gi}}{m_2 - m_1}\left[-\frac{m_2 + k_1 + f}{m_1} + \frac{m_1 + k_1 + f}{m_2}\right] = C_{gi}\frac{f(k_2 + k_3)}{k_1 k_3 + f(k_2 + k_3)} \qquad \text{(A.22)}$$

$$\lim_{t\to\infty} C_p(t) = \frac{f k_1 C_{gi}}{r(m_1 - m_2)}\left[-\frac{1}{m_1} + \frac{1}{m_2}\right] = \frac{f k_1 C_{gi}}{r(k_1 k_3 + f(k_2 + k_3))} \qquad \text{(A.23)}$$

$$\lim_{t\to\infty} C_c(t) = \frac{k_1 k_3 f C_{gi}}{r(m_1 - m_2)}\left[\frac{-1}{m_1^2}(m_1 t + 1) + \frac{1}{m_2^2}(m_2 t + 1)\right] = \frac{k_1 k_3 f C_{gi}}{m_1^2 m_2^2 r}\left[(m_1 + m_2) + m_1 m_2 t\right]. \qquad \text{(A.24)}$$

From these limits, it appears that C_g and C_p approach constant values, while C_c becomes a linearly increasing function.

A.2.2 Modeling Desorption in Moist Air

If the iodine source in the ventilating air is terminated, then iodine gas concentration in the test chamber will fall quickly. Desorption from the surface (if it occurs to any great extent) provides the only source of gaseous iodine. Thus, we expect $k_1 C_g << k_2 C_p + k_3 C_p$, which implies that Eq. (A.17) can be simplified to get
whose solution is

$$\dot{C}_p = -(k_2 + k_3)C_p , \tag{A.25a}$$

$$C_p(t) = C_p(0)e^{-(k_2 + k_3)t} . \tag{A.25b}$$

Again, the chemisorbed inventory is obtained by integration of Eq. (A.18):

$$C_c(t) = C_c(0) + \frac{k_3}{k_2 + k_3} C_2(0)\left[1 - e^{-(k_2 + k_3)t}\right] . \tag{A.26}$$

In Eqs. (A.25) and (A.26), it should be noted that t = 0 implies the beginning of the desorption process; hence, the initial surface concentrations are not zero. The total surface concentration is the sum of Eqs. (A.25) and (A.26), which can be arranged in the form of Eq. (A.13), with the definition of parameters analogous to Eq. (A.14):

$$\gamma = k_2 + k_3 , \quad C_{s\infty} = C_c(0) + \frac{k_3}{\gamma} C_p(0) , \quad C_s(t) = C_p(t) + C_c(t) . \tag{A.27}$$

A.2.3 Parameter Estimation

The principal data transient at 115°C is shown in Fig. 7 (curves A and D) of ref. 5. Some of the data points have been transcribed and are given in Table A.2. The inlet gas is composed of 56% air and 44% steam (by volume), with inlet iodine concentration of C_{gi} = 1.379 × 10^{-3} mol I_2/m^3.

Additional information on the experimental conditions were obtained from ref. 31. The sample size is a thin rectangle with surface area A_s = 25.8 cm^2 (1 in. by 2 in.), the test chamber is a tube of radius R = 1 in., and the superficial gas velocity is v_s = 0.30 cm/s. The actual length L of the test chamber could not be found, although it appeared in report figures to be about 1 ft. If this is assumed, then the fractional flow and surface-to-volume ratio is determined as

$$f = \frac{v_s}{L} = 35.433\ h^{-1} , \quad r = \frac{A_s}{\pi R^2 L} = 0.0418\ cm^{-1} . \tag{A.28}$$

On the other hand, if only the portion of the test chamber in which the sample lies is considered, then L = 2 in. In this case, we have

$$f = 212.60\ h^{-1} , \quad r = 0.251\ cm^{-1} . \tag{A.29}$$

Table A.2. Moist air adsorption data at 115°C[a]

Adsorption phase		Desorption phase	
Time (h)	Surface concentration $(mol/cm^2)\cdot 10^6$	Time (h)	Surface concentration $(mol/cm^2)\cdot 10^6$
0	0	0	8.571
4	1.161	2	8.476
8	2.459	4	8.416
12	3.972	6	8.390
16	5.493	8	8.373
20	7.049	14	8.364
24	8.571	22	8.356

[a]*Source*: H. S. Rosenberg, J. M. Genco, and D. L. Morrison, *Fission-Product Deposition and Its Enhancement Under Reactor Accident Conditions: Deposition on Containment-System Surfaces*, BMI-1865, Battelle Memorial Inst., 1969.

In either case, the ratio of the two is constant, f/r = 848.23 cm/h. In reality, it is a simplifying assumption of the modeling process that requires a value of L in the first place. A good choice would probably lie somewhere between 2 and 12 in.

The adsorption phase data are nearly linear, consistent with the analytic solution as $t \to \infty$ [cf. Eqs. (A.23), (A.24)]. This behavior permits a linear regression on the total surface concentrations in Table A.2 of the form

$$C_s(t) = M_a t + b_a \,. \tag{A.30}$$

Taking the logarithm of the surface concentrations during desorption also allows linear regression [cf. Eq. (A.13)] of the form

$$\ln (C_s - C_{s\infty}) = M_d t + b_d \,. \tag{A.31}$$

This equation is actually a nonlinear optimization because $b_d = \ln(C_s(0) - C_{s\infty})$. In practice, many values of $C_{s\infty}$ are guessed and the regression performed until the specified value of $C_{s\infty}$ corresponds to $C_s(0) - e^{b_d}$. The fitting parameters in Eqs. (A.30) and (A.31) were determined to be

$$M_a = 3.61812 \times 10^{-7},\ b_a = -2.410 \times 10^{-7},\ M_d = -0.29035,\ b_d = -15.3512\ . \quad \text{(A.32)}$$

We now seek relationships between the three rate constants k_1, k_2, and k_3, and the empirical parameters in Eq. (A.32). From Eqs. (A.24) and (A.13), it can be determined that

$$M_a = \frac{k_1 k_3 f C_{gi}}{r[k_1 k_3 + f(k_2 + k_3)]}, \quad M_d = -(k_2 + k_3), \quad b_d = C_p(0)\frac{k_2}{(k_2 + k_3)}\ . \quad \text{(A.33a,b,c)}$$

Note again that $C_p(0)$ in Eq. (A.33c) refers to the physisorbed concentration at the beginning of the desorption phase. This corresponds to the physisorbed concentration at the end of the adsorption phase and can therefore be obtained from Eq. (A.23):

$$C_p(0) = \frac{f k_1 C_{gi}}{r(k_1 k_3 + f(k_2 + k_3))}\ . \quad \text{(A.33d)}$$

We thus have four relations to determine the four unknowns k_1, k_2, k_3, and $C_p(0)$. These relations can be combined and rearranged, and the values from Eq. (A.32) used, to get

$$k_2 = -\frac{M_d^2 e^{b_d}}{M_d e^{b_d} - M_a} = 0.04276\ \text{h}^{-1}, \quad k_3 = \frac{M_a M_d}{M_d e^{b_d} - M_a} = 0.2476\ \text{h}^{-1}. \quad \text{(A.34a,b)}$$

$$k_1 = \frac{1}{k_3}\frac{r f M_a M_d}{(r M_a - f C_{gi})} = \begin{array}{ll} 18.61\ \text{h}^{-1}, & L = 12\ \text{in.} \\ 111.5\ \text{h}^{-1}, & L = 2\ \text{in.} \end{array}\ . \quad \text{(A.34c)}$$

As mentioned previously, there is some uncertainty in the appropriate mixing length L of the test section surrounding the test specimen. This uncertainty only affects the calculated value of k_1, as shown above. In practice, a value between the two is recommended. In the remainder of this work, a value of $k_1 = 90\ \text{h}^{-1}$ (corresponding to a mixing length $L = 2.48$ in.) will be used.

A.2.4 Desorption in Dry Air

These researchers ran a special experiment in which deposition in moist air was followed by desorption in dry air (see Fig. 7, curves B and C, of ref. 5). The data are shown at various points in Table A.3. Unlike the case of desorption in moist air, considerable desorption resulted. This result indicates that in dry air, chemisorbed iodine was not irreversibly bound, so that $k_4 \neq 0$ in Eq. (11.1). Thus, the desorption step is now described by the equation set

$$\dot{C}_p = -(k_2 + k_3)C_p + k_4 C_c \,, \tag{A.35a}$$

$$\dot{C}_c = k_3 C_2 - k_4 C_3 \,, \tag{A.35b}$$

which replace the single equation model of Eq. (A.25). Because this set has constant coefficients, procedures analogous to those in Sect. A.2.1 can be employed to obtain an analytic solution

$$C_p(t) = \frac{C_{p0}}{(m_2 - m_1)}\left(m_2 e^{m_2 t} - m_1 e^{m_1 t}\right) + \frac{(C_{p0} + C_{c0})k_4}{(m_2 - m_1)}\left(e^{m_2 t} - e^{m_1 t}\right) \,, \tag{A.36a}$$

$$C_c(t) = \frac{(k_3 C_{p0} - k_4 C_{c0})}{(m_2 - m_1)}\left(e^{m_2 t} - e^{m_1 t}\right) + \frac{C_{c0}}{(m_2 - m_1)}\left(m_2 e^{m_1 t} - m_1 e^{m_2 t}\right) \,, \tag{A.36b}$$

where $C_{p0} = C_p(0)$, $C_{c0} = C_c(0)$, and m_1, m_2 are the eigenvalues of system (A.35):

$$m_1 = -\beta + \sqrt{\beta^2 - \gamma} \qquad m_2 = -\beta - \sqrt{\beta^2 - \gamma}$$
$$\beta = \frac{1}{2}(k_2 + k_3 + k_4) \qquad \gamma = k_2 k_4 \tag{A.37a,b}$$

Note also that $t = 0$ corresponds to the start of the desorption phase.

For the adsorption step, Eqs. (A.16)-(A.18) still represent a reasonable model, with parameter values given in Eq. (A.34). The conditions are slightly different than those in Sect. A.2.3, with $v_s = 0.43$ cm/s, $C_{gi} = 8.629 \times 10^{-4}$ mol I_2/m^3. Using a mixing length, $L =$ 2.48 in., gives $k_1 = 90.0$ h^{-1}, $f = 245.7$ h^{-1}, $r = 0.2021$ cm^{-1}. Substitution into Eqs. (A.19) and (A.20) with $t = 20$ h yields the concentrations at the end of the adsorption step, corresponding to the beginning of the desorption phase:

$$C_{p0} = 1.005 \times 10^{-6} \qquad C_{c0} = 4.102 \times 10^{-6} \quad (\text{mol/cm}^2) \,. \tag{A.38}$$

Adding these quantities gives the total surface concentration $C_{s0} = 5.107 \times 10^{-6}$ mol/cm^2, which compares well with the data value in Table A.3. Note that although changes in the mixing length L have a noticeable effect on k_1, f, and r, their effects on C_{p0}, C_{c0}, and C_s are negligibly small (<0.1% change for 2 in. < L < 12 in.).

Table A.3. Desorption in dry air at 115°C[a]

Adsorption phase (moist air)		Desorption phase (dry air)	
Time (h)	Surface concentration $(mol/cm^2)\cdot 10^6$	Time (h)	Surface concentration $(mol/cm^2)\cdot 10^6$
0	0	0	5.786
4	0.946	12	2.837
8	2.201	39	2.158
12	3.361	61	0.971
16	4.651		
20	5.786		

[a]*Source*: H. S. Rosenberg, J. M. Genco, and D. L. Morrison, *Fission-Product Deposition and Its Enhancement Under Reactor Accident Conditions: Deposition on Containment-System Surfaces*, BMI-1865, Battelle Memorial Inst., 1969.

For the desorption step, Eqs. (A.36a) and (A.36b) are added to get the total surface concentration,

$$C_s(t) = \frac{e^{m_1 t}}{(m_2 - m_1)}[m_2 C_{c0} - (m_1 + k_3 + k_4)C_{p0}] + \frac{e^{m_2 t}}{(m_2 - m_1)}[(m_2 + k_3 + k_4)C_{p0} - m_1 C_{c0}] \ . \quad \text{(A.39)}$$

This equation represents a very nonlinear function of the unknown rate constants k_2, k_3, and k_4. Comparing Eq. (A.39) with the desorption data in Table A.3 allows a nonlinear optimization scheme to minimize the sum of square error. This resulted in $k_3 = 0$, but gave inconclusive results for k_2 and k_4. This implies that no irreversible sorption occurs without some water vapor present, which is consistent with experimental observations in absence of water (see ref. 5, page 16).

Implementing the result $k_3 = 0$ yields the simple form for Eq. (33), namely

$$C_s(t) = \frac{e^{-k_2 t}}{k_2 - k_4}[k_4 C_{c0} - (k_2 - k_4)C_{p0}] + \frac{e^{-k_4 t}}{(k_2 - k_4)} k_2 C_{c0} \ . \quad \text{(A.40)}$$

In the case of $k_2 < k_4$, the second term dies out more quickly; however, since the first term is always negative, the entire surface concentration C_s would be negative after a short time. Clearly, this cannot happen; hence, we restrict $k_2 > k_4$.

If $k_2 >> k_4$, then the second term dominates very quickly, allowing Eq. (A.40) to be represented in the linear form

$$\ln C_s = \ln\left(\frac{k_2 C_{c0}}{k_2 - k_4}\right) - k_4 t \ .$$

In fact, the desorption data in Table A.3 are well fit by the above form, yielding the regression parameters

$$k_4 = 0.02587 \ \mathrm{h}^{-1}$$

$$\ln\left(\frac{k_2 C_{c0}}{k_2 - k_4}\right) = -12.20771 \rightarrow k_2 = 5.613\ k_4 = 0.1452 \ \mathrm{h}^{-1} \ .$$

There is some concern that the assumption $k_2 >> k_4$ is not adequately satisfied. However, a recalculation using these values indicates that the first term in Eq. (A.40) contributes less than 1% to the total at all of the time points where data exist (i.e., 12, 39, and 61 h).

The previous analysis did not consider the process of physisorption itself, which is reversible. In dry air, this process is not very fast or extensive; hence, very little change in the gas concentration should occur. Assuming that $C_g = C_{gi}$ = constant, the unknown surface concentration is determined by the single equation

$$\dot{C}_p = \frac{1}{r} k_1 C_g - k_2 C_p \ ,$$

whose solution is readily found to be

$$C_p(t) = \frac{k_1 C_g}{r k_2}(1 - e^{-k_2 t}) \ .$$

From Table 2 in ref. 1, we obtain the single data point $C_p(t = 22\ \mathrm{h}) = 2.256 \times 10^{-9}$ mol/cm^2 for the conditions $C_{gi} = 5.91 \times 10^{-4}$ mol/m^3, $r = 0.465$ cm^{-1}. Using the value of k_2 determined previously, we have

$$k_1 = \frac{C_{gi}}{C_p} \frac{r k_2}{(1 - e^{-k_2 t})} = 0.2689 \ \mathrm{h}^{-1} \ .$$

APPENDIX B

KINETIC PARAMETERS FOR DEPOSITION ONTO PAINTS

The procedure for establishing rate constants here is similar to those steps followed in Appendix A; however, there is one important difference — nonlinearity. Deposition onto steel is virtually unlimited, implying that the kinetics do not depend on the number of available surface sites; hence, the governing equations are linear [cf. system (A.1)-(A.3)] and therefore amenable to analytic solutions. This is not the case with paint, since data clearly indicate that surface saturation occurs. This effect requires that the number of available surface sites be included in the analysis, resulting in a slightly nonlinear set of governing equations, and requiring numerical solution.

B.1 PROBLEM FORMULATION

The experiments and apparatus are described in refs. 5 and 95-97. In each of the experiments, a single sample is situated in a continuously flowing system which contains a known I_2 gas concentration at the inlet during the adsorption phase. This step is followed by a desorption phase in which no iodine is contained in the ventilating gas. Periodic measurements are taken of the total surface concentration during both adsorption and desorption steps. This effectively results in two data transients, one for adsorption and one for desorption, each with its own initial values and data.

Referring to the processes in Eq. (19), we define the variables

$C_1 = [I_2(g)]$ (mol/cm^3)
$C_2 = [I_2(s)]$ (mol I_2/g·paint)
$C_3 = [R_2I_2(s)]$ (mol R_2I_2/g·paint)
$C_4 = [R_2]$ (mol surface sites/g·paint)
$C_5 = C_2 + C_3$ = total surface iodine

The following rate equations then describe the transient variation of concentrations:

$$\dot{C}_1 = -k_1 C_1 + r k_2 C_2 + f(C_6 - C_1) \tag{B.1}$$

$$\dot{C}_2 = \frac{1}{r} k_1 C_1 - k_2 C_2 - k_3 C_2 C_4 \tag{B.2}$$

$$\dot{C}_3 = k_3 C_2 C_4 \tag{B.3}$$

$$\dot{C}_4 = -k_3 C_2 C_4 \tag{B.4}$$

$$\dot{C}_5 = \frac{1}{r} k_1 C_1 - k_2 C_2 , \tag{B.5}$$

where r = paint mass (g)/gas volume (L),
f = volume fractional flow rate (h^{-1}),
C_6 = inlet gas concentration (mol/L).

As described in Appendix A, Sect. A.2.3, the quantities r and f both depend on the volume V_g in the vicinity of the sample. Since this quantity is not clearly defined, both r and f will also be regarded as optimizable parameters, along with the rate constants k_1, k_2, and k_3. Initial conditions for the adsorption step are

$$C_i = 0 \qquad (i=1,2,3,5), \qquad C_4 = C_{40}^{ads} ,$$

and for the desorption step are

$$C_1 = C_6 = 0, \qquad C_2 = C_{20}^{des}, \quad C_3 = C_{30}^{des}, \quad C_4 = C_{40}^{des}, \quad C_5 = C_{50}^{des} .$$

The above quantities that are readily identifiable from data are total surface concentration (C_{50}^{des}) and total number of surface sites (C_{40}^{ads}). These quantities are listed in Table B.1 along with other relevant experimental parameters. However, the distribution between physisorbed (C_2) and chemisorbed (C_3) inventories is not known, and therefore care must be taken in the selection of C_{20}^{des} and C_{30}^{des}. In addition, the number of remaining surface sites is not known at the end of adsorption (beginning of desorption). Thus, the quantities C_{20}^{des}, C_{30}^{des}, and C_{40}^{des} are also treated as unknown parameters subject to optimization. In certain instances, additional quantities will also be optimized, including the inlet concentration, C_6, and the initial concentration, C_{50}^{des}.

Table B.1. Experimental parameters for I_2 deposition onto paint[a]

Paint type	Run designator	Temp (°C)	Concentration × 10^6			Flow rate (L/h)	Sample size		Paint mass (mg)
			C_6^{ads}	C_{40}^{ads}	C_{50}^{des}		Area (cm^2)	Length (cm)	
Vinyl	VAM 33HB-3	115	0.796	42.3	42.1	28.6	12.9	5.08	17.8
	VAM 33HB-4	170	0.737	8.2	7.9	38.9	12.9	5.08	82.2
Acrylic latex	VAM 1756-1	115	0.709	61.7	61.5	30.3	11.3	4.45	94.5
Epoxy	VAM 1756-2	170	0.701	13.9	13.9	29.7	11.3	4.45	101.5
	VAM 66-2	115	0.741	555.4	547.6	30.2	12.9	5.08	84.1
Phenolic	VAM 66-3	170	0.674	321.7	311.2	30.2	6.45	2.54	50.8
	VP 302-3	115	0.147	490.0	214.5	30.7	12.9	5.08	39.0
	VP302-5	170	0.670	293.9	293.9	30.8	6.45	2.54	35.8

[a]*Sources:* H. S. Rosenberg, J. M. Genco, and D. L. Morrison, *Fission-Product Deposition and Its Enhancement Under Reactor Accident Conditions: Deposition on Containment-System Surfaces*, BMI-1865, Battelle Memorial Inst., 1969; J. M. Genco et al., *Fission Product Deposition and Its Enhancement Under Reactor Accident Conditions*, BMI-X-10179, Battelle Columbus Laboratories, Columbus, Ohio, October 1966; J. M. Genco et al., *Fission Product Deposition and Its Enhancement Under Reactor Accident Conditions*, BMI-X-10193, Battelle Columbus Laboratories, Columbus, Ohio, April 1967; and J. M. Genco et al., *Fission Product Deposition and Its Enhancement Under Reactor Accident Conditions*, BMI-X-10222, Battelle Columbus Laboratories, Columbus, Ohio, January 1968.

B.2 Parameter Estimation

In all cases, the measured quantity is total surface concentration (C_5), which implies that optimal parameter fitting will minimize the sum of squared error

$$\min R = \sum_i (C_5(t_i) - \hat{C}_{5i})^2 , \tag{B.6}$$

where $\hat{C}_{5i}$ are data points at respective times t_i. This represents a nonlinear optimization problem, since $C_5(t_i)$ in Eq. (B.6) must be determined by solving system (B.1)-(B.5).

A numerical solution is obtained, using the following sequence of steps (note $u_i = \ell n\, k_i$):

1. The desorption data alone are used, assuming negligible gas concentration and therefore negligible adsorption. Optimization of u_2, u_3, C_{20}^{des}, and C_{40}^{des} give generally good estimates of these quantities. The assignment of C_{30}^{des} is arbitrary and does not affect the solution of system (B.1)-(B.5) or the optimization in any way.

2. The adsorption data alone are used to optimize u_1, r, f, and C_{40}^{ads}. Optimal values of u_2 and u_3 from step 1 are used, but are not subject to optimization. If step 1 has produced a viable optimization of C_{40}^{des}, then a reasonable estimate is

$$C_{40}^{ads} = C_{40}^{des} + (C_{50}^{des} - C_{20}^{des}) .$$

3. Both adsorption and desorption data are used simultaneously for optimal refinement of all parameters.

Initial parameter values for steps 1 and 2 are generally picked from a grid search, using reasonable estimates for initial concentrations. Initial values for the step 3 optimization use as initial guesses the values from the provisional optimizations in steps 1 and 2. If unique values have not been identified in steps 1 and 2, then a range of initial guesses is used in step 3. In each step, the numerical optimization procedure is that described in ref. 27. Results of each step are shown for the four paints in Table B.2.

Table B.2. Optimization results for iodine deposition onto paints

Run designator	Optimization step	Parameter[a]			Concentration × 10^6		
		u_1	u_2	u_3	C_{20}^{des}	C_{40}^{des}	C_{40}^{ads}
VAM HB33-2	1	--[b]	3.357	9.6	31.28	3	--
	2	11.24	--	--	--	--	11.37
	3	11.19	3.678	9.543	--	--	--
VAM 1756-1	1	--	2.644	9.3	41.9	3.5	--
	2	8.6	--	--	--	--	21.6
	3	8.067	1.969	9.297	--	--	--
VAM 66-2	1	--	0.5	5	250- 300	9	--
	2	9	--	--	--	--	400
	3	8.380	0.2921	4.772	--	--	--
VP 302-3	1	--	2.14	6	30	?	--
	2	7.78	--	--	--	--	380
	3	5.964	1.228	5.941	--	--	--

[a] $u_i = \ln k_i$; units of k_i are h^{-1}, h^{-1}, and $g/mol \cdot h^{-1}$, respectively.

[b] Parameter optimization not performed, or convergence to optimal value did not occur.

APPENDIX C

PARAMETER ESTIMATION FOR HYDROLYSIS REACTIONS

Aqueous iodine chemistry has been studied extensively in the past, and hundreds of experimental results have been obtained. Invariably, these involve much higher concentrations than would occur in reactor containments, and often contain salts or other "impurities" that might affect hydrolysis processes. In addition, rate constants have been determined only for certain of the reaction substeps, usually by different researchers and involving different conditions and assumptions. Unmeasured parameters are usually assigned values by heuristic estimation or speculation. It is not known that the chosen reaction set (22) is a true depiction of subprocesses. Most likely it is not, and, hence, in some ways represents an empirical model with six parameters. This implies that the rate constants are dependent on each other, and optimal values must be determined by consideration of the overall model rather than independent subprocesses. However, it is also important that sufficient data be available to clearly identify each parameter. With these considerations in mind, a recent effort was conducted at ORNL, both to obtain new experimental data and to adequately estimate the parameters in the overall model (22).

C.1 EXPERIMENTAL PROCEDURE

To provide more useful data, a number of batch experiments were performed under appropriate conditions for nuclear accident analysis. These generally involve pH values of 3 to 9, temperatures between 25 and 90°C, atmospheric pressure, and total iodine concentrations of 10^{-5} - 10^{-3} M. The results form a sufficient data base for the quantitative selection of rate constants for models discussed in previous sections.

Each batch experiment involved the dissolution of various iodine species in water, and the measurement of I^-, I_2, and IO_3^- after a specified time. For the forward (hydrolysis) reaction, a small quantity of 10^{-3} M I_2 solution is added to a borated water solution. For the reverse (Dushmann) reaction, CsI, HI, and HIO_3 are added to borated water, the pH being adjusted by the distribution of species.

Borate is typically used in experimental studies supporting reactor safety, because virtually every LWR uses borated water as a neutron absorber. Borate is also an effective buffer, allowing the reactions to proceed at nearly constant pH. Reactions between borate and the various iodine species have not been noted in any of the literature reviewed for this work, although a slight ionic strength effect may occur at neutral pH.

The measurement procedure itself is similar to that described in refs. 52 and 65 and is summarized as follows:

1. The I_2 is extracted into isooctane, and then backstripped into 0.2 M NaOH solution containing hydroxylamine-hydrochloride. The resulting iodide is measured with a specific ion electrode.

2. The I^- occurring in the original solution is measured using a specific ion electrode.

3. After removing I_2 with phenol, the IO_3^- is converted into I_3^- by the addition of excess acidified I^- via the reaction

$$IO_3^- + 8\,I^- + 6\,H^+ \rightarrow 3\,I_3^- + 3\,H_2O\ ,$$

and measured by UV-visible spectroscopy.

Typically, these steps are performed simultaneously by three different people. The concentrations of measured species are frozen in each step within 30 to 60 s (by isooctane extraction, quick measurement, and addition of acidified I^-, respectively). For long transients, this measurement time is immaterial; however, for the most rapid transients (e.g., Transient 15) the time delay of measurement may impose experimental error of 5 to 10% for some of the data points.

C.2 DATA ANALYSIS

Data from over 100 batch reactor experiments are shown in Tables C.1 and C.2, grouped according to similarities in initial concentrations, temperature, and pH. Each of these groupings is then considered as a single transient (i.e., the description of time varying behavior of a single system). The initial inventories are shown for the two different types of experiments—the Dushman reaction of I^- and IO_3^-, and the hydrolysis of I_2. Also shown are the final inventories of each measured specie, normalized by dividing by the total initial inventory.

Table C.1. Dushman reaction data

	Time (min)	Initial inventory (g-atom/dm³) × 10³			Final inventory fraction (g-atom basis)			Run No.
		I^-	IO_3^-	Total	I^-	I_2	IO_3^-	
Group 1	5	0.1	1.412	1.512	0.0339	0.0325	0.9074	69
pH = 2.8	15	0.1	1.635	1.735	0.0130	0.0515	0.9193	70
T = 25°C	30	0.1	1.654	1.754	0.0101	0.0573	0.9019	108
	60	0.1	1.451	1.551	0.0100	0.0629	0.8214	112
Group 2	5	0.1	0.900	1.000	0.0887	0.0157	0.7198	64
pH = 37	15	0.1	0.850	0.950	0.0781	0.0272	0.7183	61
T = 25°C	15	0.1	0.787	0.887	0.0827	0.0282	0.7665	77
	30	0.1	0.917	1.017	0.0562	0.0468	0.7166	65
	60	0.1	1.118	1.218	0.0216	0.0710	0.7342	63
	120	0.1	0.963	1.063	0.0212	0.0836		62
Group 3	30	0.507	0.104	0.611	0.659	0.105	0.171	101
pH = 3.2	60	0.555	0.099	0.654	0.642	0.152	0.125	104
T = 25°C	120	0.524	0.095	0.618	0.539	0.235	0.106	103
	240	0.503	0.094	0.597	0.435	0.245	0.122	111
Group 4	15	0.5693	0.0200	0.5893	0.852	0.0012	0.0289	78
pH = 3.2	30	0.5528	0.0190	0.5718	0.871	0.0191	0.0269	93
T = 25°C	30	0.5587	0.0192	0.5779	0.846	0.0167	0.0276	96
	60	0.4734	0.0191	0.4925	0.864	0.0311	0.0312	91
	60	0.5311	0.0190	0.5501	0.810	0.0330	0.0284	98
	90	0.5552	0.0198	0.5750	0.765	0.0442	0.0230	94
	120	0.5320	0.0186	0.5507	0.793	0.0716	0.0169	92
	120	0.5300	0.0193	0.5493	0.803	0.0547	0.0224	97
	150	0.5334	0.0193	0.5527	0.740	0.0550	0.0194	95
	150	0.5468	0.0191	0.5659	0.721	0.0713	0.0186	99
	240	0.5088	0.0182	0.5271	0.724	0.0855	0.0201	100
	360	0.5899	0.0202	0.6101	0.649	0.1203	0.0177	109
	360	0.5596	0.0204	0.5800	0.652	0.0644	0.0240	114
Group 5	5	0.1	0.823	0.923	0.050	0.026	0.751	81
pH = 3.0	15	0.1	0.894	0.994	0.043	0.054	0.806	79
T = 50°C	30	0.1	0.911	1.011	0.035	0.068	0.793	80
	60	0.1	0.880	0.980	0.017	0.078	0.789	82
Group 6	15	0.500	0.0191	0.519	0.795	0.0198	0.0287	87
pH = 3.2	15	0.477	0.0200	0.497	0.733	0.0227	0.0312	115
T = 50°C	30	0.535	0.0196	0.555	0.915	0.0384	0.0247	118
	60	0.490	0.0199	0.510	0.866	0.0536	0.0227	117
	120	0.493	0.0198	0.513	0.637	0.1000	0.0170	116
	240	0.536	0.0198	0.556	0.788	0.1330	0.0029	119
Group 7	15	1.998	0.0729	2.071	0.886	0.072	0.020	121
pH = 3.2	30	2.056	0.0716	2.128	0.856	0.099	0.014	120
T = 90°C	60	2.021	0.0746	2.096	0.573	0.120	0.010	122

Table C.2. Hydrolysis data

	Time (min)	Initial I_2 (g-atom/dm^3) × 10^4	Final inventory fraction (g-atom basis) I^-	I_2	IO_3^-	Run No.
Group 8	15	1.2	0.082	0.893	0.013	4
pH = 7	15	1.2		0.847	0.012	6
T = 25°C	30	1.2		0.666	0.021	2
	30	1.2	0.206	0.674	0.021	48
	60	1.2	0.228	0.730	0.031	26
	60	1.2	0.218	0.692	0.049	28
	120	1.2	0.239	0.553	0.050	27
	240	1.2	0.313	0.561	0.063	47
	360	1.2	0.356	0.475	0.089	31
	420	1.2	0.342	0.399	0.093	51
	960	1.2	0.486	0.274	0.111	30
Group 9	5	1.2	0.403	0.510	0.056	38
pH = 8	5	1.2		0.514	0.049	18
T = 25°C	10	1.2	0.460	0.539	0.065	44
	10	1.2	0.457	0.531	0.068	45
	15	1.2	0.483	0.328	0.096	37
	15	1.2		0.400	0.093	1
	30	1.2		0.225	0.114	20
	30	1.2	0.596		0.107	35
	30	1.2	0.578	0.241	0.108	36
	60	1.2		0.155	0.149	16
	60	1.2	0.661	0.202	0.119	34
	120	1.2	0.675	0.112	0.128	46
Group 10	5	1.2	0.534	0.293	0.082	43
pH = 8.5	15	1.2	0.604	0.155	0.116	42
T = 25°C	30	1.2	0.673	0.091	0.122	41
	60	1.2	0.719	0.049	0.125	40
	120	1.2	0.735	0.026	0.128	39
Group 11	3	1.2	0.671	0.165	0.126	50
pH = 9	5	1.2	0.606	0.133	0.119	24
T = 25°C	10	1.2	0.863	0.062	0.145	49
	15	1.2	0.676	0.050	0.131	23
	30	1.2	0.733	0.027	0.148	22
	60	1.2	0.807	0.016	0.160	21
Group 12	15	1.2	0.336	0.421	0.079	58
pH = 7	30	1.2	0.401	0.253	0.090	57
T = 50°C	60	1.2	0.462	0.222	0.059	59
Group 13	15	1.0508	0.274	0.529	0.067	130
pH = 5.5	30	1.1589	0.445	0.409	0.108	128
T = 90°C	60	1.0143	0.429	0.282	0.116	131
	120	0.8842	0.566	0.247	0.115	129
Group 14	10	1.0203	0.440	0.407	0.048	127
pH = 6	15	1.1590	0.542	0.355	0.091	124
T = 90°C	30	0.9548	0.592	0.228	0.095	125
	60	0.9432	0.735	0.153	0.119	126
Group 15	5	1.2	0.522	0.120	0.121	54
pH = 7	10	1.2	0.699	0.068	0.133	56
T = 90°C	15	1.2	0.595	0.045	0.133	53
	30	1.2	0.741	0.017	0.133	55

Each transient has an initial nonzero concentration either for I_2, or for I^- and IO_3^-. These are shown in columns 3 through 5 of Table C.1 and column 3 of Table C.2. Entries showing one or two significant digits were estimated using assumed compositions of initial solution ingredients; those with three or four digits were actually measured by the same procedures used for final reaction products (i.e., using either step 1, or steps 2 and 3 in Sect. 4.1). The uncertainty in either approach is probably 5 to 10%.

Note that these results involve only the end products I^-, I_2, and IO_3^-, which are stable and measurable with reliable laboratory methods. Any intermediate species are assumed to be present in small enough amounts so that (1) failure to measure them will not significantly alter the total recorded iodine inventories, and (2) only negligible quantities of volatile intermediates will evaporate. Initial concentrations of these species are assumed to be zero.

While the pH and temperature are constant, the initial species concentrations for each batch experiment within a group may vary slightly. Hence, an average value is used for the group as a whole. Table C.3 depicts these mean values, together with the standard deviations, which in most cases are less than 10% of the mean values. This error in averaging is probably no greater than the uncertainty in the individual initial concentrations. For groups whose initial inventories were estimated, rather than measured, the average is equal to this estimated value and the deviation is zero.

C.3 RATE EQUATIONS

Assuming each reaction is elementary, expressions for reaction rates in Eqs. (22) and (23) are used to obtain the overall mathematical description of system behavior. The concentration variables (mol/L) are defined as

$$y_1 = [I^-],\ y_2 = [I_2],\ y_3 = [HOI],\ y_4 = [HOI_2],\ y_5 = [HIO_3],\ y_6 = [I_3^-],\ y_H = [H^+]\ .$$

Then, the reactions (22) and (23) are modeled by the following ordinary differential equations:

$$\dot{y}_1 = u_1 y_2 - u_2 y_1 y_3 y_H + u_3 y_3^2 - u_4 y_1 y_4 y_H + u_5 y_3 y_4 - u_6 y_1 y_5 y_H - u_7 y_1 y_2 + u_8 y_6$$

$$\dot{y}_2 = -u_1 y_2 + u_2 y_1 y_3 y_H - u_7 y_1 y_2 + u_8 y_6$$

$$\dot{y}_3 = u_1 y_2 - u_2 y_1 y_3 y_H - 2u_3 y_3^2 + 2u_4 y_1 y_4 y_H - u_5 y_3 y_4 + u_6 y_1 y_5 y_H$$

$$\dot{y}_4 = u_3 y_3^2 - u_4 y_1 y_4 y_H - u_5 y_3 y_4 + u_6 y_1 y_5 y_H$$

$$\dot{y}_5 = u_5 y_3 y_4 - u_6 y_1 y_5 y_H$$

$$\dot{y}_6 = u_7 y_1 y_2 - u_8 y_6 .$$

Table C.3. Mean ($\bar{X}$) and standard deviation (σ) of initial species inventory (g-atom/dm^3) $\times 10^4$

	I^-		IO_3^-		I_2	
Transient	$\bar{X}$	σ	$\bar{X}$	σ	$\bar{X}$	σ
1	1.0	0	15.38	1.24		
2	1.0	0	9.43	1.11		
3	4.22	0.24	0.980	0.0067		
4	5.42	0.27	0.193	0.0455		
5	1.0	0	8.77	0.38		
6	5.05	0.27	0.197	0.0031		
7	5.40	0.078	0.195	0.0039		
8					1.2	0
9					1.2	0
10					1.2	0
11					1.2	0
12					1.2	0
13					1.027	0.113
14					1.019	0.099
15					1.2	0

The transients represented by the 15 groups in Tables C.1 and C.2 can each be simulated by solving this system of equations, using the average initial values shown in Table C.3. As previously discussed, the uncertainty in these values arises both from the averaging process (quantified by the standard deviation) and from errors in the initial concentrations of the batch reactor data. The total uncertainty is generally in the range of 10 to 25%, indicating that variations in these initial values should also be considered in simulating each transient. Such consideration is accomplished by treating the nonzero initial concentrations as additional parameters that can also be varied to optimize the system. (The mathematical details of this procedure are described in ref. 27.) Thus, the final result will be optimized with respect to both the nonzero initial values and the reaction rate coefficients.

C.4 INITIAL PARAMETER ESTIMATES

The mathematical optimization procedures described in ref. 27 can be rigorously applied to find local optimal values in the neighborhood of the initial guesses. To achieve global convergence, it is important that the initial guesses themselves be reasonable, and their selection is in some ways the most difficult part of the process. The initial values ultimately used in this study resulted from considerable effort, including the use of grid searches, heuristic mathematical reasoning, and an understanding of the underlying chemistry.

The Arrhenius form is commonly used to describe the temperature dependence of rate coefficients:

$$k = A\, e^{-E/RT},$$

where A is the frequency (or pre-exponential) factor, and E is the activation energy for the reaction. For a bimolecular reaction in aqueous solution, transition state theory suggests that an approximate value for A is 10^{13} $\underline{M}^{-1}s^{-1}$, provided that both interacting species are not charged.[98] For species of like charge, this value should decrease by one order of magnitude for each charge placed on a molecule; for species of opposite charge, A should increase analogously. In practice, actual frequency factors may vary from this ideal by several orders of magnitude. The activation energy is a measure of likelihood that the reaction will occur once the two molecules do interact. A value of $E = 0$ suggests that the reaction will occur spontaneously; however, a value of $E = 100$ kJ implies that reaction is unlikely. In general, it is reasonable to expect activation energies between 10 and 60 kJ, and most likely occurring between 20 and 40 kJ.

If the frequency factor is considered to lie in the range $10^{11} \leq A \leq 10^{14}$ and activation energy in the range 20 kJ $\leq E \leq$ 40 kJ, then at 25°C the rate coefficient will satisfy:

$$9.2 \leq u \leq 24.2,$$

where $u = \ln k$. This gives some idea of the likely range, although it is still quite large, and will require scoping calculations to reduce it further. Furthermore, this range should not be enforced too strictly, since it is possible that some rate constants will fall outside of it. Furthermore, reactions which are not bimolecular may easily violate these limits.

Certain equilibrium relationships are known which create relationships between the rate constants. In particular, the equilibrium constant for Eq. (22a) and the overall equilibrium constant for all three reversible reactions (22a)-(22c) are known.[39] This results in the following restrictions on the initial choices of rate constants at 25°C:

$$u_2 - u_1 = 28.4 \qquad u_4 + u_6 - u_3 - u_5 = 23.0\,.$$

C.5 PARAMETER ESTIMATION - RESULTS AND DISCUSSION

Various trial values satisfying the relations in Sect. C.4 were used for rate constants, and the rate equations solved to simulate the eight data transients at 25°C. The total error was calculated by summing all the squared error residuals between computed solution and experimental data. The best parameter values (i.e., those producing the lowest squared error) were then used as initial guesses for iterative optimization, as described in ref. 27.

Of 27 such optimizations, the final sum of squared error for 17 was decidedly better than the rest (at least 20% lower). Simple averaging of the parameter values from these superior runs yielded the mean values and standard deviations shown in the second and third columns of Table C.4. The assorted values for initial guesses within these 17 runs are given in column 4.

The results for the case with lowest overall error are given in columns 5 through 8 of Table C.4. Shown are the optimized parameter values (columns 5 and 6), the standard errors (column 7), and the initial guesses which yielded these results. As seen in the table, a variety of initial values were used, and optimal results from many different calculations were reasonably close, as measured by the standard deviations in column 3. It is interesting that the best optimization results (columns 5 through 8) did not necessarily arise from the best initial guesses. Although initial guesses for u_1 and u_4 were quite close to the final values, this is not true for the other parameters.

It is clear from both columns 3 and 7 that the last rate constant has been determined with considerably more accuracy than the others. However, all are better than order-of-magnitude estimates. It is important to realize that the standard error (column 7) measures the ability of the model [i.e., Eq. (22)] to extract rate information from the particular

Table C.4. Optimization results at 25°C

Parameter index[a] j	Results of 17 superior optimizations for parameters $v_j = \ln u_j$			Overall best optimization			
	Mean value	Standard deviation	Initial values	Optimal value[b] $u_j = \ln k$	k_j	Standard error (%)[c]	Initial guess
1	4.503	1.254	-1,3,7	3.797	44.6	43.7	3
2	34.13	1.14	27,31,35	33.78	4.68×10^{14}	56.2	31
3	13.97	0.64	5,10,15	14.05	1.26×10^{6}	77.4	5
4	29.12	2.29	27,32	26.95	5.08×10^{11}	260	27
5	15.67	1.13	10,15	15.70	6.62×10^{6}	158	10
6	18.60	0.02	11,16	18.62	1.22×10^{8}	3.7	11

[a]Corresponding to rate constants k_j in Eq. (22).

[b]Units for k_j are h^{-1} (j=1), L/mol-h (j=3,5), and L^2/mol^2-h (j=2,4,6).

[c]Expressed as % of k_j.

data used. It does not measure the effectiveness or utility of the optimization procedure or numerical methods. Thus, to improve on these parameter estimates (i.e., lower the standard error), it would be necessary to use additional data or to reconsider the reaction set being used.

Activation energies were obtained in a similar manner. The best rate constants at 25°C (i.e., columns 5 and 6 of Table C.4) were fixed and various values of activation energies were chosen. The rate coefficients at higher temperatures were then calculated as

$$k_j(T) = k_j(25°\text{C}) \exp\left[-\frac{E}{R}\left(\frac{1}{T} - \frac{1}{298}\right)\right] \qquad (T \text{ in kelvin}).$$

The rate equations were then solved for each of the data transients at 50 and 90°C. Again using the best trial values to begin iterative optimization, the final values in Table C.4 were calculated using the optimization procedures in ref. 27.

APPENDIX D

COMPARISON OF g-VALUE TO AIR AND g-VALUE TO WATER FOR HNO_3 FORMATION

The actual mechanism of HNO_3 formation in irradiated air-water systems is still unresolved. In their early work, Linacre and Marsh[99] suggested it was a gas-phase effect, due to the creation of free radicals in air. Hence, their experiments were concerned with radiation dose to air (or to nitrogen). This idea has been continued by the study of May et al.,[100] which was designed to model gas-phase formation, assuming that is how it occurs. Recent experiments at ORNL suggest that formation cannot possibly take place in the gas phase. In these studies, a small container filled halfway with purified water is irradiated. The gas space is continuously ventilated with room air and the effluent passed through a cold trap. Periodic measurements of the irradiated water showed a steady increase in $[NO_3^-]$ and a corresponding decrease in pH. However, measurements of the trap indicated no change in pH and no presence of nitrate. Thus, it appears that reaction(s) takes place either in the liquid (involving dissolved air) or at the gas-liquid interface. In either case, it makes more sense to measure the dose to liquid, since this produces the reactive species.

Because of the varied theories of HNO_3 formation, it is helpful to compare the production based on dose to water with that based on dose to air. For any region, we have the rate of energy absorption,

$$R = \iiint_V \rho \left[\int_0^\infty \left(\frac{\mu_k}{\rho} \right) E \phi(r,E) dE \right] dr \ , \qquad \text{(D.1)}$$

where

R = rate of energy absorption (MeV/s),
ρ = density of medium (g/cm^3),
E = incident photon energy (MeV),
ϕ = gamma flux density (photons/cm^2-s-MeV),
μ_k = linear energy absorption coefficient (cm^{-1}).

If the material region is homogeneous, then ρ is independent of location, and Eq. (A.1) can be revised to give

$$R = \rho V \int_0^\infty E\left(\frac{\mu_k}{\rho}\right)\bar{\phi}(E)\,dE\ , \tag{D.2}$$

where $\bar{\phi}(E)$ is the volume average flux,

$$\bar{\phi}(E) = \frac{\iiint_V \phi(r,e)\,dr}{\iiint_V dr} = \frac{1}{V}\iiint_V \phi(r,E)\,dr\ .$$

If an experimental vessel contains distinct regions of air and water, then Eq. (D.2) can be applied to each:

$$R_g = \rho_g V_g \int_0^\infty E\left(\frac{\mu_k}{\rho}\right)_g \bar{\phi}_g(E)\,dE\ , \tag{D.3}$$

$$R_l = \rho_l V_l \int_0^\infty E\left(\frac{\mu_k}{\rho}\right)_l \bar{\phi}_l(E)\,dE\ . \tag{D.4}$$

Most radiation chemistry experiments use small containers, whose dimensions are but a fraction of the mean-free path of the source radiation (^{60}Co has two dominant decay modes, both of which have mean-free path > 15 cm). For this reason, the flux should vary only slightly throughout the vessel, and it is reasonable to assume $\bar{\phi}_g(E) \approx \bar{\phi}_l(E)$. Furthermore, the energy absorption mass coefficients in air and water are approximately the same through a large range of energies, $(\mu_k/\rho)_g \approx (\mu_k/\rho)_l$ (see ref. 101). Thus, the energy integral terms in Eqs. (D.3) and (D.4) are approximately equal, which implies

$$\frac{R_g}{R_l} = \frac{\rho_g V_g}{\rho_l V_l}\ .$$

For the data in Table 8, $V_g = V_l$, and at nominal temperature and pressure $\rho_l/\rho_g \cong 840$. Thus, the doses to water and air should differ approximately as

$$R_l = 840\ R_g\ .$$

The g-values for reactions should differ inversely. As mentioned in Eq. (34), when measured in terms of dose to water, the HNO_3 formation rate is

$$g(HNO_3) = 0.0068 \text{ molecules/100 eV absorbed in water .}$$

This suggests that if dose to air is intended, the g-value should be

$$g(HNO_3) = (0.0068)\ (840) = 5.7 \text{ molecules/100 eV absorbed in air.}$$

This value is about a factor of 3 higher than that suggested by other researchers.[99,100] However, considering the approximations involved (and that some consider dose to nitrogen rather than air), this value is a reasonable comparison.

APPENDIX E

INSTRUCTIONS FOR DATA INPUT/OUTPUT FOR pH CALCULATIONS

1. PTOT is pressure (atm). For most cases, this can be left at 1.0.

2. T is water pool temperature in (K).

3. B(J,1) values are the amounts of each element (g-atom/m^3), as described in Table E.1.

4. The desired output is HCON, the hydrogen ion concentration (mol/L), or HP, the pH.

Table E.1. Elemental inventories for pH calculation

J	Element[a]	Comments
1	H	Count 2 g-atom for every mole of water in the pool. Other species containing H can also contribute. For example, H_3BO_3 and HNO_3 would contribute 3 and 1 g-atom/mol, respectively.
2	O	Count 1 g-atom for every mole of water in the pool. Other contributors might be H_3PO_3 and HNO_3, both contributing 3 g-atom/mol.
3	B	Most likely in the form of H_3BO_3 (1 g-atom/mol), but possibly $Cs_2B_4O_7$ (4 g-atom/mol) or others may also be present.
4	K	This includes all alkali metals such as CsOH, Na_2O, KH_2PO_2, K_2O, which contribute 1, 2, 1, and 2 g-atom/mol, respectively.
5	C	The amount of CO_2 in normal air is already included. Another source is Cs_2CO_3 (1 g-atom/mol).
6	N	Nitrogen occurs here only as NO_3^-. However, all strong acids are treated as if they were nitric acid. (For HI entering water, count 1 g-atom for the purpose of calculating pH.)
7	P	This is most likely in the form K_2HPO_4 or KH_2PO_4 (1 g-atom/mol), both of which are additives to control pH.
8	Ca	This would likely come only from core-concrete debris.
9	Ar	This includes all noble gases.

[a]Corresponding to B(J,1) input values.

INTERNAL DISTRIBUTION

1. F. Barrera
2-13. E. C. Beahm
14. J. T. Bell
15. G. F. Flanagan
16. R. K. Genung
17. S. R. Greene
18. S. A. Hodge
19. M. J. Kania
20-21. T. S. Kress
22. B. L. Lepard
23. R. A. Lorenz
24. J. C. Mailen
25. R. H. Morris
26. L. Norris
27. M. F. Osborne
28. L. J. Ott
29. C. V. Parks
30. C. E. Pugh
31-33. C. H. Shappert
34. R. P. Taleyarkhan
35. J. S. Watson
36-48. C. F. Weber
49. R. M. Westfall
50. G. E. Whitesides
51. R. P. Wichner
52. ORNL Y-12 Technical Library Document Reference Section
53-54. Laboratory Records Dept.
55. Laboratory Records, ORNL-RC
56. Document Reference Section
57. Central Research Library
58. ORNL Patent Section

EXTERNAL DISTRIBUTION

59. Office of Assistant Manager for Energy Research and Development, DOE Field Office, Oak Ridge, P.O. Box 2001, Oak Ridge, TN 37831
60. Director, Division of Reactor Safety Research, U.S. Nuclear Regulatory Commission, Washington, DC 20555
61-62. Office of Scientific and Technical Information, P.O. Box 2001, Oak Ridge, TN 37831
63. Division of Technical Information and Document Control, U.S. Nuclear Regulatory Commission, Washington, DC 20555
64. C. A. Alexander, Battelle Memorial Institute, 505 King Ave., Columbus, OH 43201
65. E. G. Basanski, Principal Research Associate, Department of Nuclear Safety,
66. I.V. Kurchatov Institute of Atomic Energy, Kurchatov Square, 123182 Moscow, Russia
67. B. R. Bowsher, Chemical Physics Department, Safety & Performance Division, AEA Thermal Reactor Services, AEA Technology, Winfrith Technology Centre, Dorchester, Dorset DT2 8DH, United Kingdom
68. M. L. Brown, 15 Barrock St., Thurso Caithness, Scotland KW14 7DB
69. F. Eltawila, Accident Evaluation Branch, U.S. Nuclear Regulatory Commission, NLN-344, Washington, DC 20555
70. M. Furrer, Group Leader, Paul Scherrer Institut, CH-5232 Villigen PSI, Switzerland
71. S. Hagen, Bau 601, Kernforschungszentrum Karlsruhe, Postface 3640, D7500 Karlsruhe 1, Federal Republic of Germany
72. R. R. Hobbins, EG&G Idaho, Inc., P.O. Box 1625, Idaho Falls, ID 83401

73. C. Hueber, DERS/SEMAR (Batiment 702), Institut de Protection et de Surete Nucleaire, Commissariat a l'Energie Atomique, Centre d'Etudes Nucleaires de Cadarache, F-13108 Saint-Paul-lez-Durance CEDEX 147, France
74. F. C. Inglesias, AECL, Chalk River Nuclear Laboratories, Chalk River, Ontario, KOJ 1JO, Canada
75. K. Ishigure, Department of Nuclear Engineering, Faculty of Engineering, University of Tokyo, 7-3-1 Hongo, Bunkyo-ku, Tokyo, Japan
76. H. K. Lee, Spent Fuel Storage and Disposal Technology Section, Korea Advanced E
77. R. Y. Lee, Accident Evaluation Branch, U.S. Nuclear Regulatory Commission, NLN-353, Washington, DC 20555
78. Y. Y. Liu, Argonne National Laboratory, 9700 S. Cass Ave., Argonne, IL
79. R. O. Meyer, Accident Evaluation Branch, U.S. Nuclear Regulatory Commission, NLN-344, Washington, DC 20555
80. W. Morell, Department Manager, Siemens AG/UB-KWU E141, Hammerbacherstrasse 12+14, D-8520 Erlangen, Federal Republic of Germany
81. T. Nakamura, Reactivity Accident Laboratory, Dai-2-Genken-Shinhara-Jutaku-304, 1-23-5, Shinhara, Mito-shi, 310, Japan
82. L. A. Neimark, Argonne National Laboratory, 9700 S. Cass Ave., Argonne, IL 60439
83. K. S. Norwood, 8 Appleford Drive, Abingdon, Oxon OX14 ORA, United Kingdom
84. D. J. Osetek, Sandia National Laboratories, P.O. Box 5800, Albuquerque, NM 87185
85. F. Panisko, Pacific Northwest Laboratory, P.O. Box 999, Richland, WA 99352
86. D. A. Petti, EG&G Idaho, Inc., P.O. Box 1625, Idaho Falls, ID 83401
87. D. Powers, Sandia National Laboratories, P.O. Box 5800, Albuquerque, NM 87185
88. K. O. Reil, Sandia National Laboratories, P.O. Box 5800, Albuquerque, NM 87185
89. J. Rest, Argonne National Laboratory, 9700 S. Cass Ave., Argonne, IL 60439
90. R. L. Ritzman, Technical Advisor, Nuclear Power Division, Electric Power Research Institute, 3412 Hillview Ave., P.O. Box 10412, Palo Alto, CA 94303
91. N. H. Sagert, Branch Manager, AECL Research, Whiteshell Laboratories, Pinawa, Manitoba, ROE 1LO, Canada
92. H. E. Sims, Section Leader, Radiation Chemistry, Reactor Chemistry Department, Thermal Reactor Services, Bldg. Chem. 540.2, AEA Technology, Harwell, Didcot, Oxon OX11 ORA, United Kingdom
93. K. Soda, Head, Severe Accident Research Laboratory, Department of Fuel Safety Research, Nuclear Safety Research Center, Japan Atomic Energy Research Institute, Tokai Research Establishment, Tokai-mura, Naka-gun, Ibaraki-ken, 319-11, Japan
94. L. Soffer, Section Leader, Office of Nuclear Regulatory Research, U.S. Nuclear Regulatory Commission, Washington, DC 20555
95. K. Y. Suh, Fauske & Associates, Inc., 16W070 West 83rd St., Burr Ridge, IL 60521
96. Y.-C. Tong, Institute of Nuclear Energy Research, P.O. Box 3-6, Lung-Tan,

97. A. C. Vikis, Director, Chemistry Division, AECL Research, Whiteshell Laboratories, Pinawa, Manitoba, ROE 1LO, Canada
98. D. Williams, Technology Division, AEE Winfrith, Dorchester, Dorset, England
99. S. J. Wisbey, B.220, AERE Harwell, Didcot, Oxon OX11 ORA, United Kingdom
100. T. Yamashita, Nuclear Fuel Chemistry Laboratory, Department of Chemistry, Japan Atomic Energy Research Institute, Tokai-mura, Naka-gun, Ibaraki-ken, 319-11, Japan

END

DATE FILMED

4 / 29 / 93